

Chapter 2

Remote-Sensing Technologies and Data Processing Algorithms

2.1 Remote Sensing Methods

Remote sensing of the land covers, atmosphere and World Ocean aquatories is based on the registration of background or reflected and scattered electromagnetic radiation. Such knowledge is necessary to get data about the properties of environmental elements as it explains the dependence of thermal emission on its own physical and geothermal parameters. Also the scattering mechanisms and active radiation reflection are functions of these parameters (Borodin 2008; Bui Ta Long 1998; Shutko et al. 1994, 2010; Krapivin and Shutko 2002, 2012; Petty 1995; Schimel 1995; Golovachev et al. 2004; Cheremisin 2013; Savinikh et al. 2007).

The waves (or frequencies) of electromagnetic emission used for remote sensing in environmental monitoring systems occupy a wide spectrum from 0.3 μm to 1.3 m and cover the subranges: near ultraviolet (0.3–0.4 μm), visible (0.4–0.76 μm), near infrared (IR: 0.76–1.5 μm), middle and far IR (1.5 μm –1 mm), super high frequency (SHF: 1 mm–1.3 m). The SHF-range is divided into three basic subranges: millimeters (1–10 mm), centimeters (1–10 cm), and decimeters (10–130 dm). Two subranges called usually as L-band (15.8–63 cm) and P-band (63–100 cm) are used by many authors.

The real range choosed for objective study of the environment has to take on board many conditions such as the absorption and scattering of electromagnetic waves by the Earth's atmosphere and its interactions with the Earth's land covers and water surfaces. The atmosphere is an extremely limiting factor when choosing a working range for remote monitoring. For instance, the P-band can used for abyssal sensing from the flying laboratories, but its application in satellite monitoring systems is beset with problems because the ionosphere acts as a screen. A similar situation is found with ultraviolet radiation which is intensively absorbed by atmospheric gases. In order words, there is a question about the atmosphere clarity for specific wavelengths. For example, some wavelengths in the IR and submillimeter ranges are intensively absorbed by water vapor which practically precludes

them from consideration as remote-sensing tools. Clouds have a powerful effect on light radiation and create obstacles to land surface observation from space over many territories (Klyuev 2000; Justice et al. 1995; Grankov 1994; Asrar and Dozier 1994).

Knowledge of the atmosphere admitting function in the given synoptical and geographical conditions is the key task under the synthesis of the remote monitoring system. As a rule this task is solved during the realization of measurements. For this, one or several channels use waves that are relatively powerfully absorbed or are dispersed by different atmosphere components; these are added to the basic channels. The content of relative component is determined by the effect of these waves relaxation on the various latitudes (or the integrated content, depending on the task). The measurement results correction is introduced by the basic channels using these additional data.

The specified physical special features of the environment remote sensing are inherent to the super high frequency and ultra short waves ranges which are the foundation of the radiometric geoinformation monitoring systems. These systems allowed the many tasks involved in operative identification of natural phenomena to be solved and new methods and technologies for remote diagnosis of natural and natural/technogenic systems to be developed.

Microwave methods can be conditionally divided into two classes: active and passive. The methods that study the character of the reflection, scattering and absorption of the waves emitted by the source with known spectral density are defined as active. The optical range includes such sources: the Sun, lasers and other light emitters. Active methods used widely in radiolocation systems are in the radio range. The power of reflected and dispersed radiation, its spectral composition and polarization characteristics, phase and propagation time are the study objects in this case.

Passive methods are based on the heat emission analysis of natural formations. The fact that thermal emission is determined by substance temperature and its physical parameters is taken into account here. That is why passive methods are used for the temperature measurement and for the determination of different environmental parameters. These measurements are effective particularly under multi-channel sensing co-ordinated with the data processing algorithms (Sarkisyan 2000; Sellers et al. 1996; Krapivin and Mkrtchyan 1991; Bondur et al. 2010; Krapivin et al. 2010a, b).

Let us now move on and consider the specific features of radiophysical methods (i.e., those in which the radio waves are used). Basic attention is here concentrated on the SHF-range since namely this range is applied in the remote sensing systems located on fly-laboratories and satellites (Kondratyev 2000a; Kondratyev et al. 1990a; Krapivin and Phillips 2001; Shutko et al. 2010). Microwave radiometer systems are used intensively on numerous satellites. These systems secure the operative control of more than twenty basic geophysical parameters forming weather and climatic processes (Bondur et al. 2009).

Main specific features of radiometric methods are connected with high radio-clearness of the atmosphere. It is one of its advantage in comparison with optical

and infrared methods. The possibility of the letters is restricted mainly by absorbing and dispersing qualities of the atmosphere. The main problem here is cloud which is opaque in these wavelengths and, hence, the receipt of necessary data about the environment state is prevented. This makes it difficult to obtain operative data when such tasks as the diagnosis of extraordinary and disastrous natural or technogenic anomalies need to be solved. Certainly, the use of devices of optical and infrared ranges is possible only in the regions with small cloudiness. Hence, main advantage of radiophysical methods for the remote monitoring is its all-weatheriness. Nevertheless, there are still problems here, which scientists from many countries are addressing. For example, the absorption line of water vapors exists for $\lambda = 1.35$ cm, and the oxygen absorption zone effects for $\lambda = 0.5$ cm.

Radio waves can penetrate under the vegetation cover canopy and into the soil layer depth. That is why the use of radiophysical methods allow to assess the vegetation and soil state and to define many its properties (Krapivin 2000b; Krapivin et al. 1998b; Metternicht 1998; Burkov and Krapivin 2009; Krapivin and Vilкова 1990).

The remote sensing topics cover many theoretical and experimental investigations of the most current specializations within the fields of geoscience, ecology, radiophysics, biochemistry, oceanology, applied mathematics, cybernetics, climatology, and other sciences (Klyuev 2000; Grankov and Milshin 2004, 2010; Haarbrink et al. 2011). This chapter mainly considers the role played by the microwave range in the measurement of environmental parameters. It consists in development and experimental validation of the high-precision remote sensing methods with aim:

- (1) to study natural and anthropogenic processes,
- (2) to establish relationships between atmospheric, ionospheric and surface phenomena,
- (3) to find the long-scale changes connected with climatic, meteorological, seismological and human activity,
- (4) to investigate the field of microwave and optical remote sensing for detection of areas of water seepage through irrigation constructions, levees and dykes and for revealing of areas with dangerously high groundwater level, and
- (5) to develop a synergetic remote sensing technology for raised groundwater and seepage detection by using jointly spectral microwave and optical approach.

This chapter describes an experience in the remote sensing of the Earth from space. This experience allows obtaining the radio holographic data base for establishing regular and statistical relationships describing influence of the natural and anthropogenic factors on the ionosphere, atmosphere, and developing the adaptive models for simulation of the greenhouse effect.

Existing experience in remote sensing is characterized by different applications. For example, remote sensing methods for the land surface monitoring given possibility to introduce series of indices that help to solve numerous tasks:

- (1) NDVI—Normalized Difference Vegetation Index is an index of plant “greenness” or photosynthetic activity, and is one of the most commonly used vegetation indices.
- (2) EVI—Enhanced Vegetation Index was specifically developed to:
 - be more sensitive to changes in areas having high biomass (a serious shortcoming of NDVI),
 - reduce the influence of atmospheric conditions on vegetation index values, and
 - correct for canopy background signals.

EVI tends to be more sensitive to plant canopy differences like leaf area index (LAI), canopy structure, and plant phenology and stress than does NDVI which generally responds just to the amount of chlorophyll present.

- (3) SAVI—Soil-adjusted Vegetation Index was developed as a modification of the NDVI to correct for the influence of soil brightness when vegetative cover is low
- (4) MSAVI—Modified Soil-adjusted Vegetation Index is soil adjusted vegetation indices that seeks to address some of the limitation of NDVI when applied to areas with a high degree of exposed soil surface.
- (5) SATVI—Soil-adjusted Total Vegetation Index is a modification of several earlier vegetation indices that correlates with the amount of green and senescent vegetation present on the ground.
- (6) Microwave Vegetation Index (MVI) uses microwave readings from two different frequencies to determine the cover of vegetation. Each of these different frequencies has the ability to penetrate vegetation canopy to a different degree, and the relative difference in reflectance between these two can be interpreted to give an index of vegetation cover.
- (7) Normalized Burn Ratio (NBR) was defined to highlight areas that have burned and to index the severity of a burn using Landsat TM imagery.
- (8) Biological Crust Index uses a unique feature of the phycobilin pigment found in cyanobacterial soil crusts, resulting in a relatively higher reflectance in the blue spectral region compared to soil without cyanobacteria.
- (9) Burned Area Reflectance Classification (BARC) is a method using remotely sensed data to assess the severity of fire damage to vegetated areas developed by the US Forest Service and US Geological Survey.

Remote sensing methods widely penetrate to other areas. The fundamental task that is subject of many studies consists in development and experimental validation of the high-precision methods and algorithms for restoration of the time-spatial distribution of the physical parameters of the atmosphere, ionosphere and the Earth’s surface using the radio fields measured on some interface or curve in space (radio hologram). Radio hologram can be registered using small satellite in space or an airplane in the atmosphere. Application of the satellite radio holography for global geophysical monitoring is justified by existence of the space radio systems

designed for radio navigation, radio communication and other civilian tasks. Many of these radio systems are emitting permanently radio signals having high coherence and stability properties. This allows one to develop radio holographic methods that can be realized with help of the high stability and coherence of the radio signals of the space radio systems. The radio holographic analysis of the satellite radio holograms can be used as a tool for elaborating the data base containing important geophysical information on the global scale with aim to reveal natural and anthropogenic processes, to establish relationships between atmospheric, ionospheric and surface phenomena and to find the long-scale changes connected with climatic, meteorological, seismological and human activity. The database can be elaborated by means of radio holographic processing of the radio holograms registered by exiting and future satellite missions (e.g. Mir, GPS/MET, CHAMP, SAC-C radio occultation experiments). The next fundamental and practical problems are needed to solve:

1. Elaborating the radio holographic methods for high-precision determination of the spatial distribution of the physical parameters of the atmosphere, ionosphere and the Earth's surface.
2. Development of the database for global geophysical monitoring of the physical parameters of the atmosphere, ionosphere and the Earth's surface using radio holograms registered by low orbital satellites.
3. Analysis of the elaborated data base with aim to find the radio-physical parameters that are sensitive to long-scale changes in the state of the atmosphere, ionosphere and the Earth's surface.
4. Elaboration of the radio holographic technology for bistatic radiolocation of the atmospheric boundary layer and the terrestrial surfaces. The aims of this technology are:
 - to determine the humidity and the vertical gradients of the refractivity in the boundary layer of the atmosphere; and
 - to measure parameters of the terrestrial surfaces (wind roughness and long-scale waves in the oceans, ice distribution in the polar regions).

Elaboration of the polarimetric and interferometer methods for studying physical parameters of the land surfaces: the electric permittivity, conductivity, soil moisture, foliage parameters and the long-scale relief changes connected with seismic and anthropogenic activity. Elaboration of the database of the global geophysical monitoring of the Earth's surface and the atmospheric boundary layer by means of the processing of the radio holograms registered by MIR, GPS/MET, CHAMP, SAC-C missions.

5. Investigation of the ionospheric effects of the natural and anthropogenic processes by means of analysis of the radio holograms registered on the communication line satellite-satellite and Earth-satellite.
6. Modeling the greenhouse effect by means of the analysis of the developed global geophysical database.

The experience of elaborating the theory of the radio holographic investigation of Earth and its gas-plasma environment from space was described in publications by Liou et al. (2003, 2010), Pavelyev et al. (2002, 2003, 2010).

Positive scientific results are achieved owing to the combined use of remote sensing and ecoinformatics tools. With the global effect of climate change, ecoinformatics is an emerging drench of research where new techniques, tools and infrastructure are being developed to enable more in-depth study of processes in the nature/society system with effective employment of scientific data collection instruments such as sensors, satellites, scientific experiments and simulations. As Myers and Atkinson (2008) remark, ecoinformatics is the combination of multiple environmental datasets and modeling tools used to test ecological hypotheses and derive information.

2.2 Remote Sensing Techniques

Remote sensing is the observation and measurement of objects from a distance, i.e. instruments or recorders are not in direct contact with objects under investigation. Remote sensing depends upon measuring some kind of energy that is emitted, transmitted, or reflected from an object in order to determine certain physical properties of the object. One of the most common types of remote sensing is microwave radiometry, which along with many other techniques is used for the equipment of flying laboratory and satellites.

There are several types of instrumentation that can be used for environmental investigations. For examination of soil type, or surface moisture, the ones that come to mind are thermal infrared radiometers, active radar systems, and the passive microwave radiometers. A system of non-scanning single-beam microwave radiometers was designed in Kotelnikov Institute of Radioengineering and Electronics (Shutko et al. 2010). The basic technical parameters of this system are given in Tables 2.1 and 2.2. Common view of portable radiometers is given in Figs. 2.1 and 2.2.

Table 2.1 Set of portable microwave radiometers

Parameter	Characteristic
Frequency (GHz)	1.41; 1.67; 5.0
Polarization	V or H
Antennas	
Slot array	19.7" × 19.7"; 16.3" × 16.3"
Dipole array	7.9" × 6.5"
Incidence angle	Fixed angles 0–30° off nadir
Sensitivity (K)	0.5
Beamwidth (3-dB)	30°
Platform	Boom truck, land-rover, small aircraft
Weight (kg)	12
Power required (VA)	30

Table 2.2 Characteristics of microwave radiometers designed in Kotelnikov Institute of Radioengineering and Electronics, Russian Academy of Sciences (Shutko and Krapivin 2011; Krapivin and Shutko 2012)

Frequency (GHz)	Wavelength (cm)	Range	Pixels/scan	Spatial resolution (H)	Mode
37	0.8	Ka	32	0.04	Scanning
15.2	2	X	16	0.08	Scanning
13.3	2.25	X	12	0.09	Scanning
5.5	5.5	C	6	0.13	Scanning
1.4	18/21	L	2	0.65	Twin-beam

H is height above ground



S-Band Radiometer for «Interkosmos 21» Satellite



S-Band Radiometer for «Mir» Station



4.3-cm Polarization Radiometer



30-cm Radiometer



8- mm Radiometer



21-cm Radiometer

3-mm Scanning Radiometer



Fig. 2.1 Set of portable radiometers produced by Special Design Office of Kotelnikov Institute of Radioengineering and Electronics of Russian Academy of Sciences (Krapivin and Shutko 2012; Verba et al. 2014)

The radar systems, including Interferometric Synthetic Aperture Radar (IFSAR), share the same frequency band as the microwave radiometers. Therefore they have similar wave propagation characteristics, although the radar systems are actively transmitting and measuring the return values. The radar/IFSAR systems rely on surface texture to reduce surface boundary conditions.

Passive microwave systems only record the naturally emitted radiation, which is a function of the soil moisture content within the first several centimeters/decimeters and is less influenced by surface roughness. From a given height above the

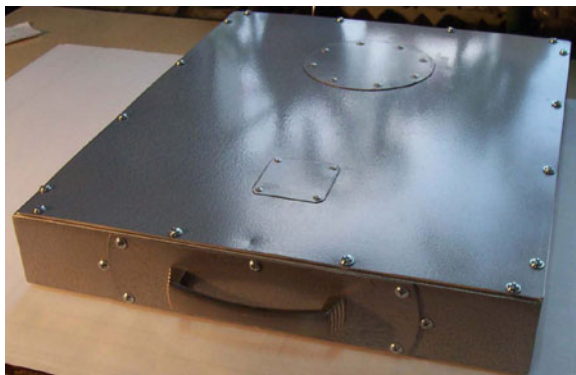


Fig. 2.2 21 cm microwave radiometer produced by Special Design Office of Kotelnikov Institute of Radioengineering and Electronics of Russian Academy of Sciences (Krapivin and Shutko 2012)

ground surface radar systems have a much smaller ground sample distance, or pixel size, than the passive systems. To compensate, the passive system can be flown on light aircraft at very low altitudes, as low as 500 ft above the mean terrain.

Thermal infrared radiometers (TIR) and the microwave radiometers both measure natural radiation from a thermodynamic process. TIR sensors are further influenced by cloud, fog, smoke, solar radiation and other similar atmospheric conditions. However, TIR operating in 10–12.5 μ wavelengths range are mainly sensitive to the temperature variations which take place within a thin surface layer of the object being imaged. This temperature variation could be the result of many things, such as warm water, or steam leaking from underground pipes, poor insulation properties on buildings, effluent from a manufacturing process, etc.

Microwave radiometers, on the other hand, measure the natural radiation at mm, cm and dm wavelengths that is primarily a function of soil moisture content in the first couple of centimeters/decimeters of the Earth's surface.

Considerable experience of remote sensing in global scale was started with the launch of orbital space station “Mir” which was complex science-research complex (Fig. 2.3). This station was launched at February 20, 1986 and was submerged at March 23, 2001 in the Pacific Ocean.

Instrument complex of Mir space station for remote sensing functions was equipped in specialized modules that were named as Spectr and Priroda (Nature). Module Spectr has optical-visual and photometric instruments as well as lidar and photographic cameras for the monitoring of the atmosphere, oceans, land surface, as well as for medical-biological investigations. Priroda (Nature) conceived for remote-sensing research from orbit, was also sitting on the ground partially completed until Russian-US cooperation revived the project. It became the last element, which completed the construction of Mir. Module Mir had specialized complex of sensors:

- trace, panoramic and scanning microwave radiometers (radiometric system Ikar, Tables 2.3 and 2.4);



Fig. 2.3 Russia's Mir space station (<http://spaceflight.nasa.gov/gallery/images/shuttle/sts-91/html/91727051.html>)

- 64-channels IR-spectrometric system Istok;
- UV-spectrometric systems of visual and IR-range; and
- active radiophysical and optical systems.

Solution of specific environmental tasks requires the optimization of instrumental and algorithmic means. It can be realized by means of the GIMS-technology methods. The ratio between experimental and theoretical methods in this case is defined by the complexity of environmental system that is to be studied. Cumulative experience of the GIMS application is based on the solution of national problems in many countries where different remote sensing platform were created. Historically this experience was started in 1980 with equipping of flying laboratories based on bi-plane AN-2, twin-engine plane IL-14, 4-engine plane IL-18, helicopters MI-2, MI-8 and Ka-26 (Krapivin and Shutko 2011, 2012; Shutko et al. 2010; Haarbrink et al. 2011). In the ensuing years, this set of carriers was widened.

Table 2.3 Trace and panoramic radiometers of radiometric system Ikar

Radiometer characteristic	Panoramic	Trace Ikar-N
Wavelength (cm)	2.25; 6.0	0.3; 0.8; 1.35; 2.25; 6.0.
Fluctuating sensitivity (time for integration is 1 s) (K)	0.15	0.15
Measuring range of radiobrightness temperature (K)	50–350	50–350
Antenna beam width (3 dB level) (°)	12	9
Spatial resolution (for altitude of 400 km) (km)	80	60
Observation angle (°)	40	0, 0
Swath (for altitude of 400 km) (km)	750	60
Required power (W)	30	100
Mass (kg)	40	50
Informativity (Kb/s)	0.5	1.0
Sampling digit capacity (bits)	10	10

Table 2.4 Scanning radiometers of radiometric system Ikar

Radiometer characteristic	P-400	Delta
Wavelength (cm)	4.0	0.8; 1.35; 2.25
Fluctuating sensitivity (time for integration is 1 s) (K)	0.15	0.15–0.4
Measuring range of radio brightness temperature (K)	50–350	50–350
Antenna beam width (3 dB level) (°)	5.0	1.1; 1.7; 3.0
Beam shift angle at channels (°)	0.0	0.0; –1.1; 2.4
Spatial resolution (for altitude of 400 km) (km)	50	10.0; 15.5; 28.0
Observation angle (from nadir) (°)	40	40.0; 37.9; 42.4
Scan time (s)	3.4	2.56
Swath (for altitude of 400 km) (km)	400	660
Угол сканирования, град	72	165
Потребляемая мощность (Вт)	30	50
Масса (кг)	46	100
Информативность (кбит/с)	1.5	10
Разрядность квантования (бит)	10	10

One of examples when multi-purpose flying laboratory was used successfully is IL-18-based (hull No 75423) regional monitoring system (Borodin et al. 1982). IL-18 on-board complex is represented in Fig. 2.4.

Flying laboratory IL-18 has given a possibility to solve numerous environmental tasks practically in real time. On-board system represented in Fig. 2.4 registered environmental characteristics and at the same time processed existing and delivered by sensors information. Figure 2.5 explains a structure of on-board information-modeling system that interrogated all sensors with time period equaled to 0.01 s and taking into consideration of navigation information all results were referred to the geographical coordinates.

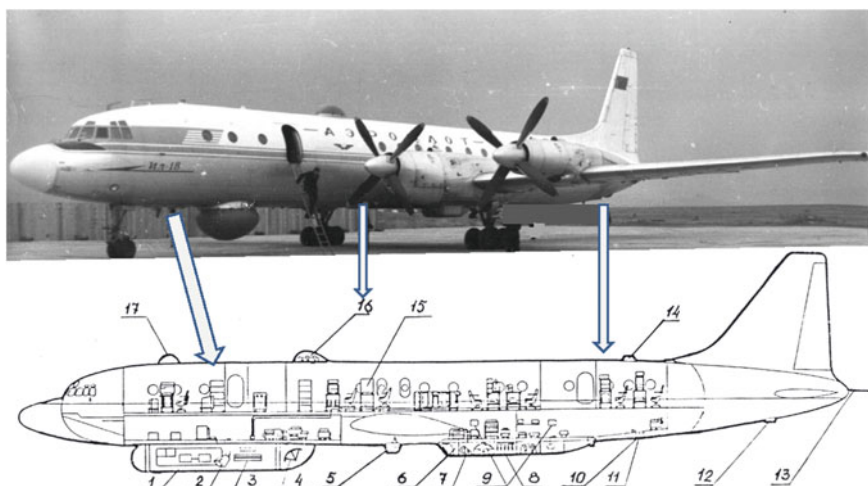


Fig. 2.4 Scheme of positioning the antenna systems and photo-hatches on-board of flying laboratory IL-18. Notation: *Antennas*: 1, 3—radio locators with synthetic aperture, wavelengths—2.0 and 10.0 cm; 2, 6—trace polarimeters, wavelength—0.8 and 2.25 cm; 4—six-channel scanning polarimeter, wavelength—0.8, 1.35, 2.25, 10, 20 and 27 cm; 7, 9—precision altimeter and interferometer of side looking, wavelength—2.2 cm; 13—sub-surface sounding station of decimetric range; *Photo-hatches*: 5, 10, 12—large-format and frame TV, aerocamera; 11, 14—radiometers of mm range; 16—trace radiometers, wavelength—0.8, 1.35, and 2.25 cm; 15—gravimetric and inertial devices; 17—astro-hatch

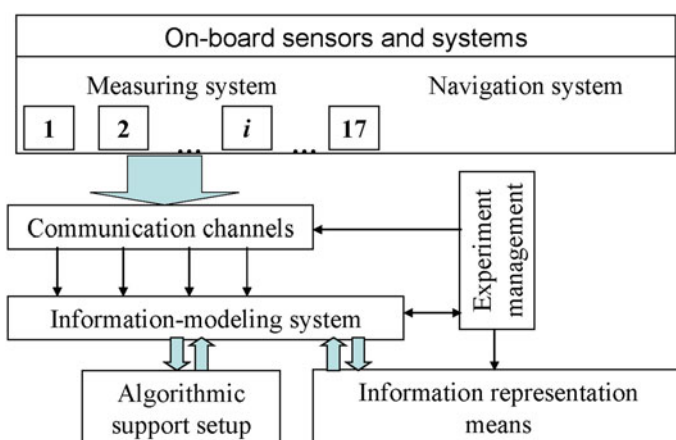


Fig. 2.5 Typical structure of on-board information-modeling system realized in flying laboratory IL-18

Long-term exploitation of flying laboratory IL-18 in Former USSR has showed the availability of using the multi-purpose remote sensing systems under solution of environmental problems on large territories. Unfortunately, this laboratory was

destroyed in 1990 when USSR was broken. However, this experience was developed in Russia (Krapivin and Shutko 2012).

One of effective multi-frequency polarimetric synthetic aperture radar system was created in the 90s by the Russian Corporation Vega for surface and subsurface sensing. It is airborne IMARC SAR system. This Corporation created radiometer system Radius operating at the wavelengths of 0.8, 2, 5.5, 21 and 43 cm (Fig. 2.6, Table 2.5). Main features of the IMARC SAR complex are given in Table 2.6.

The IMARC is a four-wavelength polarimetric airborne SAR system designed at Radioengineering Corporation Vega (Kutuza et al. 2000). Radar system operates at wavelengths: X (3.9 cm), L (23 cm), P (68 cm), and VHF (2.54 m); polarizations in all bands: VV, HH, VH, and HV; spatial resolution is around 12 ± 8 m; maximum swath is 24 km. The carrier of this system was a twin-turbine jet airplane TU-134A and other planes. The main IMARC SAR mission goals were to map the characteristics of Earth covers (including soil hydrological regimes), to map the ground terrain in a presence of vegetation with eliminating of the influence of vegetation and, to produce elevation models, to detect areas with on-ground and underground irregularities, etc. (Shutko et al. 2010; Krapivin and Shutko 2012).

Airborne SAR system IMARC can use for solution the following tasks:

- surface sensing of ocean, ice and vegetation;
- subsurface sensing of scattering objects and deep layers.



Fig. 2.6 General view of the scanning SHF—radiometric system “Radius” (2 and 5 cm) (Shutko et al. 2006a, 2007, 2010; Krapivin and Shutko 2012; Verba et al. 2014)

Table 2.5 Scanning radiometer “Radius” characteristics

Frequency (GHz)	Wavelength (cm)	Band	Pixels/scan	Resolution (H)	Mode
37	0.8	Ka	32	0.04	Scanning
15.2	2	X	16	0.08	Scanning
5.5	5.5	C	6	0.13	Scanning
1.4	21	L	2	0.5	Scanning
0.7	43	S	1	–	Non scanning

Power consumption is 200–300 W, power supply is 27 VDC; weight is 100–120 kg

H is height above ground

Table 2.6 The IMARC SAR complex parameters

Parameter	Value			
Frequency	X	L	P	VHF
Wavelength (cm)	3.9	23	68	254
Polarization	VV, HH, VH, HV			
Resolution (m)	4–6	8–10	10–15	15–20
Antennas: gain (dB)	30	14–17	14–17	9–11
Width in azimuth (°)	18	24	24	40
Width in elevation (°)	24	24	24	60

Multi-frequency polarimetric SAR gives new possibilities for operative remote sensing of sea, soil, vegetation, ice cover and other Earth surfaces. The algorithms used for deep-layer remote sensing, which is undertaken layer-by-layer, make it possible to solve a narrow set of environmental problems.

The larger the wavelength, the higher the influence of deeper soil layers—this fact allows the development of methods of thick-layer deep sensing using multi-frequency radar systems. For subsurface sensing the use of long waves of P and VHF bands is required.

Information about soil properties (soil moisture) profiles can be received from the analysis of measurements of scattering at different wavelengths. To calculate the influence of soil moisture profile into backscattering cross section it is necessary to develop the models of reflection from the layers situated at different depth. Solution of the inverse problem can be obtained by setting the measurement of backscatter at several wavelengths and at different polarization modes. For complete information about soil moisture profile it is necessary to solve the problem of images interpretation in broad band of wavelengths including meter band where attenuation in soil and vegetation is comparably low.

The results of multi-band radar survey obtained with the help of 4-bands airborne SAR IMARC (Radioengineering Corporation Vega) illustrate the possibility of measuring of hydrological soil regimes and water lenses allocation in Kara-Kum desert. Lenses of underground water at the depth of 50–70 m were detected. Results were validated by control well-boring. We can see at radar images:

- (1) dry river-Uzboy bed;
- (2) sand dunes of 6–15 m height;
- (3) underground water lenses;
- (4) transmission facilities.

Application of GIMS technology depends on just how complex the solution to the environmental tasks under consideration is in a given time period at a given precision. An effective instrument using GIMS technology was synthesized by Miramap (a private-sector Dutch Company) in response to a European Space Incubator initiative from the ESA Technology Transfer & Promotion (TTP) Office. The TTP office is contributing to the capitalization of space-based technology and know-how for the benefit of Europe's economy and science. The innovation of microwave radiometer (MR) mapping company (Miramap) was nominated for the Holland Innovation Price in 2005 and was quoted in several newspapers and magazines such as the Dutch Financial Times.

The Miramap instrument consists of three microwave sensors in X-band, C-band and L-band which are all Global Navigation Satellite System (GNSS) integrated (Fig. 2.7, Tables 2.7, 2.8, 2.9 and 2.10). The X-band and C-band sensor makes a conical scan at constant incidence angle over a wide swath, while the L-band sensor makes a twin-beam oscillating scan. The small instrument sizes and weights enable use of a low-cost light aircraft as the observing platform, providing decision makers with a new affordable tool. The platform on which these instruments are flown is a



Fig. 2.7 Miramap sensor aircraft (Shutko et al. 2010; Krapivin and Shutko 2012)

Table 2.7 Miramap microwave sensor specifications

Parameter/band	X-band	C-band	L-band
Frequency (GHz)	15.2	5.5	1.4
Wavelength (cm)	2.0	5.5	21
Pixels/Scan	16	6	2
Incidence angle (°)	30	30	15
Beam width (°)	3.5	5	25
Polarization	H	H	H
Sensitivity (K/s)	0.15	0.2	1
Absolute accuracy (K)	±5	±5	±5

Table 2.8 Microwave Radiometer Mapping Company (Miramap, Noordwijk, the Netherlands): Sensor specification

Sensor	Type	Wavelength	Project specs	Use
Digital photo camera	Rollei AIC 50 mm lens	Visible 0.4–0.7 μ	10 cm GSD sub-pixel precision	Detailed visible interpretation
Lidar scanner	Optech altimeter	SW infrared 1,064 nm	2 cm GSD 0.1 m precision	Elevation model
Passive microwave scanner	Radius (IREE-Vega design)	Microwave 2, 5, 21 cm	5 m GSD 0.15 K	(Sub) surface detection of wet and dry areas
Thermal camera	Flir systems	LW infrared 7.5–13 μ	3 m GSD 0.1 °C	Surface temperature

Table 2.9 Miramap company platforms and remote sensing instrumentation

Platforms/instrumentation	Aircraft laboratory	Unmanned plane/helicopter	Specific car/rover	In situ data collecting instruments
Microwave radiometers	Exists	Exists	Exists	Exists
Infrared radiometers	Exists	Exists	Exists	Exists
Optical color digital cameras	Exists	Exists	Exists	Exists
Lidar (3-D) land surface relief easurer	Exists	No exists	No exists	No exists
Georadar	No exists	No exists	Exists	Exists

Table 2.10 Miramap product specifications

Parameters	Operating range	Max abs error
Soil moisture (g/cm ³)	0.02–0.5	0.07
Depth to water Table (m)	0.05–5	0.3–0.6
Plant biomass (kg/m ²)	0–3	0.2
Pollutant concentrations (ppt)	1–30	1–5

reliable and safe twin Aero Commander (Krapivin and Shutko 2012; Krapivin et al. 2012a). The aircraft is specially modified to simultaneously carry a range of other instruments, such as (digital) photogrammetric cameras, lidar scanners, thermal infrared and multi-spectral sensors. The capability to measure such a comprehensive range of remotely sensed parameters from a single low-cost airborne platform is unique worldwide.

With whole set of sensor shown in Tables 2.7, 2.8 and 2.9, company Miramap provides the customers exactly with the parameters and environmental conditions given in Table 1.18 including:

- surface soil moisture,
- underground moistening,
- depth to a shallow water table (down to 2 m in humid areas and down to 3–5 m in arid/dry areas),
- located on the surface and shallowly buried metal objects of a reasonable size under the conditions of dry ground,
- contours of water seepage through hydrotechnical constructions (levees, dams, destroyed drainage systems, different kinds of leaks),
- biomass of vegetation above a water surface or wet ground,
- increase in temperature in land, forested and volcano areas,
- changes in salinity/mineralization and temperature of a water surface,
- water surface pollution, oil slicks on a water surface,
- on-ground snow melting,
- ice on a water surface and on the roads, runways.

Some indices of the effectiveness of the GIMS-technology realized in framework of Miramap's flying research laboratory are the following:

(1) Soil moisture content

- operating range is $0.02\text{--}0.5\text{ g/cm}^3$
- maximum absolute error is:
 - when vegetation biomass is less than 2 kg/m^2 — 0.05 g/cm^3 ;
 - when vegetation biomass is greater than 2 kg/m^2 — 0.07 g/cm^3 .

(2) Depth to a shallow water table

- operating range is:
 - for humid or swampy areas— $0.2\text{--}2\text{ m}$;
 - for dry arid areas, deserts— $0.2\text{--}5\text{ m}$;
- maximum absolute error is $0.3\text{--}0.6\text{ m}$.

(3) Plant biomass (above wet soil or water surface):

- operating range is $0\text{--}3\text{ kg/m}^2$;
- maximum absolute error is 0.2 kg/m^2 .

(4) Salt and pollutant concentration of water areas (off-shore zones, lakes):

- operating range is 1–300 ppt;
- maximum absolute error is 1–5 ppt;
- relative error is 0.5 ppt.

Large-scale investigations on the creation of microwave research carrying platforms were realized by Microwave Remote Sensing Division (MRSD) in 2002 through 2005 within the NASA Center for Hydrology, Soil Climatology and Remote Sensing (HSCaRS) at Alabama Agricultural and Mechanical University (AAMU). This Division was capable of performing microwave radiometric data interpretation and conducting studies in field conditions, from mobile platform and unmanned helicopter.

The antennas, radiometers, data collection system and an embedded Global Positioning System (GPS) receiver were mounted on the manned Rover type mobile platform and unmanned helicopter platform Microwave Autonomous Copter System (MACS) for measuring the soil-plant system radiation. All radiometers were mounted on a folding mounting panel to observe horizontally polarized radiation when folding the panel is situated between the nadir through zenith looking angle. The GPS information was used to register the microwave reading to a common coordinate system of the study area. The data capture rate was set to 1 measurement per second in each of the radiometric channels and GPS readings.

The manned “Rover” type mobile platform is a modified Gator utility vehicle. This two-seater vehicle has a 286 cc, air-cooled, 4-cycle gasoline engine. Its towing capacity is 500 lb (226 kg) with a top speed of 20 mph (32 km/h). The instrument platform (or mounting frame) for the radiometers and other instruments was assembled at AAMU research station. The aluminum folding panel of 1.5 m × 1.5 m connecting all system components was designed so that the incidence angle from 0° (nadir) to 180° (sky) could be easily obtainable (Figs. 2.8 and 2.9 and Table 2.11). The radiometers were mounted with the antennas viewing off to the right hand side of the platform at an incidence angle of 10°. The radiometer “Rover” shuttled back and forth in a north-south direction at a speed of 2–5 mph. using the developed remote sensing system data obtained from a height of 2 m provided the spatial resolution of 1.4 m of land area.

The unmanned helicopter platform MACS was equipped with a 6 cm radiometer (incidence angle 5°) mounted on the nose of the AutoCopter™ onto a stabilized gimbal with pan/tilt interface which attenuates vibrations (Fig. 2.10, and Table 2.12). The MACS is a modified AutoCopter™, a small unmanned helicopter platform that can fly autonomously (fly a pre-programmed flight path) or semi-autonomously (with an operator directing the maneuvers). This is a product of Neural-Robotics, Inc. (NRI) of Huntsville, AL.

The unmanned helicopter advantage is its patented flight control system consisting of multiple neural network modules working together. The result is an autonomous helicopter that adapts to changing conditions and provides an extremely stable platform for hundreds of applications. The AutoCopter™ is 2.18 m in length (from tip of tail rotor to tip of main rotor) and weighs approximately 13.6 kg.



Fig. 2.8 General view of the manned “Rover” type mobile platform equipped with three portable microwave radiometers, operating at the wavelengths 6, 18, and 21 cm. Also equipped with a folding panel of $1.5 \text{ m} \times 1.5 \text{ m}$ for instrumentation installation along with GPS receiver, data acquisition system and power supply battery (Shutko et al. 2010; Krapivin and Shutko 2012; Verba et al. 2014)

It carries a payload of up to 6.8 kg. Basic avionics consist of a PC/104 computer, altitude and heading reference system (AHRS), GPS receiver (WAAS-compatible), downward pointing range finder (ultrasonic sensor), barometric pressure sensor, and heading-hold gyro. The standard transmitter is used as the “ground station.”

The Ground Control Station (GCS) with a flight planning program “Way Planner” was used with the AutoCopter™. This is a self-contained Windows-based application that unlocks the power of fully autonomous flight. The program enables mission planning in 2D using stored satellite images. Flight plans were uploaded to the AutoCopter™ via data link enabling the aircraft to takeoff, climb, fly its programmed route, and land fully autonomously. The programmed flight consisted of an autonomous launch with 16 waypoints, a climb to 30 m, followed by a transition to forward flight at a velocity of 2 m/s and auto-landing.

During flight the aircraft has the ability to state data (aircraft altitude, speed, and other parameters in real time on the GCS screen in 2D and 3D. While maintaining airspeed, altitude and heading, 8 flight lines were flown at a distance of $\sim 500 \text{ m}$ at 30 m intervals. The time it took the helicopter to fly from waypoint to waypoint (north-south direction) was $\sim 4.5 \text{ min}$ totaling $\sim 40 \text{ min}$ of flight time. Because the

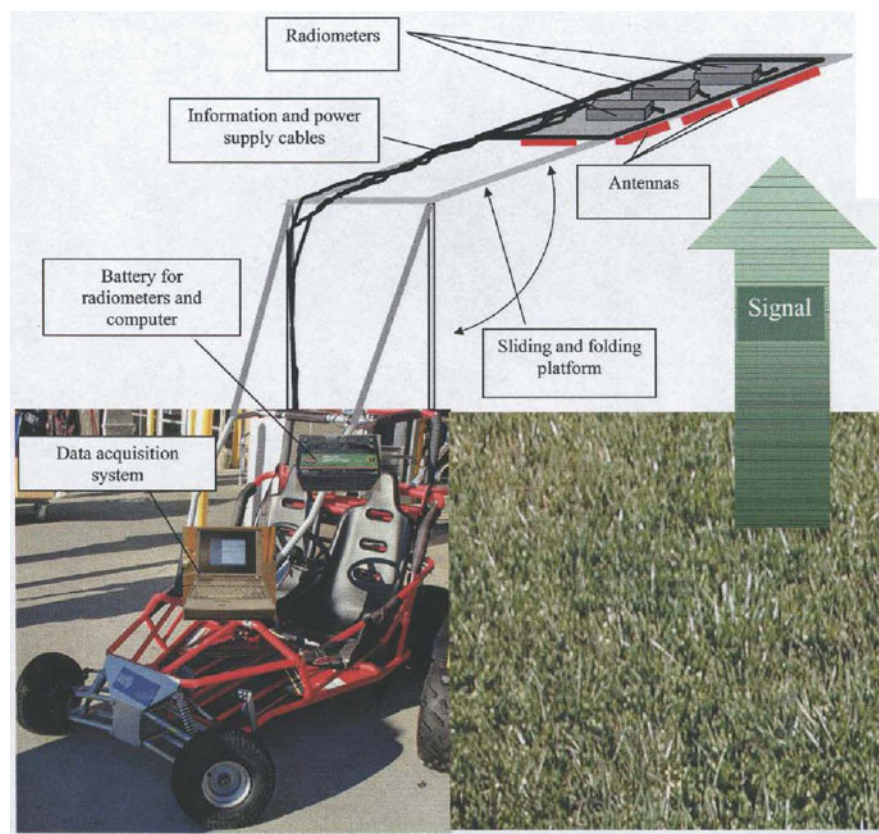


Fig. 2.9 Subsystems and microwave radiometers on mobile platform “Rover” (Shutko et al. 2010; Krapivin and Shutko 2012)

Table 2.11 Characteristics of the microwave platform “Rover”

Parameter	Value
Frequencies	1.41, 1.67 and 5 GHz
Polarization	H or V
Antennas	19.7" × 19.7"; 16.3" × 16.3"; slot array; 7.9" × 6.5"; dipole array
Incidence angle	Fixed angles 0–30° off nadir
Sensitivity	0.5 K
Beam width	(3-dB); 30°
Weight	12 kg
Power required	30 VA



Fig. 2.10 Photograph of the unmanned aerial vehicle (UAV) helicopter “Microwave Autonomous Copter System” (MACS) equipped with a 6 cm radiometer, data acquisition system, GPS receiver and power supply battery (Shutko et al. 2010)

Table 2.12 Characteristics of the microwave autonomous copter system (Krapivin and Shutko 2012)

Parameter	Value
<i>Physical characteristics</i>	
Length	3.58 m
Weight	22.68 kg
Main blades	1.03 m
Engine	120 cc
Range	161 km
Payload capacity	20.41 kg
Fuel tank	32 oz
<i>Passive sensor packages</i>	
Wavelengths	3, 6, or 21 cm
Sensitivity	0.3–0.5 K
3-db beam width	30°
Power supply	27 V DC
Power consumption	15 VA
Weight	2–6 kg
<i>Others</i>	
Frequencies	1.4 or/and 5 GHz
Polarization	H or V
Antennas	Flat panels w/30° 3-dB
Incidence angle range	Fixed angles 0–30°
Sensitivity	0.5 K
Flight time	2 h

aircraft flew below 500 ft it was exempt from FAA regulations. Using the developed remote sensing system, data obtained from an altitude of 30 m provided the spatial resolution of 20 m of land area.

2.3 Microwave Radiometry and Remote Sensing of the Environment

Microwave radiometry, or passive microwave remote sensing, is one of the radio-physical methods used for remote observations of the environment. It is based on measurements of the natural electromagnetic radiation of objects in the millimeter to decimeter range of wavelengths. The theoretical aspects of radiophysical monitoring are determined by organizing a measurement procedure in the active or passive regimes of electromagnetic radiation propagation. An active sensing technology is based on the radiolocation methods, and a passive one is based on the background radiation registration. In both cases, theoretical tasks of microwave monitoring are connected with the study of electromagnetic waves propagation in the environment and, of course in the first place, in the atmosphere and near ionosphere (Kondratyev and Fedchenko 1992; Yakovlev 2001; Yakovlev et al. 2009; Chukhlantsev 2006; Gulyaev et al. 2009; Pavelyev et al. 2010).

In the active regime the talk is about the propagation of electromagnetic waves of various ranges from the emitter to the receiver. Two cases are possible here. In the first case, the transmitter and receiver have different position in the environment and the decision about the assessment of the environment parameters is accepted on the base of registered distortion of transmitted signal. In the second case, the transmitter and receiver are combined so that estimation of the environment parameters is made on the base of analysis of the emitted signal absorption and distortion of received its reflection. Clearly, the time it takes the signal to propagate in the environment is the information parameter. An active form of microwave monitoring is typical for the atmosphere radiotranslusense method.

Basic advantage of microwave remote sensing lies in its largely immune to clouds, precipitation, smoke, etc. and a capacity to penetrate sand, soil, rock, vegetation, dry snow, ice, etc. Knowledge of the physical processes associated with energy emission at microwave range gives a possibility to calculate a variety of surface and atmospheric parameters, including air temperature, sea surface temperature, salinity, soil moisture, sea ice, precipitation, the total amount of water vapor and the total amount of liquid water in the atmospheric column directly above or below the instrument.

The passive methods of microwave monitoring are based on SHF-radiometry. The existence of resonance absorption fields in SHF range allows remote reconstruction of meteorological atmosphere parameters such as the vertical profiles of temperature, humidity, total water vapor mass, water storage in the clouds, and precipitation intensity, etc. The possibility to receive data not only about the properties of water and

land surfaces but also about deep characteristics depends on the choice of electromagnetic range. In the infrared range, total emission is formed into very thin surface layer. Electromagnetic waves of microwave range are absorbed powerfully by the land and water surfaces. The depth of its spread into the water environment is measured in hundredth of millimetre; whereas dry soils, continental ices, and dry snow this value can reach several tens of wavelengths. It allows to realize the remote investigations of soil, ice and snow covers up to considerable depths.

Penetrating ability of radio-waves gives the advantage particularly under the sensing of land covers. Vegetation without a dense canopy (grass, cereals, etc.) absorbs radio waves weakly and this is the reason radio-observation of soil covers through this vegetation is possible. Radio-waves can spread across the soil up to the depth reaching one metre.

Main defect of microwave radiometric observations consists in the comparative low spatial resolution in comparison with the optical range. In the radio-range the high spatial resolution is achieved by the multichannel application and specific data processing methods. It demands large economic investments.

Let us consider some aspects of active location. Let us supposed that irradiation at the nadir of a smooth plot is realized. In this case the signal power reflected from the land surface equals $W = pGA|\kappa_0|^2(16\pi H^2)^{-1}$, where p is the emitted power, G is the coefficient of directed action of antenna, A is the efficient antenna area, H is the antenna height above the ground surface, κ_0 is the surface reflection coefficient. If all instrumental parameters and antenna height are known the ratio of power accepted to that of the one received determines the value of the reflection coefficient. In the case when the soil is uniform by depth the reflection coefficient equals $\kappa_0 = (\varepsilon^{1/2} - 1)/(\varepsilon^{1/2} + 1)$, where ε is the dielectric ground permittivity. For the estimation of ε the following approximate formula exists

$$\varepsilon = \left(\varepsilon_w^{1/2} p_w + \varepsilon_s^{1/2} [1 - p_w] \right)^2, \quad (2.1)$$

where ε_w is the dielectric water permittivity, p_w is the relative volume concentration of free moisture in the soil, $\varepsilon_s \approx (1 + 0.5\rho_s)^2$ is the dielectric permittivity of dry ground, and ρ_s is the dry ground density ($1\text{--}2 \text{ g cm}^{-3}$).

From Eq. (2.1) it is seen that reflected signal power give a possibility to determine the reflection coefficient and, consequently, dielectric ground permeability. The value of ε defines the ground density when it is dry or the water content if it is wet.

Dielectric properties of land covers are basic to use the radiometric methods for its diagnosis under different situations. Specifically, the knowledge of spectral coefficient for the emission in the millimetre range allows to estimate the properties of snow or ice layer.

The reflection coefficient is determined as well as by passive methods using the measurements of radiothermal emission intensity. The intensity of background radiation at microwave range according to the Kirghof law is characterized by the brightness temperature

$$T_j = \kappa T_e \quad (2.2)$$

where κ is the emission coefficient (or absorbing surface ability, or the blackness level), T_e is the effective surface temperature.

Expression (2.2) characterizes the thermal emission of the surface but does not take into account the emission falling on the surface or reflected by it. The coefficient κ is described by Frenel reflective formula. The thermodynamic and brightness temperatures are measured in Kelvins: $T(K) = t(^{\circ}C) + 273$. The emissivity is a function of dielectric permittivity of the object/surface of observation. For a land surface, the dielectric permittivity is first of all a function of soil moisture. The higher a soil moisture content, the higher the permittivity of soil, the lower the emissivity/intensity of radiation/brightness temperature of this piece of land.

For a water surface, the dielectric permittivity is first of all a function of electric conductivity of a water solution that is dependent on a concentration of salts, acids, on a presence of oil films and many other chemical substances. For example, the higher salinity of water, the higher the dielectric permittivity of water solution, the lower the emissivity/intensity of radiation/brightness temperature of this water body. Within the 2–30 cm band, for $t = 10\text{--}30^{\circ}C$, the radiation characteristics of several surface types are shown in Table 2.13. Table 2.14 shows the sensitivity of radiation in the X-band (2–3 cm) and L-band (18–30 cm) to the changes in free water content in bare soil, soil density, salinity and temperature of the soil surface. These data show that the main parameter affecting the intensity of a bare soil radiation, practically independent of spectral band, is the soil moisture. Based on this sensitivity it is feasible to estimate the value of soil moisture without a priori data on the soil parameters.

The power registered by completely concerted receiver equals $W = \kappa T_j \Delta f$ where Δf is the received emission branch. In the case when the model of soil with the flat

Table 2.13 Basic microwave radiation characteristics of some typical surface types

Surface	$T_j(K)$	κ
Metal	0	0
Water surface	90–110	0.3–0.4
Very wet soil	160–180	0.55–0.65
Very dry soil	250–270	0.85–0.93

Table 2.14 Sensitivity of a bare soil microwave radiation to variations in soil moisture (W), soil density (D), salinity (S), and surface temperature (T)

Wavelength (cm)	Spectral band	$\Delta T/\Delta W$ (K/g/cm ³)	$\Delta T/\Delta D$ (K/g/cm ³)	$\Delta T/\Delta S$ (K/ppm)	$\Delta T/\Delta T$ (K/ $^{\circ}C$)
2–3	X	–200	–15	0.05	0.5
18–30	L	–(200 to 300)	–10	–0.5	0.1

surface is considered the emission and reflection coefficients are correlated by the formula $\kappa = |\kappa_0|^2$. Consequently the knowledge of emission coefficient allows to estimate the reflection coefficient and electrophysical properties of ground. Under this it is necessary to know the soil temperature T or to calibrate the radiometer using the land covers with emission coefficients which are known. Theoretical bases of remote methods, as a rule, have approximate character. This has to do with the need for simplified prepositions. For example, among the simplifications often used are uniformity of environmental parameters distribution by the depths or height, absolute transparency of the area, the land covers smoothness. The models synthesized under these simplifications reflect restricted spectrum of the studied phenomenon properties. That is why the estimation of model adequation is necessary.

The problem of wavelengths choice and the combination of its ranges with the classes of solved tasks is now within sight of many investigators. Theoretical foundation of this choice lies in the area of the thermal radiation transmission theory. Specifically, for the monochromatic case the transmission equation has

$$dI(z)/dz = J(z) - \alpha I(z), \quad (2.3)$$

where α is the absorption coefficient, $J(z)$ is the emission source distributed by z , $I(z)$ is the emission intensity in the point z . Under this for the unscattering atmosphere the following equation is valid: $J(z) = \varepsilon_1(z)B(z)$, where ε is the atmosphere emissivity,

$$B(z) = 2hf^3c^{-2} \left[\exp\{hf(kT)^{-1}\} \right]^{-1};$$

h , c and k are fundamental constants, $f = \nu c$ is the frequency. For the microwave branch where the observed frequency is in the region of a few hundred gigahertz or less it takes place a condition $hf \ll kT$ and the Rayleigh-Jeans approximation is valid: $B(z) = 2kT\lambda^{-2}$. Here $k = 1.38 \times 10^{-20}$ mW Hz⁻¹K⁻¹ is the Boltzmann's constant, λ is the wavelength.

The Eq. (2.3) has solution

$$T_j = \kappa T_e \tau(0, \infty) + \int_0^\infty T(u)Q(u)du, \quad (2.4)$$

where

$$\tau(a, b) = \exp \left[- \int_a^b \alpha(z)dz \right].$$

Table 2.15 The value of brightness temperatures which are typical for the some land covers

Land cover	Wavelength, λ (cm)			
	0.8		1.35	
	$T_{j,min}$	$T_{j,max}$	$T_{j,min}$	$T_{j,max}$
Desert	251	261	245	270
Cultivated steppe	255	268	257	277
Steppe covered by snow	246	261	241	260
The ice covered by snow	247	263	231	253
The ice	239	247	235	254
Sea surface	136	171	110	168

The weight function $Q(u) = \partial \tau(u, \infty) / \partial u$ describes an influence of various atmospheric layers to the receiving signal. The formula (2.4) makes the expression (2.2) into a whole. The examples of specific values T_j are given in Table 2.15.

Microwave measurement calibration is important in remote monitoring. Calibration procedure can be defined as the process of relating signals that can be extracted from a measurement radiometric system to the physical characteristics of a target such as its brightness temperature. The main goal of a calibration process is in getting all measurements to account with a unique scale. In the passive regime for this aim the objects having known brightness temperature are used (see Table 2.16). Usually it is selected the forest or the freshwater reservoir. In this case the radiobrightness temperature of forest is equaled to the thermodynamical temperature of the trees canopy, and the radiobrightness temperature of reservoir is calculated with the known algorithms (Yakimov 1996; Ferm and Hultberg 1999; Burkov and Krapivin 2009; Krapivin and Shutko 2012).

2.3.1 Remote-Sensing Technologies in the Infrared and Optical Bands

There exist no less than 10 technologies for remote sensing of the environment. Between them are those not widely known and not widely applicable for our case, namely: ultra-sound methods, radar sensing beyond the horizon, solar radiation sensing and a few others.

Table 2.16 Emission coefficient for the some natural and anthropogenic microwave standards (Shutko 1987)

Land cover	Microwave range	
	Centimetres	Decimetres
Dry sand	0.93 ± 0.03	0.93 ± 0.03
Concrete	0.84 ± 0.02	0.82 ± 0.02
Asphalt	0.85 ± 0.03	0.83 ± 0.02
Dense forest	0.95–0.98	0.92–0.96
Fresh water	0.38 ± 0.01	0.36 ± 0.01
Watering soils	0.58 ± 0.03	0.56 ± 0.03

For our case—that is, using the GIMS as the key instrument to solve environmental problems, for decision-making procedures in the GIMS, for geoscience and remote sensing, and for oceanic engineering—and for the very typical example of diagnosing and preventing at an earlier stage the buildup of extensive moisture in the soil, water barrier failure, and flood development the most acceptable, useful and effective, instruments, and technologies that have been proven in a number of domestic and international campaigns are the following:

- (1) Optical (digital photo and/or video cameras, spectrometers).
- (2) Lidar (Laser 3-D scanner).
- (3) Thermal IR-radiometers.
- (4) Microwave radiometers.
- (5) Radar (Synthetic Aperture Radar—SAR).
- (6) Short pulse nadir viewing subsurface dielectric irregularities finder.
- (7) Georadar (subsurface dielectric irregularities finder of on-ground location, also nadir viewing).

Table 2.17 presents the effectiveness estimates of first 5 of total 7 rather widely used instruments with regard to their application for remote sensing of water and land areas. Crosses in the Table 2.7 indicate the degree of capability (and thus of usefulness) of different sensors to registration of different parameter variations or changes in different situations in typical/characteristic environments. Three crosses indicate the highest possible rank of effectiveness, one cross—minimum one.

Why are five of the seven, rather than seven of the seven, presented types of sensors discussed? The answers are as follows:

- (a) sensors 6 and 7 are still not used so widely as the first 5 sensors,
- (b) these two sensors were not used in the development of the GIMS, and
- (c) special conditions are needed to organize a flight campaign and to include in it these sensors and Radar, including Synthetic Aperture Radar, which are effective and useful, but heavy, of a big size and expensive tools for aircraft and spacecraft remote sensing.

These technologies are under the development primarily in JPL and Vega Radio Corporation in Russia and available for potential users.

Table 2.17 gives rough but effective assessments of how basic remote sensors, operating at both passive and active microwaves in the infrared and optical bands, behave under the basic parameters and conditions inherent in the following scenarios:

- Oceanic, sea or fresh/water surface.
- Plane and rough water surface.
- Foam-covered and oil spill-covered water surface.
- Water-vegetative canopy system.
- Bare land surface.
- Vegetation-covered soil.
- Atmosphere-tree crown system (when sensing upward through the canopy).

Table 2.17 Typical remote sensing technologies, their information content and effectiveness

Sensors and parameters they determine	O	L	T	M	R
Sea/water surface temperature			++ or +++	++ or +++	
Sea/water surface natural salinity				++ or +++	
Oil pollution on water surface	+		+	++	+++
Water pollution with dissoluble chemicals	+			++	+
Water pollution with waste outflow	+			++	+
Soil moisture	+		+ or ++	+++	+ or ++
Sub-surface moisture (depth to water table)				+++	+ or ++
Zones of water seepage through water barriers	+	+	+	+++	+
Flooding	+ or ++	+ or ++	+	+++	+++
General: water regime of terrain	+ or ++	+	+	+++	++
Terrain relief	+	++ or +++	+	+ or ++	++ or +++
Water areas and/or wet lands overgrowing with vegetation	+	+	+	++	+++
Vegetation classification	++	+		+	+ or ++
Vegetation biomass, dynamics, seasonal changes	+	+		+	++
Monitoring crowns of separately standing trees				++ or +++	
Monitoring vegetation sick rate	+ or ++		+		+
Deforestation	+ or ++		+		+
Monitoring timber/forest clearance	+ or ++		+		+
Risk of forest or peat fire	+ or ++		+ or ++	++ or +++	+
Revealing epicenter and/or border of fire in foggy and smoky condition	+ or ++		++ or +++	++ or +++	
Monitoring terrain traffic ability	+ or ++	+ or ++	++ or +++	++ or +++	++ or +++

O Optical (digital photo and/or video cameras, spectrometers), *L* Lidar (Laser 3-D scanner), *T* Thermal IR-radiometers, *M* Microwave radiometers, and *R* Radar (SAR) (Krapivin and Shutko 2012)

As we mentioned above, the crosses in Table 2.17 characterize the information content (usefulness) of different sensors, beginning from a single cross (the lowest rate of usefulness) and moving to three crosses (highest usefulness). Thus this table allows one to obtain preliminary assessments of the effectiveness of the expected results of some experimental campaign under the development.

Of course, Table 2.17 reflects the expert-level opinion regarding the usefulness of different sensors. This opinion was created by them based on multi year studies

of the spectral properties of different environments. This personal experience was used to develop, test, and put into practice truly multi-spectral remote-sensing technologies providing state-of-the art information by means of an optimum set of sensors, such as those installed on board of the Dutch/U.S./Russia Miramap aircraft equipped with the above mentioned multi-spectral passive/radiometric microwave, thermal infrared, color digital orthophoto cameras, and lidar (laser 3-D scanner working in the near-infrared band).

2.4 Monitoring of the Soil-Plant Formations

Land cover change is an important environmental process. Studying and monitoring this change are significant when assessing the variations and dynamics of the global biogeochemical cycles of greenhouse gases. One of effective satellite instruments that gives a possibility to detect the disturbances of the globe's land surface is the Moderate Resolution Imaging Spectroradiometer (MODIS) of NASA's Earth Observing System (EOS).

MODIS is a key instrument aboard the Terra (EOS AM) and Aqua (EOS PM) satellites. Terra's orbit around the Earth is timed so that it passes from north to south across the equator in the morning, while Aqua passes south to north over the equator in the afternoon. Terra MODIS and Aqua MODIS are viewing the entire Earth's surface every 1–2 days, acquiring data in 36 spectral bands, or groups of wavelengths. These data will improve our understanding of global dynamics and processes occurring on the land, in the oceans, and in the lower atmosphere. MODIS is playing a vital role in the development of validated, global, interactive Earth system models able to predict global change accurately enough to assist policy makers in making sound decisions concerning the protection of our environment.

Understanding Earth system processes and their interdependencies through observation, theory, and modeling, is the objective of many international programs such as the International Geosphere-Biosphere Programme (IGBP), the International Human Dimensions Programme (IHDP), the World Climate Research Programme (WCRP), and the Global Carbon Project (GCP). However, this is only possible if reliable and operative information about the land covers is available. Undoubtedly, the use of this information demands the creation of algorithms and models to improve the quality of environmental monitoring.

A remote monitoring of the soil-plant formations is aimed at assessing biological productivity, understanding interactions inside the *soil-vegetation-atmosphere* system, evaluating biome dynamics, modeling biogeochemical cycles paying particular attention to the role played by vegetation, and controlling vegetation resources.

Land covers are characterized by high landscape diversity having various soil and plant types, water-salt and temperature regimes, the cultivating of surface layer, and macrorelief. The soil includes solid particles, water (soil mixture) and air. Solid

particles consist of mineral and organic matter. Basic mass of majority soils forms mineral substances (mineral soils): particles of size more 3 mm form the stony soil part, particles from 0.01 to 1 mm are called as “physical sand”, and particles less 0.01 mm are “physical” clay. The minerals that make up the soil consist basically of two oxides: SiO_2 and Al_2O_3 . The content of organic substances (mainly humus) fluctuates in such soils between 1 and 10 % by the weight. All these circumstances, when the monitoring system of land covers is designed, lead to the necessity of microwave channels choice to be informative. The many lengthy investigations in this field facilitate choosing the most effective wave range for monitoring many types of vegetation and soils. Studies of agricultural systems, forest, and arid zones are inevitable very detailed. Such areas as the control of hydrological soil regime under the forest canopy and the study of reforestation dynamics in the regions of clearing and forest fires are perspective scientific fields to be studied at the nearest time in the microwave monitoring. This can be done by using the decimeter range in which the forest canopy is transparent in the microwave range and, consequently, soil up to the ground waters level can be sensed. Experimental characteristics of the natural microwave L-band emission of a forest are described by Chukhlantsev and Shutko (1988), Phillips et al. (2004), and Chukhlantsev (2006).

A possibility of wood-bushes vegetation inventory by means of radiolocation sensing is based on the correlation between the coefficients of SHF waves back scattering and the structure and dielectric properties of vegetation. Using radiolocation systems to control forests is stipulated by the possibilities of additional data being received together with remote measurements in the visible and IR ranges (Savin and Bondur 2000).

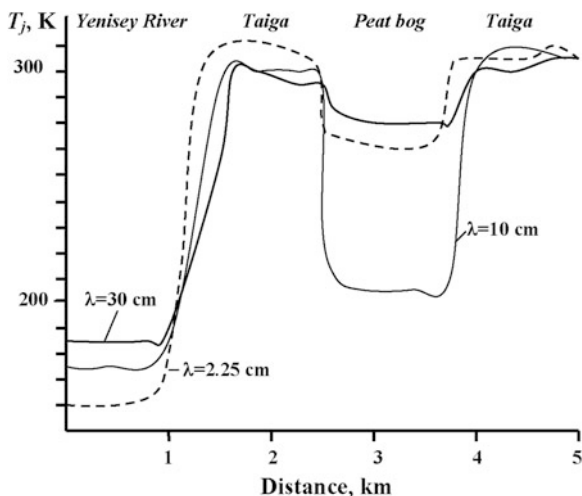
Global mapping of vegetation in the scale determined by economic needs of given region is main task of the satellite based radiolocators under the forest observations. Specifically, the forest protection from the fires is one of directions in the development of remote monitoring to assess the vegetation state. Present satellite- and aviation- based monitoring systems solve many significant problems:

- Operative assessment of the forest's fire risk;
- The forest watering mapping under the putting out fire in the forest;
- The mapping of the forest fires contours through the smoke layer and trees canopy;
- The determination of the energetic fire parameters;
- The forest state determination after fire;

Investigations of radiothermal emission from natural layers of a forest that are combustible such as the lichen, mosses, grass rags, died pine needles, and scrub have brought about methodologies to identify forest fire parameters based on the measurements of radiothermal emission in microwave range of electromagnetic spectrum. The examples of radiobrightness temperature in the forest burning zone are given in Figs. 2.11 and 2.12. The leading and rear edges of fire and the burnt forest in between can clearly be distinguished.

Comparing radiobrightness temperatures registered in different wavelengths shows that forest fires emissivity increases with the wavelength decrease and

Fig. 2.11 An example of the registerograms received by means of flying laboratory IL-18 near Eniseysk city using radiometers of 2.25 cm (1), 10 cm (2), and 30 cm (3) wavelengths



depends on the fire type. Given in Fig. 2.12 averaged results for the dependencies of radiobrightness temperatures spectrum from various components of forest fire under different wavelengths allow to classify these components with high precision.

The GIMS synthesis with the functions of forest fire control on the large areas demands the creation of applied models describing the forest fire-ripening processes. The foundation of such models is, certainly, the knowledge how the intensity of radiothermal emission of forest landscape element depends on its water-content. Many observations show that statistical characteristics of the forest

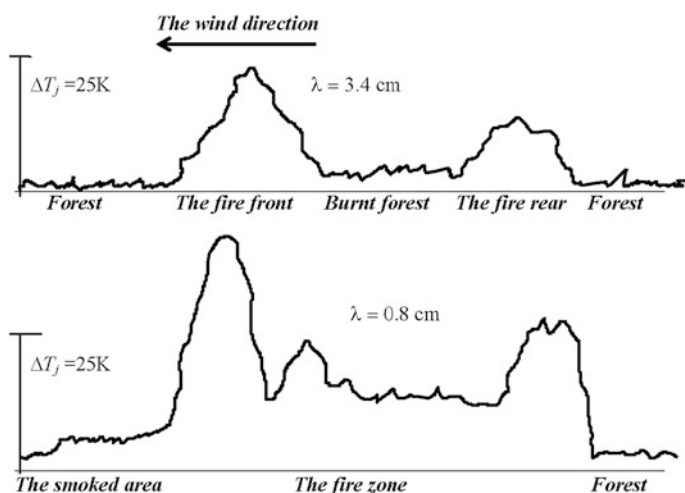


Fig. 2.12 Fragment of the registerograms in the wildfire zone near Krasnoyarsk received by means of flying laboratory IL-18

microwave emissions are changed with the fire-ripening growth for the layers of combustible timbers. Specifically, such a dependence can be represented in the following form (Yakimov 1996):

$$T_j = \kappa(\lambda, w)T_S(1 - \exp\{-\alpha(\lambda, w)h\}) + T_{jS}\exp\{-\alpha(\lambda, w)h\},$$

where κ and α are emission and absorption coefficient, respectively; w is the water content in the timber, h is the thickness of emitting layer, T_S is the soil temperature, T_{jS} is the soil brightness temperature. The following deciding factor, based on the calculating the first-order (M) and second-order (σ) moment for the set of T_j corresponding to the forest territory and registered on the wavelength $\lambda = 2.25$ cm were proposed by Yakimov (1996). The value M (mean) is compared with the threshold equaled to $d = 7.251\sigma + 249.876$. If $M \geq d$ then forest plot has average or higher fire-dangerous. If $M < d$ then fire-dangerous of given forest plot is low. This deciding rule is to be extended by the forest fire model. An example of such a model is one describing forest fire as a running wave or as self-supporting process of local energy release into the active environment.

The millimeter range (1–30 mm and 30–300 GHz bands) is best for land cover diagnosis. As numerous experimental investigations show, adding millimeter range channels to the monitoring system enhances the accuracy of soil-plant formations classification by separating out roughnesses and small formations. It is especially important for anthropogenic landscape monitoring.

McCloy and Lucht (2004) developed a method for comparing the complex spatio-temporal patterns present in two long-time series of data of the seasonal cycles of vegetation for a large part of the global land surface. It is based on the use of two datasets derived from global satellite observations (AVHRR) and Lund-Potsdam-Jena dynamic global vegetation model (LPJ-DGVM). McCloy and Lucht (2004) showed that the LPJ model generally corresponds well with natural vegetation whereas the former is primarily dependent on climate. Due to a lack of representation of agriculture in the model, the correspondence with actual vegetative status was poor.

2.5 Microwave Monitoring of the Soil Moisture

2.5.1 Introduction

A series of world wide large scale Soil Moisture Experiments (SMEX) have been conducted from 1997 to 2005 by the National Aeronautics and Space Administration (NASA) and the United States Department of Agriculture (USDA), Hydrology and Remote Sensing Laboratory, with the involvement of institutions in the USA, Japan and Brazil (Jackson et al. 2002). The primary objective of those

experiments was to evaluate the capabilities of satellite microwave sensors for soil moisture mapping on a planetary scale. The experiments to date have all utilized a combination of aircraft microwave measurements and in situ measurements to achieve the goal.

Soil moisture was recognized by the NASA Post 2002 Program as a critical measurement. Operational determination of soil moisture spatial-temporal variability plays a leading role in regional and global studies of the water, biogeochemical and energy cycles. The efforts are targeted on the improvement of spacecraft microwave radiometric assessments of soil moisture to the level of data acceptability when reliable predictions of regional to global hydrologic regimes can be provided. Soil moisture is a key state variable in hydrology: it is the switch that controls the proportion of rainfall that percolates, runs off, or evaporated from the land. It is the life-giving substance for vegetation. Soil moisture integrates precipitation and evaporation over periods of days to weeks and introduces a significant element of memory in the atmosphere-land system. There is strong climatological and modeling evidence that the fast recycling of water through evapotranspiration and precipitation is the primary factor in the persistence of dry or wet anomalies over large continental regions during summer. As a result, soil moisture is possibly one of the most significant land surface boundary conditions controlling the exchange of water and energy with the atmosphere.

Remote sensing of the environment by means of passive microwaves or microwave radiometry is based on retrieval algorithms that relate the environmental parameters (such as soil moisture, vegetation type and biomass, forest stem volume, water equivalent, physical temperature, and others) to the remotely sensed radiation characteristics (spectral brightness temperature, polarization). Microwave emission from a natural object is governed by the interaction of electromagnetic waves with a natural medium that is determined by its geometrical structure and dielectric and electric properties of the medium constituents. In turn, these properties are connected with geophysical and biophysical parameters of the medium that enables the retrieval of these parameters from remotely measured characteristics of electromagnetic waves emitted or scattered by the object. Therefore, dielectric and electric properties of natural media constituents and their relationships to geophysical and biophysical parameters play a crucial role in microwave remote sensing of the environment. Besides, the dielectric permittivity of a medium or its real part and its imaginary part determines the penetration depth of electromagnetic waves in the medium that is very important for subsurface remote sensing of soil moisture and for soil moisture sensing under vegetative canopies.

The impact of microwave radiometer pixel size on the reliability of soil moisture assessments for different landscapes and minimization of the number of in situ locations for sampling soil moisture, temperature and vegetation parameters are key elements of the study. As a result, a combined approach for soil moisture mapping from a regional to global scale using microwave radiometric observations, laboratory tests, in situ measurements and mathematical modeling of the soil-vegetation system inherent in different landscapes is to be developed as a highly calibration

and validation input to the series of the NASA and USDA Soil Moisture Experiments (SMEX) in the interests of hydrological science, technology and applications. In this aspect, the following problems are arising in the microwave monitoring of soil moisture:

- development of models parameterizing biometrical, soil properties and radiometric data for typical sites;
- comparative evaluation of seasonal patterns in series of satellite, ground-truth (and/or aerial) and laboratory data and simulations of soil-vegetation model;
- conduct intercomparisons of radiation data and mean values of soil moisture data at different depths with regard for the type of vegetation cover and amount of biomass;
- choice of constructive scheme for the data calibration basing on the available radiative transfer model and results of measurements;
- spectral radiometric data processing related to soil moisture and vegetation cover parameters and results of modeling;
- development of mathematical model for soil-vegetation system dynamics using satellite, field and laboratory data;
- combining approach to parameterization of data needed for description of water balance in soil-vegetation system and of data delivered from microwave satellite (AMSR-E/Aqua, etc.) spacecraft observations, ground based microwave observations, laboratory tests, in situ measurements (sampling) and mathematical modeling; and
- using data of attenuation in vegetation and dielectric properties of soil and vegetation samples as calibration and validation input to the GIMS.

2.5.2 Microwave Technology

The fundamental principles of soil moisture retrieval by means of the use of passive microwave sensors and microwave radiometric technique for measuring soil moisture properties have been established by Shutko (1986) and his disciples. During a series of experiments, microwave radiometers were put on satellites, aircraft, and ground-based vehicles. L-band passive microwave measurements were the most informative in these experiments. Numerous investigations of sensitivity of microwave measurements to vegetation biomass and soil moisture have shown that remote sensing data give a possibility to solve important tasks from hydrology and agriculture and to realize operational diagnostics of damage of stressful natural processes. For instance, Ferrazzoli et al. (1992) carried out a comparative evaluation of the potential of active and passive radiometers in estimating vegetation biomass and soil moisture content. It was shown that low frequency data (L band) at a steep incidence angle (10°) confirm that both the backscattering coefficient and the normalized temperature are correlated and sensitive to soil moisture content.

Interrelations between the characteristics of the microwave emission field of moistened soil and of the soil liquid water content, soil density, temperature and mineralization level of liquid water are the properties studied both theoretically and by field measurements. Both research and field studies show that microwave radiometric measurements permit estimates of 7–10 moisture levels in the top 0.1–1.0 wavelengths of soil and 3–7 grades of the subsurface water level between 0 and 1.5–3.5 m.

The soil moisture is divided into solidly united, loosely united, and free. United moisture is the water adsorbed by ground particles at the surface and takes the form of a film of thickness equal to no more than six to eight molecular layers. The volume of united moisture in the soil layer is determined by the soil type and is fluctuated in the wide interval from 2–3 % for sandy soil to 30–40 % for clay and loess soils. United water is unattainable by plants and does not influence the salt regime of soil. That is why the monitoring system is to realize that kind of moisture classification in the soil.

The soil moisture is expressed in percent of dry soil weight. Radiation models of different types of soil moisture that consider soil density, temperature, and salinity have been studied in great detail. The data required to ascertain moisture levels can be obtained by means of brightness temperature contrasts, degree of polarization, and spectral characteristics at centimeter and decimeter wavelengths. Wavelengths 2.25, 18 and 30 cm proved to be the most informative to solve this task. The microwave radiation model describing the land cover emissivity under the conditions of heterogeneously moistened layer is based on the existence of vertical heterogeneity in the dielectric permeability coefficient (see Formula (2.1)): $\varepsilon \cong (1 + 0.5\rho_s)^2$. The value of ε is informative indicator of the moisture soil variation. As soil moisture begin to grows the ε increases at first slowly, if soil was dry, then it increases more rapidly. The weak dependence of ε on the initial moisture stage, explained by moisture tied up in the soil, can be characterized as having small dielectric permeability. The variety of experimental dependencies of ε from the soil types and moisturizing levels was given by many authors (Shutko 1986; Engman and Chauhan 1995; Borodin and Krapivin 1998; Schmugge 1990; Tsegaye et al. 2005). Such a knowledge base combined with application of GIMS technology allows ascertaining water content, $W_s(z)$, diagnostics in the soil layer. Basic types of moisture profiles $W_s(z)$ of real soils and corresponding profiles, $\varepsilon(z)$, of dielectric constant were described by Reutov and Shutko (1986). Four major types of vertical moisture profiles have been identified from an analysis of the moistening characteristics of the various climatic zones in the Former Soviet Union. In other climatic zones it is necessary to have such identification. As a matter of fact the task is reduced to the function $W_s(z)$ reconstruction when the values $W_{si} = W_s(z_i)$ are known and the following conditions are satisfied:

$$\partial W_s / \partial z|_{z=0} \leq C, \quad 0 \leq W_s(z) \leq K_s(z), \quad (2.5)$$

where $K_s(z)$ is the given function.

Practice has shown that, irrespective of the climatic zone, microwave radiometers need to be used to achieve acceptable precision when reconstructing the vertical profile of moisture in a soil layer to a depth of one meter. There is *a priori* information about average soil moisture for depths 50 cm (W_{s2}) and 100 cm (W_{s3}). The value W_{s1} is estimated by means of microwave radiometers with wavelengths $\lambda = 10$ and 30 cm. Then the following approximation $W_s^*(z) = az^3 + bz^2 + cz + d$ is considered, where unknown coefficients are calculated from the condition of minimal deviation between the $W_s^*(z_i)$ and W_{si} ($i = 1, 2, 3$). For this to be done conditions (2.5) have to be realized. This methodology allows soil moisture to be determined by remote monitoring over large areas with an error no greater than 0.3 g cm^{-3} for a biomass of vegetable cover no smaller than 2 kg m^{-2} and with an error up to 0.07 g cm^{-3} for a biomass greater than 2 kg m^{-2} .

The knowledge of function $W_s(z)$ allows to use the model of water balance of territory to reconstruct the dynamical soil properties and other water balance elements as the functions of geophysical and ecological parameters. Experimental valuation of thickness of upper soil layer on the lower boundary of which every 6 days after rain or watering the capillary connections breaking is taken place (Fig. 2.13). Typical thickness of this dried up layer oscillates between 3 and 5 cm.

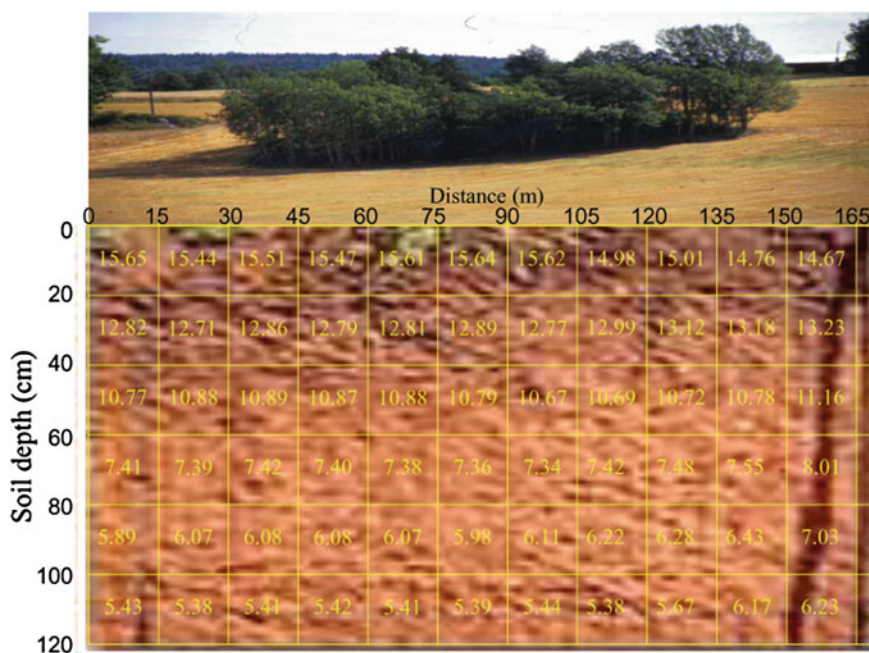


Fig. 2.13 Fragment of the vertical profile of soil moisture (%) calculated on basis of monitoring data in framework of International hydrophysical experiment on the Bulgarian territory in the 2007 summer (Krapivin and Shutko 2012; Verba et al. 2013)

Table 2.18 The reflection coefficients for the microwaves under different soil moistening

Moisture content in the soil (g cm^{-3})	Thickness of the soil layer (cm)				
	0.5	1.0	2.0	3.0	5.0
$\lambda = 18 \text{ cm}$					
0.001	0.98	0.94	0.95	0.96	0.97
0.02	0.91	0.92	0.93	0.95	0.97
0.05	0.88	0.89	0.92	0.95	0.96
0.1	0.82	0.84	0.89	0.95	0.96
0.2	0.73	0.76	0.85	0.94	0.95
0.3	0.65	0.69	0.83	0.94	0.93
0.4	0.59	0.64	0.82	0.94	0.93
0.5	0.53	0.59	0.82	0.92	0.92
$\lambda = 30 \text{ cm}$					
0.001	0.93	0.93	0.94	0.95	0.96
0.02	0.91	0.91	0.92	0.93	0.96
0.05	0.88	0.88	0.89	0.92	0.96
0.1	0.82	0.83	0.85	0.89	0.96
0.2	0.72	0.73	0.78	0.85	0.96
0.3	0.64	0.66	0.73	0.83	0.95
0.4	0.57	0.59	0.69	0.82	0.94
0.5	0.52	0.55	0.66	0.81	0.92

The reflection coefficient estimations for the microwave range reflected from this layer are given in Table 2.18.

Optimal choice of the electromagnetic radiation range and model synthesis based on methodologies to measure the moisture content in the soil demands further investigation of the conditions that influence emission fields in the *atmosphere-soil-vegetation* system (Grankov and Mil'shin 1994; Engman and Chauhan 1995). These investigations are to be correlated with application of remote sensing to agricultural crop forecasting and in selected water resources management.

Figure 2.14 presents the sample of microwave radiometers application and the use of spatial interpolation methods to solve the task of agriculture fields monitoring providing the soil moisture mapping. This can be done radiometers with 18 and 27 cm wavelengths located on a flying laboratory. The experiments of such type are realized in the climatic conditions of Moldavia, Ukraine, Bulgaria, Cuba, Vietnam, Russia, and USA (Shutko et al. 2010; Krapivin and Shutko 2012). These experiments showed GIMS technology allows specific geophysical conditions to have practically valid results from monitoring. To reconstruct the spatial distribution of soil moisture with precision of 20 %, the flying laboratory in most cases needs to fly parallel routes at height $H \approx 200 \text{ m}$ with a distance between them of no more than 500 m. The interval between measurements, when the precision of forecast for synoptical parameters is 10 % and for precipitation is 15 %, can be monthly if the precision of soil moisture estimation is planned to be less than 50 %.

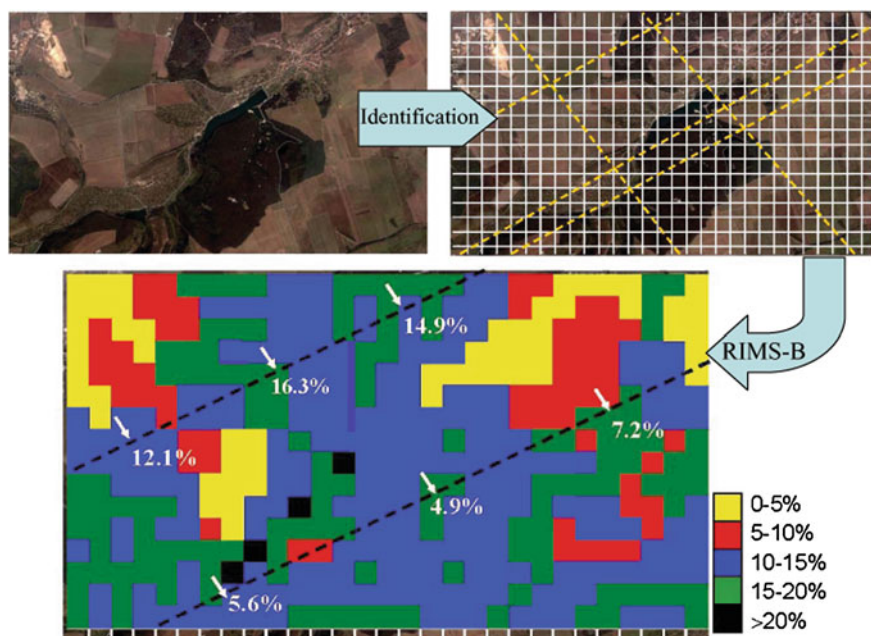


Fig. 2.14 Stages of the monitoring procedure realization to assess the soil moisture distribution in the Nikolovo village environs using the land, remote and computer calculations during the International Experiment GIMS-Bulgaria-2007 (Shutko et al. 2010; Shutko and Krapivin 2011). Spatial resolution is 250 m. *Arrows* show the places where the soil moisture was measured in situ. *Dashed lines* correspond to the traces of flight-laboratory (Soldatov 2011)

Guha et al. (2003) considered a series of experiments using the Electronically Scanned Thin Array Radiometer (ESTAR). The Southern Great Plains Experiment (SGPE-99), within the framework of which ESTAR-derived soil moisture fields were studied, took place in a region of the United States that is characterized by a relatively homogeneous geography, variable surface flux properties, and large seasonal variation in temperature and specific humidity. In addition to ESTAR, 4 different microwave radiometers operating in the L-(1-2 GHz), S-(2-4 GHz), and C-(4-8 GHz) bands were flown on aircraft. The instruments included the Polarimetric Scanning Radiometer (PSR/C) the Step Frequency Microwave Radiometer (Step-C), and the Airborne C-band Microwave Radiometer (ACMR) operating in the C-band and the Passive and Active L- and S- Band System (PALS) in the L- and S- bands. Passive microwave data were also collected by the Tropical Rainfall Measuring Mission (TRMM) satellite and the Special Sensor Microwave Imager (SSM/I) sensor.

Within these measurements, the problem of distinguishing between the water contents in soil and vegetation cover was solved. An empirically derived piecewise function was used to solve this problem. The vegetation water content (VWC) was calculated with the following correlation:

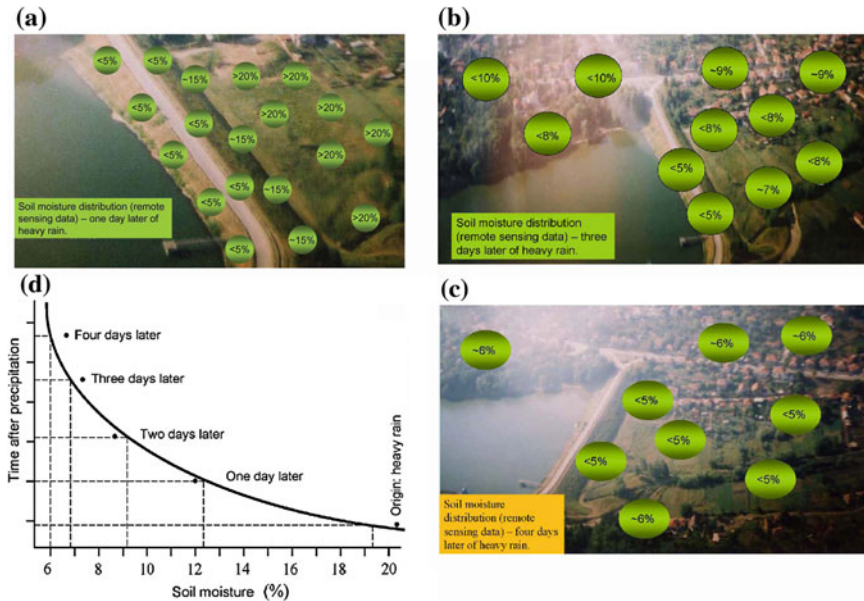


Fig. 2.15 Results of soil moisture retrieval in its dynamics in the Rusenski Lom region (Bulgaria) as results of combined use of remote sensing measurements and the RIMS-B application

$$VWC = \begin{cases} 1.9134(NDVI)^2 - 0.3215(NDVI) & \text{when } NDVI \leq 0.5; \\ 4.2857(NDVI)^2 - 1.5429 & \text{when } NDVI > 0.5; \end{cases}$$

where VWC is measured in kg m^{-2} .

Figure 2.15 demonstrates some results received by means of the GIMS using for remote sensing data processing. Detailed and geo-referenced maps identifying the locations of saturated and dry levees can be produced using microwave radiometric measurements from a light aircraft or helicopter, and integrated with GPS for positioning and orientation. The development of synergetic remote sensing technology for raised groundwater and seepage detection by the joint use of microwave and optical data along with GIS databases is an effective and most contemporary way of supporting risk assessment and facilitating disaster prevention and management.

2.5.3 Geoinformation System to Monitor Agriculture

The GIMS technology was set up to solve the wide range of problems arising in agriculture (Reutov and Shutko 1986; Shutko 1986; Chukhlantsev 1986; Chukhlantsev and Shutko 1988; Shutko et al. 2006a, b, 2010; Krapivin and Shutko 2012). The properties of the interaction of electromagnetic energy with the soil-plant formations

have been of considerable interest to scientists and engineers who designed the Geo-Information Monitoring System of Agricultural Function (GIMSAF).

Microwave radiometric technique for measuring soil moisture characteristics have been developed and widely used in many regions by Shutko et al. (2010). This experience was used in the GIMSAF to find a procedure to determine the water content and moisture profiles in soil layers a meter thick and without vegetation cover by means of remote sensing. The procedure is based on the dependence of microwave emissivity of soil on its moisture. The procedure takes into account the variations of temperature, density and roughness of natural soils.

The GIMSAF performs:

- collection of information pertaining to the current parameters of the *soil-vegetation* system (moisture, shallow water table, soil salinity, biomass of the vegetation) over regions of various area;
- processing of the information above within the framework of a model simulating the biogeocenotic, physical and chemical processes in the *soil-vegetation* system with the aim of evaluating its current state and predicting its development and potential productivity;
- represents current and predicted information as a schematic maps with spatio-temporal detailing within a controlled structure;
- making technological decisions that are optimum from the point of view of providing the maximal biological productivity of agriculture vegetation;

The GIMSAF structure includes units of:

- collection of information;
- initial information processing and accumulation of data for simulating the agricultural vegetation productivity and water conditions;
- predicting the geosystem state;
- evaluation of the disparity between the measured and predicted trends in the geosystem processes;
- making decision pertaining to the measurement scheduling and geosystem controlling;
- service support in operation with input and output data.

The data collection unit is based on remotely sensed data and prior knowledge of the state of an object and meteorological parameters. Remote pickups switch on a microwave radiometric complex provided with computer programs that permit to obtain operational area information at the desired degree of detailing concerning the soil moisture content to a depth of 0–100 cm, the subsoil water level to a depth of 0–3 m, the salt concentration of the soil in a range of 3–90 g L⁻¹, the vegetation biomass, the degree of mineralization and contamination in reservoirs. Moisture measurement operating range is 0.0–0.6 g cm⁻³ with maximal absolute error equaled to the vegetation biomass less and more 200 t ha⁻¹ to 0.05 and 0.05–0.08 g cm⁻³, respectively.

The operation of the information processing units is based on a computer program package providing spatio-temporal interpolation of remote trace measurements and

point surface measurements in addition to information flow stabilization in the event of the information collection system failing. The program package also realizes the description of the dynamics of the moisture and biological, physical, chemical and energetic processes in the interaction between the soil, vegetation, atmosphere and energy sources including factors of anthropogenic effects.

The adaptation of the information processing units to the actual conditions in the region studied is accomplished by introducing sets of coefficients and characteristic dependencies.

The trend-correcting and decision making units are based on evaluating the state of the object under consideration, predicting its development, and ascertaining the sensitivity of the system to potential production and technological measures put forward by experts.

Let us now list some of the features of the GIMSAF and some of its differences from similarly designated systems:

- use of remote radiophysical sensors pickups providing area, operative and quantitative information on the state of objects;
- ability to function at various levels of information support (remote, surface and a priori data set or part of them or without such data);
- fully open to further development regarding technological and software support and full compatibility with any sensor, information, consulting, and expert systems;
- algorithms that have the ability to adapt make the system self-regulating and, in particular, noise immune;
- compatible means of bringing about production and technological decisions.

Application results are expected to include:

- obtaining reliable operative, area and quantitative information on the parameters of the object and its general state with prediction;
- evaluation of the expediency and efficiency of anthropogenic effect on the agriculture and melioration objects;
- optimum productional and technological decisions made with the help of a simulational experiment and providing an increase in the object control efficiency.

Developing GIMSAF based on a joint use of remote measurements, in situ data, GIS information and mathematical modeling of temporal-spatial variations in soil-vegetation systems in local, regional and global scales needs the following subsystems and phases of whole system accomplishment:

- Dual-channel multi-polarized SAR measurements from spacecraft with a spatial resolution of 5–10 m for obtaining basic/strategic/global information about the condition of corn crop fields.
- Selective dual-channel multi-polarized SAR measurements from aircraft with a spatial resolution of 1.5–5 m for obtaining synchronous with spacecraft information about the condition of agriculture vegetation in a regional scale.

- Selective four-channel, dual-channel and dual-polarized microwave radiometric measurements from aircraft for determination of corn crop germination and corn crop biomass in the areas with big and medium size fields; comparison of this data with SAR estimates of vegetation biomass and yield assessments; SAR estimates calibration and validation.
- Technical calibration of SAR and microwave radiometric signals with corresponding technical means.
- The real-time or near-real-time data processing in form of maps and interpretation in terms of crop germination at early phase of growth, crop biomass before harvesting, vegetation homogeneity inside the corn fields and finally of the expected yield.
- Additional information: Disaster management, revealing flooding, drought, hurricanes, others, observing annual dynamics inside and around the crop fields.

2.6 Microwave Radiometric Observations of Temperature Anomalies

The microwave range is an informative component of the multi-channel systems that monitor temperature anomalies on the Earth surface such as forest fires, peat bog fires, areas of geothermal activity, etc. Measurements of radiation contrasts make it possible to localize on a land surface the areas with anomalously high and low brightness temperature values due to the temperature variations with respect to a mean value of effective background radiation. Numerous experimental investigations shown that radiobrightness contrasts registered by the radiometers with wavelengths 0.8 and 3.4 cm in the areas of the burnings in the forests, peat bogs, and peateries can achieve values $\Delta T_j \in [200, 300]\text{K}$. The most important result is that the microwave range is sensitive to the surface temperature variations, and hence, the detection of possible burning hotbeds can be preventive. Specifically, microwave monitoring of the peat bogs allows to fix interior zones of the temperature anomalies when external signs are absent.

Wildfires and peat burning are extreme events for many regions of Russia, Australia, USA, Canada and other countries. Wildfires occur on every continent except Antarctica. They are a force that we cannot really control, and thus understanding, appreciating, and learning to live with wildfire is ultimately our wisest public policy. These events cause principal changes to forest ecosystem dynamics and influence on regional climate. Population considers these events as disasters bringing economical losses and victims. Therefore, earlier detection of these events with timely warnings is main task of environmental monitoring systems. Solution of tasks arising here is subject of numerous publications (Alvarado et al. 1998; Johnson and Miyanishi 2001; Wuerthner 2006; Johnson 1996; Fuller 1991; Perona and Brebbia 2010; Brebbia 2012).

Johnson (1996) assembles the relevant studies of fire intensity, rate of spread, fuel consumption, fire frequency, and fire weather in the North American boreal forest. The central thesis is that the North American boreal forest has at least four wildfire characteristics that are important in understanding the dynamics of its plant populations:

- the large size of the burns with respect to dispersal distances;
- the short recurrence time of fire with respect to tree lifespans;
- the high mortality of plants due to the predominance of crown fires; and
- a good germination surface due to the large area of the forest floor that is covered by ash.

Perona and Brebbia (2010) note that as in the past, future forest fire scenarios are impacted by climatic trends and changes in climatic extremes, as well as by anthropogenic pressure. It is to be expected that future trends, especially in the Mediterranean regions, will certainly lead to an increasing impact of human pressure on the natural environment. Increases in tourism and enlargement of urban residential areas invading the countryside are basic causes of anthropogenic changes in the environment. Forecasting the effects of both factors (climatic and anthropogenic) and separating their effects on forest fires frequencies may be particularly difficult, but is essential to improve our knowledge of forest fire occurrence probability and to better organize prevention and fighting activities. At the same time, estimation of the possible increase of fire risk over coming years is important, taking into account also the diverse fire prone environments present in the Mediterranean as well as many other areas (mountain slopes, coastal zones, large islands, etc.). Book written by Perona and Brebbia (2010) contains peer-reviewed papers presented at the Second International Conference on Modeling, Monitoring and Management of Forest Fires held in Kos, Greece, in 2010. The papers covered important topics in the field of prevention and fighting of forest fires, including: Computational Methods and Experiments; Air Quality and Health Risk Models; Detection, Monitoring and Response Systems; Decision Support Systems; Resource Optimization; Risk Assessment and Vulnerability Assessment.

Brebbia (2012) includes selected papers presented at the Third International Conference on Modeling, Monitoring and Management of Forest Fires, held in May 2012. The Conference is the third in a series of biennial conferences organized by the Wessex Institute of Technology on the topic of applying computer techniques to the difficult field of forest fire prevention, management, and mitigation. In order to prevent or reduce major loss of life and property, and damage to the environment, it is important to be able to analyze the behavior of forest fires. To do so requires the development of computer codes that can take into consideration a large number of different parameters.

Main problem of wildfire control is earlier detection of fire point. The problems arising here are solved by many authors (Artemov et al. 1974; Borodin et al. 1976, 1978; Borodin and Mitnik 1977; Solimini 1995; Bonafoni et al. 2011). One of efficient methods is microwave radiometry technology which gives possibility to detect temperature anomalies in forested areas. Numerous experimental investigations have

shown that wavelengths 0.8 and 3.4 cm register radio-brightness contrasts $\Delta T_b \in [200, 300]$ °K. The most important fact is that microwave range is sensitive to the surface temperature change what allows the detection of heat sources on the peat bogs and in forests. It is indicated that microwave monitoring of peat bogs and forests can detect the fire point with warning.

In common case, passive radiation of the surface registered at the wavelengths λ_1 and λ_2 gives $\Delta T_b \approx \kappa \Delta z dT_s/dz$ where $\Delta z = z_2 - z_1$ ($z_2 > z_1$) is the difference of the depth between sub-surface layers, $dT_s/dz = -Q/k_T$, Q is the heat flux intensity, k_T is the thermal-conductivity coefficient for layer Δz . SHF-radiometer sensitivity usually equals $dT_s/dz \approx 0.1\text{--}1.0$ °/m. It allows measurement of water content in vegetation biomass what gives the possibility to assess fire dangerousness using corresponding models. Effectiveness of microwave monitoring of forested areas depends on the model structure of vegetation environment. Ground fire is the most problematic object for its detection because of presence of radiation attenuation in the vegetation cover. Multi-channel sensing promotes the solution of many tasks, arising here, by means of cluster analysis application.

Use of three-layers model of the flame-smoke-tree crown gives $\alpha_P = (1 - \exp\{-\kappa_1\})\exp(-\kappa_2)\exp(-\kappa_3)$ where α_P is the emissivity of fireplace of the lower forest fire, κ_i is the attenuation coefficient for flame radiation ($i = 1$), smoke ($i = 2$) and the whole of crown ($i = 3$). Attenuation coefficient of tree crown is function of tree types. It is determined that absorption in crown grows strongly with decrease of wavelengths. Figure 2.16 shows a dependence of radio-brightness contrasts from wavelengths.

Observations show that statistical characteristics of SHF-radiation for forested areas are changed with growth of fire readiness for layers of combustible forest materials. As an example, such dependence can be written in the form (Yakimov 1996):

$$T_b = \kappa(\lambda, w)T_s(1 - \exp\{-\alpha(\lambda, w)h\} + T_{bs}\exp\{-\alpha(\lambda, w)h\},$$

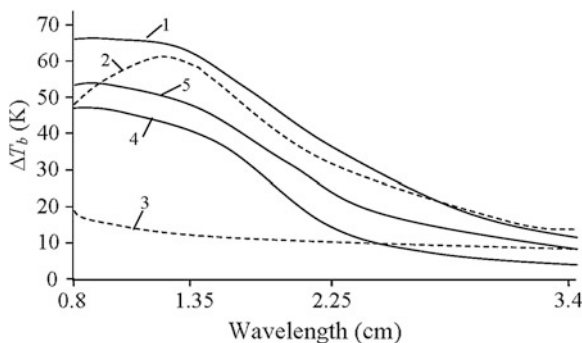


Fig. 2.16 Averaged spectr of radio-brightness contrasts for separate elements of the forest fire: 1—smoked zone, 2—fire front, 3—burned-out zone, 4—fire back, 5—boundary between fire front and burned-out zone

where κ and α are the radiation and attenuation coefficients, respectively; w is the medium moisture content; h is the radiative layer depth; T_s is the soil temperature; T_{bs} is the soil brightness temperature. Yakimov (1996) proposed the following decision rule based on the calculation of mathematical average M^* and standard deviation σ^* for series of T_b for forested area using wavelength 2.25 cm. Value M^* is compared with threshold $d = 7.2514\sigma^* + 249.876$. If $M^* \geq d$ then considered forested area has average or higher forest fire dangerous. If $M^* < d$ then fire dangerous of considered area is low.

The forest fire scale depends on the series of factors such as water content in vegetations, topography, and wind direction. Water content in the plants is the most important factor regulating the speed of forest fire evolution. Maki et al. (2004) and Rahimzadeh-Bajgiran et al. (2012) studied relations between different indexes of forest fires and determined that the most perspective indexes are:

- vegetation dryness index (VDI);
- temperature vegetation dryness index (TVDI);
- water deficit index (WDI); and
- normalized difference water index (NDWI).

To assess the water content in vegetation it is needed to use indicators FMC (fuel moisture content) and EWT (equivalent water thickness):

$$FMC/100 \% = (FW - DW)/FW, \quad EWT \text{ (g/cm}^2\text{)} = (FW - DW)/\sigma,$$

where σ is the area of leaves in crown (cm^2), FW is the wet weight of vegetations (g) and DW is the dry weight of vegetation (g).

Indicators NDWI, WDI and VDI are calculated by means of the following formulae:

$$\begin{aligned} NDWI &= (T_{b,NIR} - T_{b,SNIR}) / (T_{b,NIR} + T_{b,SNIR}), \\ WDI &= 1 - \Delta_1/\Delta_2, \quad VDI = 1 - \Delta_3/\Delta_4, \end{aligned}$$

where $T_{b,NIR}$ is the brightness temperature registered in near IR range, $T_{b,SNIR}$ is the brightness temperature registered in short-wave IR range, Δ_1 is the distance on the phase plane (NDWI, NDVI) between conditions when water deficit (D) and excess (C) take place under low-density vegetation, Δ_2 is the distance between conditions of dense (A) and low-density (B) vegetation, Δ_3 and Δ_4 are distances between measured NDVI and NDWI and between sides of parallelogram with corners in points A, B, C and D (dense vegetation and moisture excess) on plane (NDWI, NDVI) under NDVI = const, respectively. Index NDWI is calculated basing on the measurements received from satellite SPOT in channels 430–470, 610–680, 780–890 and 1,580–1,750 nm. NDVI value is usually assessed with use of measurements received by means of sensors in red and near IR ranges from satellite Landsat.

Table 2.19 Values of coefficients in (2.6)

Vegetation	a_{EWT}	b_{EWT}	R_{EWT}	a_{FMC}	b_{FMC}	R_{FMC}
<i>Nerium oleander</i> var. <i>indicum</i>	-0.10697	0.62268	0.82	155.89	-34.087	0.06
<i>Betula platyphylla</i> var. <i>japonica</i>	-0.03136	0.3339	0.88	135.59	212.72	0.26
<i>Liriodendron tulipifera</i>	-0.00951	0.17521	0.87	68.312	539.65	0.56
Others	-0.02442	0.27963	0.79	119.42	204.69	0.28

Maki et al. (2004) proposed linear approximations:

$$\text{EWT} = a_{\text{EWT}} + b_{\text{EWT}}\text{NDWI}, \text{ FMC} = a_{\text{FMC}} + b_{\text{FMC}}\text{NDWI} \tag{2.6}$$

coefficients of which are shown in Table 2.19.

Experimental results of the fire dangerous assessment are represented in Figs. 2.17, 2.18, 2.19, 2.20 and 2.21. Figure 2.16 shows profile of radio-brightness temperature fixed by means of radiometer 0.8 cm under monitoring of burned peat piles, peat bog and forest fire. Increase of radio-brightness temperature for case of burned peat piles equals to 100–200 K. Increase of radio-brightness temperature for case of peat bog monitoring is 100–300 K. Finally, increase of radio-brightness temperature for forest fire case is 30–70 K. These variations exceed levels of phone radiation variations (5–20 K) and equipment noise (1–5 K).

Figures 2.18 and 2.19 show radio-thermal specters of peat bogs from which it is followed that emissivity coefficient of peat bog has anomalous decrease for wavelengths 10–20 cm and has considerable increase of absorption coefficient. These features follow from capillary-porous peat structure with abrupt differences of volumetric and dielectric characteristics of peat particles in space between of which there exist large quantity of coupled water and air.

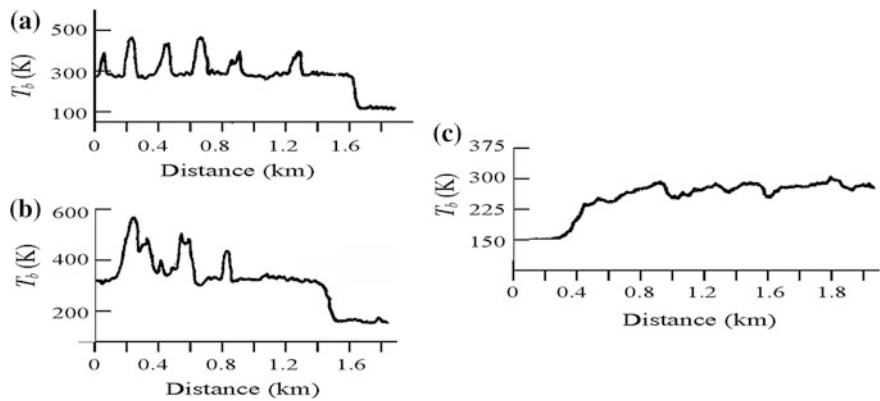


Fig. 2.17 Profiles of radio-brightness temperature at the wavelength 0.8 cm received under remote sensing measurements above the stacks of burning peat (a), fuming peat bog (b), and forest fire (c). Level 150 K corresponds to radio-brightness of water surface

Fig. 2.18 Spectral characteristics of peat emissivity coefficient under weighed humidity: 1—45 %; 2—54 %; 3—67 %; 4—78 %

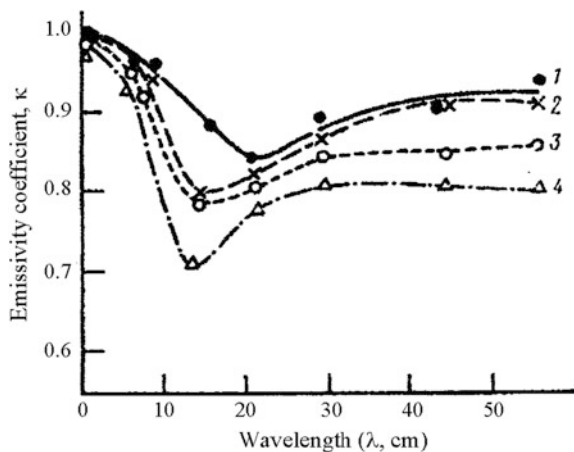


Fig. 2.19 Spectral characteristics of absorption coefficient for peat under weighed humidity: 1—40 %; 2—53 %; 3—63 %; 4—70 %; 5—73 %

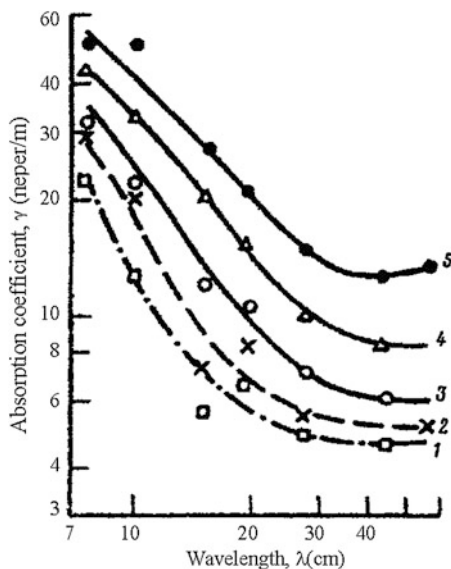


Figure 2.22 shows the stability of averaged maximal variations of radio-brightness temperatures registered in different directions of flying laboratory traces. Total error of radio-brightness contrasts is near to 2 K. Results given here show that microwave radiometers allow the detection of fire in its beginning with high probability.

Another important area for the application of microwave radiometry is remote control of geothermal sources. Microwave monitoring facilitates analyzing the

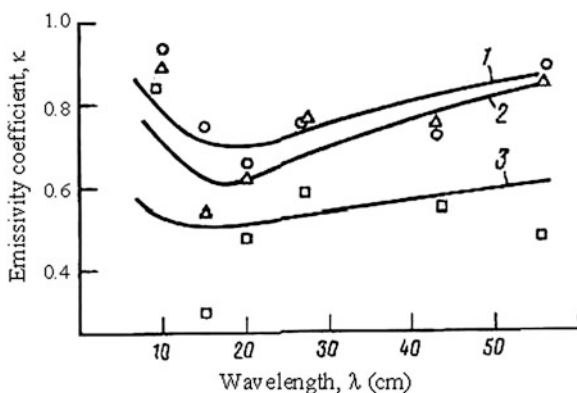
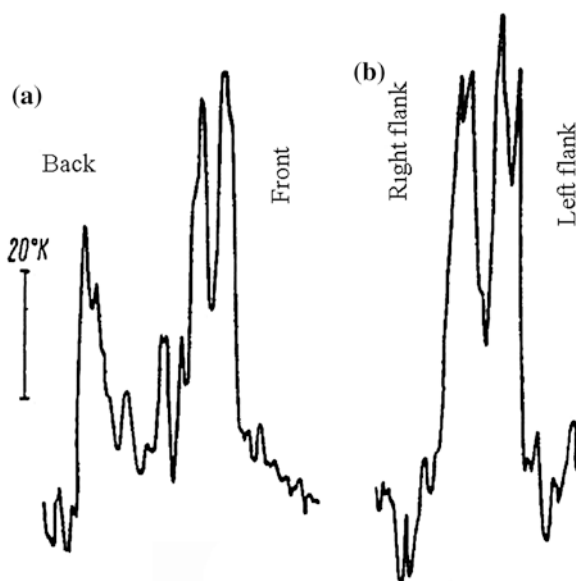


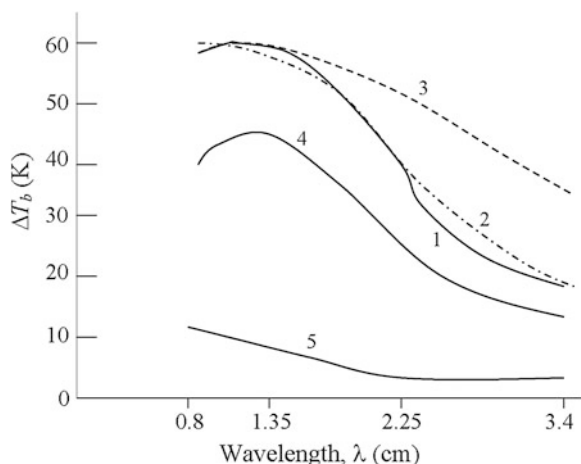
Fig. 2.20 Spectral dependence of peat emissivity coefficient under weighed moisture: 1—45 % (marker of measurement data is *circle*); 2—53 % (marker of measurement data is *triangle*); 3—78 % (marker of measurement data is *square*)

Fig. 2.21 Spectral characteristics of slash fire (*chain line*), peat bog (*solid line*), and sphagnum bog (*dotted line*) in dynamics of drying and moistening: 1—during rainfall; 2—after heavy rainfall; and 3—2 days later rainfall



activity and classifying geophysical structures in areas where geothermal sources are active. In such areas the water content of rocks is insignificant and, hence, the depth of electromagnetic wave spread is increased to equal the inverse value of the absorption coefficient per unit of depth z . Multi-channel measurements based on use of the microwave range use and application of GIMS technology allow soils to be reliably classified and thermal situations mapped. Figure 2.23 demonstrates the map of Tolbachik volcano zone (Ostry Tolbachik—55° 57'N, 160° 25'E;

Fig. 2.22 Averaged spectral characteristics of different fire zones: 1—front, 2—left flank, 3—right flank, 4—back, and 5—faded zone



Plosky Tolbachik—55° 49'N, 160° 24'E). This map was formed on the base of radiobrightness temperature spectres represented in the Fig. 2.24.

In connection with the change climate problem the forest fires monitoring gains specific role in the global ecoinformatics. The forest state and its influence on the greenhouse gases concentration is impossible for the reliable assessment of the present and future tendencies in the environment change. That is the reason a global geoinformation monitoring system has to have built into it a function to effect such an assessment. For such a function to be brought about there needs to be a model that can identify the forest state from radiothermal radiation. For such a model to be created there needs to be knowledge of the dependencies of forest radiothermal radiation on different wavelengths to reconstruct the moisture content of forest timber at various layers and its combustibility. Investigations of many authors shown that application of microwave sensing in the range 0.8 ÷ 20 cm allows to estimate the fire-dangerous for the waterlogged forests.

Multi-channel sensing allows using cluster analysis algorithms to distinguish and classify fire risk classes. The accuracy of this methodology depends on the detail of description by the model of the forest structure reflecting the canopy state and trees density. The most difficult to identify are forest edge fires. In this case the three-layers model of the *flame-smoke-canopy* system is effective:

$$\alpha_p = (1 - \exp\{-\kappa_1\})\exp(-\kappa_2)\exp(-\kappa_3),$$

where α_p is the emissive ability of the forest near-land fire hotbed, κ_i is the emission relaxation coefficient by the flame ($i = 1$), by the smoke ($i = 2$), and by the canopy ($i = 3$). The emission relaxation coefficients are functions of the trees type. It was established that absorption in the canopy increases with high speed as the wavelength is decreasing. Consequently, the receipt of emissions and the discovery of forest near-land fires become difficult when trees have a compact structure. Nevertheless, wavelengths 0.8–1.5 cm enable forest fires to be estimated with high

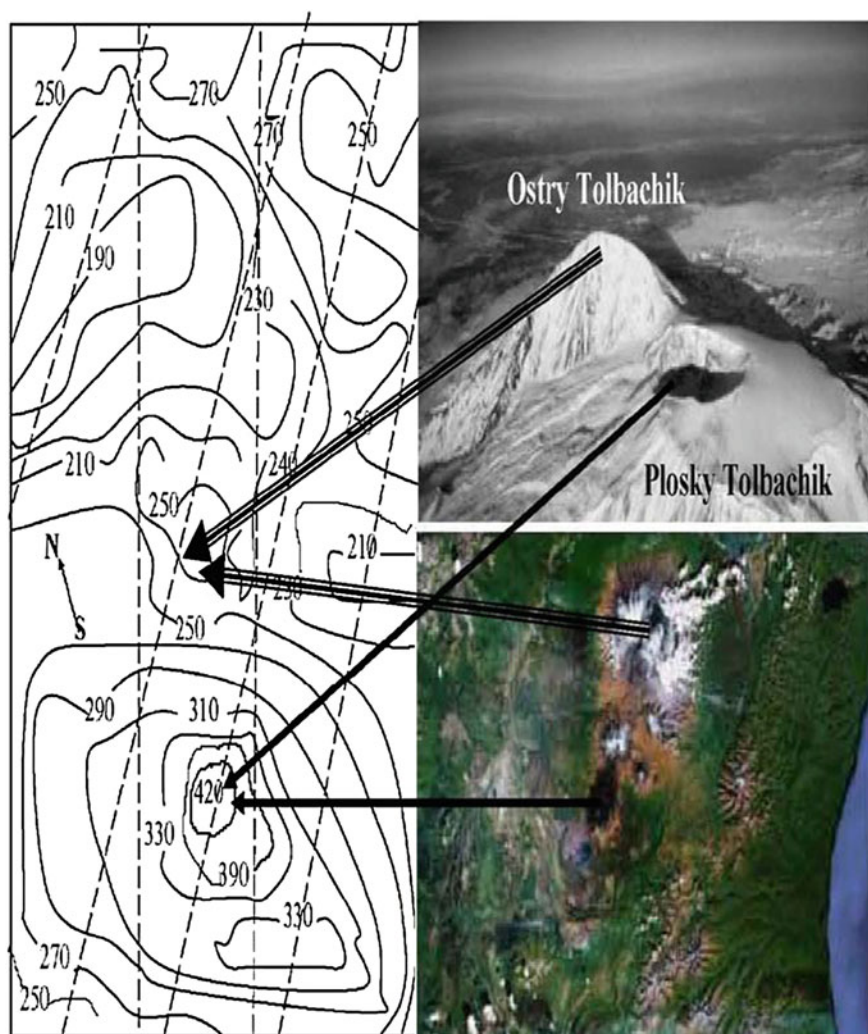
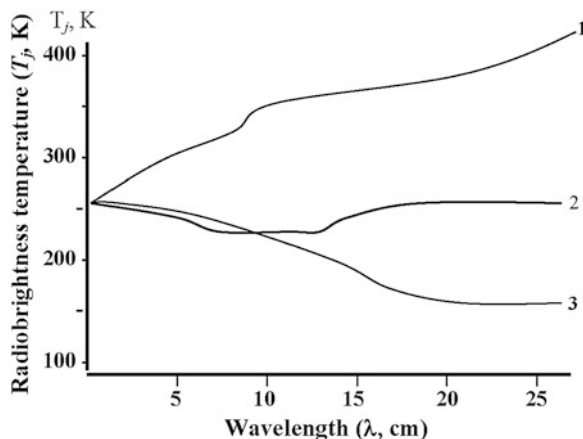


Fig. 2.23 A map of radiobrightness temperature T_b distribution in the area of Greet Tolbachik Volcano on the Kamchatka by means of flying laboratory IL-18 at wavelength $\lambda = 27$ cm. This map was reconstructed by means of the GIMS-technology basing on the trass data

reliability in most cases. It is connected with that main contribution to the microwave emission by the fire hotbed gives the flame particles having the sizes up to 100–300 μm . The burning zone gives the radiobrightness temperature increase on the wavelength 0.8 cm equaled about 200 K. It exceeds the radiometers sensitivity limit. Therefore, microwave monitoring of forest fires in contradiction to optical methods does not depend on the weather conditions.

Fig. 2.24 The radiobrightness temperature spectra for Greet Tolbachik Volcano. Notations: 1—fresh lava flow, 2—isohermic cold lavas, 3—slag fields with the presence of subsurface moisture (Borodin and Krapivin 1998)



The problem of temperature anomalies diagnosis demands the development of specific algorithms for the data processing. Joint use of microwave radiometers and model of *atmosphere-soil-vegetation* system allow to have the efficient technology to solve this problem. Microwave observations provide estimates of the vertical profiles of temperature in the ground as a result of the dependence of effectively emitted layer on wavelength. Two wavelengths are normally used in practice. Applied model describing the temperature profile is based on the assumption about the profile form. Thus, the effectiveness of microwave radiometry for thermal source detection and intensity measurement depends on just how adequate this assumption is. The minimum temperature gradient determined from the radiation data at two wavelengths is approximately $0.3\text{--}1\text{ }^{\circ}\text{C}\cdot\text{cm}^{-1}$. Note that effectiveness of microwave range is much higher then infrared radiometry due to the ability of electromagnetic microwaves for penetration into a soil.

2.7 The Atmosphere Microwave Monitoring

The present state of industrial technologies, energy supply, and transportation worldwide coupled with the, growing number of massive industrial complexes are in continuous conflict with ecological standards for natural environment quality, leading to greater risks of accidents, anthropogenic and natural catastrophes, and natural disasters in many parts of the world. All of which highlights the necessity for uninterrupted control of the most vulnerable environment subsystem—the atmosphere. A role of microwave methods to solve this problem consists in the expansion of the atmosphere monitoring system functions basing on the optical control principles. Since the atmosphere is almost limpid for many radio waves its effectiveness under the atmosphere parameters measurement turn out to be insignificant especially in the local scales. Nevertheless, numerous experimental investigations using a flying

laboratory and satellites show that microwave sensing of the atmosphere is not as good as optical methods on the short traces but is indispensable for atmospheric control over large areas. A choice of wave range for the atmosphere sensing is determined both by the special features of given task and by spatial scales.

A concept of assumed ecological loading on the atmosphere essentially depends on the level of spatial-temporal consideration of the proceeding processes in the interaction between natural environment and anthropogenic factors. Four levels corresponding to the ecological monitoring systems can be shown.

The global level (planetary) predicts the impact of anthropogenic influences on the atmosphere during intervals from several months to tens of years. Macrolevel (continental) considers the processes connected with the trans-boundary moving of the atmosphere pollutants between the countries or continents. A functioning of monitoring systems is regulated by legislative statements. Spatial and temporal scales spread thousands km and several months to year, respectively. Mesolevel (regional) considers the atmosphere pollution process over restricted territory with the selection of pollution sources and its chemical components. The spatial structure of considered processes is detailed by 100 m–100 km. Temporal scales is changed from several hours to units days. The monitoring systems of this significance level control the atmosphere state in the large industrial cities. Microlevel (local) considers the processes of atmosphere pollution over the areas having linear sizes from several to hundreds meters with the timescales from units to 10 min. The monitoring systems of this level registers single phenomenon with detail study of spatial distributions of atmosphere parameters in the local area. Such systems usually are used to control the atmosphere contamination in the zone of dangerous industries.

The atmosphere pollution sources are divided on stationary and unstationary one. Each source is characterized by the quantity of emitted contaminants with the specific properties per unit time, by the temperature of emitted aerial mixture, by the altitude above the earth surface, by the velocity of emitted mixture, and by the geographical coordinates. Under this the source types are distinguished by the geometric form (point, linear, areal) and by the emission regime (continuous action, periodical, emitting a volley). Moreover, atmospheric pollution sources can be classified by their hazard levels. In the first place large chemical industries, ground and underground oil- and gas- reservoirs, gas- and product- pipes, industrial reservoirs of liquid ammonia, chlorine, concentrated sulphuric acid, and also industries connected with the emission of sulphur gas, nitrogen oxides, and hydrogen sulfide are selected (Straub 1989; Liou et al. 2010; Krapivin and Nazaryan 1997).

Classificational characteristics of scaleness and of physical-chemical state of atmosphere pollution sources simplify the monitoring system design. Although pollution source categories can be precisely classified, adequate monitoring systems often do not exist. Nevertheless, in each concrete case such correlations are inevitably established when an atmospheric pollutant dynamics model is created.

Remote sensing methods of the atmosphere are based on the study of electromagnetic and acoustic waves propagation. In the laser sensing optical radiation scattering on the aerosol and atmosphere gases molecules is used. In the radiolocation sensing the effects of turbulent pulsation is taken into account. Laser sensing

is certainly effective at determining the chemical composition of the atmosphere, wind speed, temperature, cloud parameters, and dust formations (Klyuev 2000). The diagnostics of water content in the clouds, compound of atmosphere gases and aerosols by its thermal radiation in the microwave range is based on the spectral measurements (Strelkov and Soldatova 1989).

Many authors use the millimeter wavelength band to diagnose atmospheric gases. Strelkov (1995, 1996) implemented the estimates of atmospheric track optical depths between two satellites on admixture gases CO and N₂O resonance absorption frequency in millimetre and submillimetre bands with taking into account the data on their atmospheric concentrations. It was shown that optical depths are completely defined by admixture gases from the sighting distances ≈ 15 km and can be measured, which indicates the use of the active remote sensing method of the atmosphere for CO and N₂O contents definition. Intrusion of these gases to the atmosphere is caused by anthropogenic factors to a considerable extent. But it is problem for many biogeochemical processes such as ozone cycle. That is why possibility of the measurement of these gases concentration with satellite systems is significant achievement.

Strelkov (1996) developed new method for measuring the concentration of water vapor in the mesopause by active sensing at resonance wavelengths of the rotational spectrum. He showed that for two-frequency sensing, simultaneous measurement of the height profiles of the concentration of water vapor and of the temperature within the mesopause is possible. This method is based on the fact that within the mesopause water vapor completely determines the optical depth of the sensing path in the centres of its spectral lines with wavelengths $\lambda \geq 0.5$ mm. Moreover the absorption coefficient in the centre of the line with resonance frequency f_i is described by the expression

$$\alpha_i = \frac{8\pi^2 N}{3hcG(T)} f_i |\mu_i| \left\{ \exp \left[-\frac{hcf_{i1}}{kT} \right] - \exp \left[\frac{hcf_{i2}}{kT} \right] \right\} \frac{c}{\Delta f_i(P, T)},$$

where N is the concentration of water vapor molecules, h is the Planck's constant ($=6.55 \times 10^{-34}$ J), c is the speed of light ($=3 \times 10^8$ m s⁻¹), k is the Boltzmann's constant ($=1.3 \times 10^{-23}$ J K⁻¹), $G(T)$ is the rotational statistical sum, f_{i1} and f_{i2} are the lower and upper energy levels of transition with frequency $f_i = f_{i2} - f_{i1}$, μ_i is the dipole moment matrix element for transition with frequency f_i , Δf_i is the half-width of the line which depends on the pressure P and the air temperature T , z is the height.

Scientific and technical achievements in the satellite monitoring of atmosphere gases are important in connection with the greenhouse effect and ozone problems (Kondratyev and Varotsos 2000; Zuev 2000; Krapivin and Nitu 2011). The active and passive sensing of some atmospheric gases from satellite board with millimetre and submillimetre wavelengths allow to measure the content of O₂, O₃, N₂O, H₂O, CO, BrO, ClO and HCl. For example, the possibility of active sensing of the added gas is equivalent to the possibility of reliable measurement of the inter satellites trace optical depth, τ , stipulated by the gas:

$$\tau(f, z_m) = 2 \int_{z_m}^H \frac{\gamma(t, z)(R + z)dz}{\sqrt{(R + z)^2 - (R + z_m)^2}},$$

where γ is the gas absorption coefficient, f is the sensing frequency, z is the height, z_m is the minimal distance of trace from Earth's surface, R is the Earth's radius, H is the height of satellites orbits. A possibility of passive sensing of ClO, for instance, is defined by the expression for the limb brightness temperature:

$$T_j(f, z_m) = 2 \int_{z_m}^H \frac{T(z)\gamma(f, z)(R + z)}{\sqrt{(R + z)^2 - (R + z_m)^2}} \times [Q_1(z) + Q_2(z)]dz,$$

where

$$Q_1(z) = 0.5 \exp \left(- \int_z^H \frac{\gamma(f, \xi)(R + \xi)d\xi}{\sqrt{(R + \xi)^2 - (R + z_m)^2}} \right),$$

$$Q_2(z) = 0.5 \exp \left(-\tau(f, z_m) + \int_z^H \frac{\gamma(f, \xi)d\xi}{\sqrt{(R + \xi)^2 - (R + z_m)^2}} \right)$$

The radio-translusense method with using two satellites at frequencies of strong gas absorption lines proves to be effective approach to the ozone layer characteristic measuring (Strelkov 1995; Yakovlev 2001; Yakovlev et al. 2009). Enhancement of this method is given by Yakovlev et al. (2009). Radio-eclipsing method of the Earth sensing is proposed. Principal scheme of this method is characterized in Fig. 2.25.

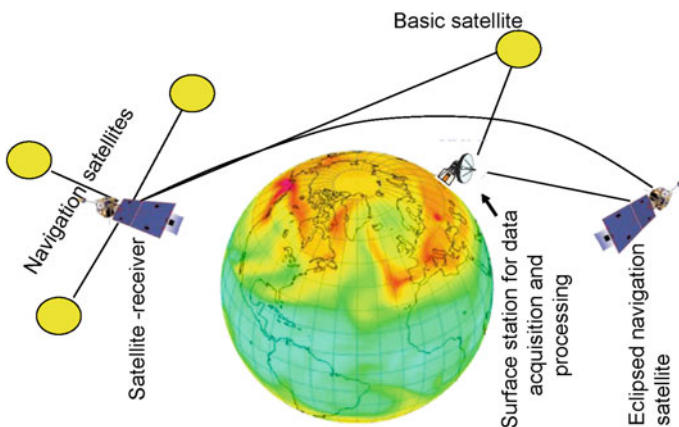


Fig. 2.25 Schematic diagram of global monitoring system based on the radio translusense method

This method is based on the effect of variations in the intensity of electromagnetic field, as well as in the phase and frequency of radiowaves under the transmission of atmosphere and ionosphere. Eclipse monitoring of the atmosphere and ionosphere is dependent on the inverse problem being solved so that it can define the vertical profiles of electron concentrations, refraction coefficients and atmospheric temperatures. Subsequent development of this method would involve creation of algorithms that might make it possible to identify atmospheric and ionospheric characteristics based on regular measurements.

According to the estimations by many authors the greatest role of microwave radiometry is displayed under the precipitation and clouds monitoring. For the first time these possibilities were demonstrated by the experiments with satellite "Cosmos-243" in 1968, and then many space microwave measurements were realized by means of SMMR (Scanning Multichannel Microwave Radiometer), SSM/I, TRMM, and multichannel on-board systems placed on the cosmic station "Mir" what was sunk in 2001.

Local measurements of water vapor concentration in the atmosphere reliable are registered with wavelength 1.35 cm. Under this the dependence of atmosphere radiobrightness temperature on the integrated content of water vapor can be well described by a linear function with a slope equal to $\approx 19 \text{ K g}^{-1} \text{ cm}^{-1}$.

The application of radio waves from the centimeter and millimeter ranges to diagnose atmospheric properties has been pretty successful because of weak, unlike the optical and IR ranges, interaction with cloud particles, dust, and atmospheric gas molecules. Radio wave interaction with rain drops, on the contrary, is resonant and expressed by the intensive absorption and scattering of wave energy. Therefore, microwave devices of the active and passive sensing at present time are unique means giving a possibility to receive from space the data about the precipitation parameters in global scale.

Microwave observations of precipitation are based on the measurements and calculations of four Stokes parameters (Zagorin 1999; Zagorin and Kutuza 1998; Kutuza et al. 1998, 2000): $S = \{S_1, S_2, S_3, S_4\}$, where S_1 is the total intensity of radiation, S_2 is the difference between the radiation intensivities of horizontal and vertical signal polarization, S_3 is the difference of radiation intensivities with linear orthogonal polarizations respect to the coordinates system turned by 45° , S_4 is the difference of radiation intensivities of right and left circular polarization. The Reileigh-Jeans approximation gives $S_1 = 2k_B T_j \lambda^{-2}$, where k_B is the Boltzmann's constant ($= 1.38 \times 10^{-20} \text{ mW Hz}^{-1} \text{ K}^{-1}$), λ is the wavelength. These parameters are the functions of radiobrightness temperatures T_j of radiation, receiving by the channels of vertical, T_v , horizontal, T_h , under the angle $\pm 45^\circ$, $T_{\pm 45}$, and circular (right, T_r , and left, T_l) polarizations, and also they are expressed as functions of complex amplitude for the vertical, E_v , and horizontal, E_h , components of electric field intensity of radiothermal emission (Zagorin and Kutuza 1998):

$$S = \begin{pmatrix} S_1 \\ S_2 \\ S_3 \\ S_4 \end{pmatrix} = \begin{pmatrix} T_V + T_h \\ T_V - T_h \\ T_{+45} - T_{-45} \\ T_l - T_r \end{pmatrix} = \frac{\lambda^2}{2k_g} \begin{pmatrix} |E_V|^2 + |E_h|^2 \\ |E_V|^2 - |E_h|^2 \\ 2\text{Re}(E_V E_h^*) \\ 2\text{Im}(E_V E_h^*) \end{pmatrix}$$

The Stock's parameters, measured directly in field experiments, together with other measurements and using cluster analysis allow clouds and rains types to be realized. Figures 2.26 and 2.27 give data about the correlation of the Stock's parameters with the rain intensity calculated by Zagorin (1999). The maximum

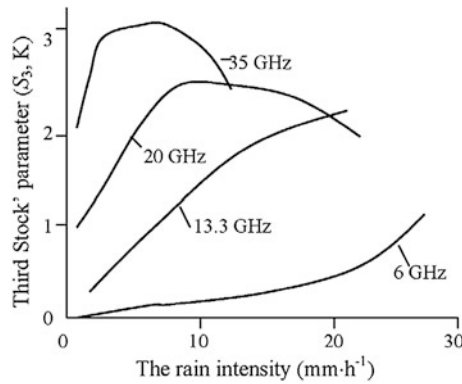
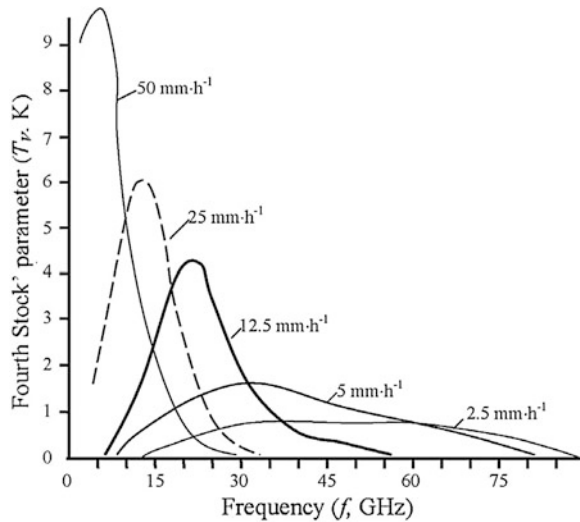


Fig. 2.26 A dependence of third Stock's parameter from the rainfall intensity. A thickness of the rain layer is 3 km. A descending microwave emission with the angle of 50° to the zenith is considered. The drops slope angle is equaled to 5° (Zagorin 1999)

Fig. 2.27 A spectral dependence of fourth Stock's parameter for the microwave Sun radiation dispersed by the rainfall drops in the layer of 4 km. (Zagorin 1999; Zagorin and Kutuza 1998)



spectral dependencies of the second, third, and fourth Stock's parameters on microwave Sun radiation dispersed as a result of rain intensity increasing are displaced to the low-frequency region (up to ≈ 6 GHz). So, for the rain layer having the thickness in 4 km under the Sun observation under corner in 20° regarding the horizon the maximal values of S_2 , S_3 and S_4 are achieved under the rain intensity $r = 12.5 \text{ mm h}^{-1}$ and for the frequency ≈ 13.5 GHz. They are equaled: $S_2 = 220 \text{ K}$, $S_3 = 44.6 \text{ K}$ and $S_4 = 5.95 \text{ K}$. When $r = 50 \text{ mm h}^{-1}$ and frequency ≈ 6 GHz these parameters are the following: $S_2 = 483 \text{ K}$, $S_3 = 101.5 \text{ K}$, and $S_4 = 28.5 \text{ K}$.

Polarization radiometry of precipitation is based on two effects: the nonspherical form of rain drops and the existence of a distinct direction in which the symmetrical axes of falling drops are oriented. This means that the emission and absorption of radio waves having vertical and horizontal polarizations that differ in directions from the orientation of symmetrical axes of rain drops can be distinguished. For this reason the azimuth symmetry of radiothermal field of the rain emission is absent. And this means that microwave emission of the rain is partly polarized. Therefore, the task of precipitation diagnostics is reduced to finding the degree of dependence of the emission polarization parameters (polarization degree, slop angle of polarization plane, polarization ellipse form, etc.) on characteristics of the state of the environment in which rain is dispersing.

The first polarization radiometric measurements of the rain descending microwave emission were realized by Kutuza (1977), and then were motivated and developed by the experiments and theoretically in the subsequent investigations. The results of measurements of T_j in general and difference channels of microwave radiometer at $\lambda = 2.25 \text{ cm}$ (13.3 GHz) given the estimations of degree of linear polarization of rain radio-emission. When intensity of steady downpour was changed between 0.5 and 2.5 mm h^{-1} it was equaled to 5.5% . The rains having the convective type with the intensity more 5 mm h^{-1} had the degree of linear polarization which was increased until 8.5% . These estimations guarantee the distinct delimitation of the rain zones.

The methodology set up to estimate the parameters involved in the distribution of rain drops by size developed by Gasiewski and Kunkee (1994) is based on the measurements of two Stock's parameters, S_1 and S_2 . The gist of methodology consists in solving an inverse task under the preposition that non-spherical drops have an exponential distribution with two unknown parameters determined by the data about S_1 and S_2 . The contribution of values of third and fourth Stock's parameters to the solution of rain diagnostics task is determined by the expansion of estimated parameters. So, S_3 is proportional to the differential relaxation, Δ_1 , of radiowave. The fourth Stock's parameter is proportional to the product of Δ_1 and differential phase displacement, Δ_2 . A value of $\Delta = \Delta_1 + i\Delta_2$ is called as the rain anisotropy parameter and it can be measured directly. Theoretical dependencies of Δ from different parameters of the rain are studied by Gasiewski and Kunkee (1994). It was shown that the spreading in the distribution by the slop corner to the vertical of projections of drops symmetry axis in the plane which is orthogonal to the direction of wave spreading exercise largest influence on the precision of Δ estimation. Statistical models describing the orientation of drops allow the average

value and dispersion to be connected with the Gaussian distribution law of drops according to the orientations of wind field parameters (Zagorin 1999). It was discovered that when dispersion of drops orientation less 30 % theoretical and experimental estimations of Δ are similar in the value. It allows to use the developed models of rain in practice.

The atmosphere microwave control supposes the existence of radiation source in the microwave range. Such a source can be Sun, the radio-emission of which in its calm state (when the flashes are absent) within the frequency region $\lambda \in [2, 100]$ GHz can be characterized by $T_j \in [5 \times 10^3, 1.5 \times 10^4]$ K. Non-polarized microwave radiation of Sun is relaxed and polarized by the rain, and average relation $S_2/S_1 \approx 0.0528$. The radiometers dislocation and choice of its ranges for such microwave source is actual task of present radiophysics. This task is combined with the formation of T_j level on the radiometer output as the function of fields composition on its antenna. This composition depends on the character of litter surface the repeated reflections of radiowaves from which are to take into account under the solution of inverse task arising in the atmosphere radiometry. In the conditions when the atmosphere-litter surface system has a symmetry by the azimuth, and when emitting and scattering atmosphere particles are oriented chatically, and the litter surface is mirrory- or diffusely- reflecting, then $S_1 \neq 0$, $S_2 \neq 0$, $S_3 = S_4 = 0$. When the symmetry by the azimuth is absent, and when atmosphere particles have the orientation direction differing from vertical, and when spreading surface roughness is characterized by the asymmetrical distribution of slopes we receive: $S_1 \neq 0$, $S_2 \neq 0$, $S_3 \neq 0$, $S_4 \neq 0$. The fourth Stock's parameter S_4 which characterizes the polarization ellipticity, becomes unequal to zero when the radiothermal emission undergoes no less two-fold scattering into the hydrometers volume or on the surface roughness (Zagorin 1999).

An important stage in precipitation monitoring is clearly optimizing registered radiation frequencies. This was partly done by Sasaki et al. (1989), who based on measurements showed that the frequencies near 1 GHz are the most informative. This result is corroborated by the curves given in Figs. 2.28 and 2.29.

The perspectivism of the radiophysical methods used for the design of an atmospheric control system is substantiated by the many theoretical and empirical investigations. The basic problem consists in forming a knowledge base to maintain correlations between atmospheric characteristics (properties) and the behavior of electromagnetic waves inside the atmosphere. The basis on which atmospheric process models have been built reflecting the combinations of spatiotemporal scales is again an important element in the study of these correlations.

As it follows from the investigations by Yakovlev (2001) effective methodics of the atmosphere monitoring system design is connected with the radio occultation studies of the atmosphere and ionosphere. The setup necessary to bring about such measurements is based on placing the transmitter on a satellite orbiting Earth and placing the receiver on a geostationary satellite. As result such structure secures continuous regime of atmosphere vertical transection with the obtaining of its parameters distribution by the altitude. The task is reduced to identifying the values

Fig. 2.28 The state image of informational space of brightness temperatures in the section of the most representative frequencies

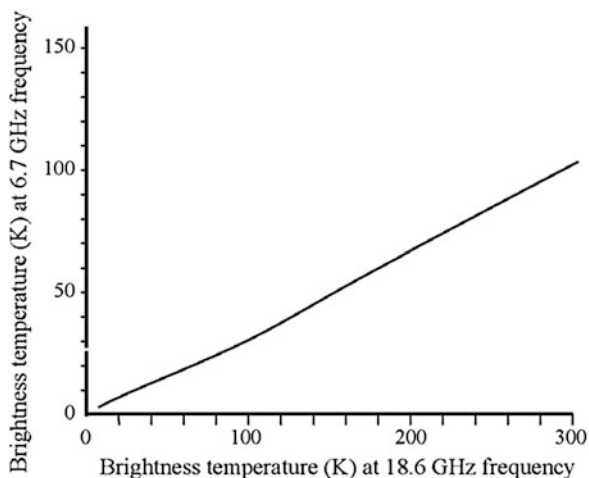
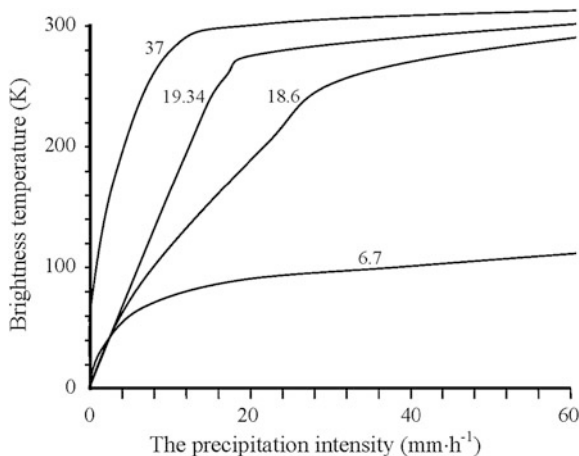


Fig. 2.29 The comparative rainfall rate dependence of the sky brightness temperature for different frequencies (they are shown on the curves, GHz) (Sasaki et al. 1989)



of these parameters using data about signal absorption and fluctuation as a result of propagating along the changing tracks between satellites.

The influence of the atmosphere and ionosphere on the parameters of refraction, fluctuation, relaxation, absorption, decay, and change in signal frequency has been studied in detail. Depending on the orbit position of the satellite this influence makes it possible to receive data about the atmosphere and ionosphere in concrete regions of the planet. A total spatial image for part or of the atmosphere can be had by data processing using GIMS technology.

It is possible to distinguish between the direct and inverse tasks of radio-translucense. The direct task arises when the atmosphere model is used to determine the above mentioned changes in electromagnetic waves for a given satellite

trajectory. The inverse task consists in the determination of the atmosphere and ionosphere parameters through experimental data describing the signal variations.

The method of atmosphere radio-translusense can be used when the microwave emission receiver is sited on the Earth's surface. Using the Doppler effect on wavelength 1.35 cm (22.235 GHz) in this case allows the vertical distribution of water vapor in the uppermost atmosphere to be received with acceptable precision.

Atmospheric microwave sensing can be expanded to consider the possibility of estimating a wider set of its parameters. To do so would mean solving a complex mathematical task connected with the prognosis of the microwaves relaxation according to sensing routes in the atmosphere. Millimetre range causes special interest in this respect. According to the investigations by Meriakri (1992) and Strelkov (1995) many gases have discrete absorption spectre in the waves of millimetre and submillimetre ranges. This allows the average concentration of the gas component along the sensing route to be calculated based on estimating electromagnetic wave absorption. An example of such a calculation is given in Table 2.20.

A special feature of the millimeter range is the possibility to form narrowly directed radio-bundles because of the relatively small apertures of the emitters. The task of atmosphere parameter estimation can be transformed to registering variations in signal relaxation on the sensing route between the receiver and transmitter followed by solving a suitable integral equation that takes into account the refraction of electromagnetic waves in the troposphere, cross-diffraction of signal bundles, and possible variations in the vertical distribution of refraction indicators along the route. Monitoring systems of low atmosphere also call for the influence of land covers on the propagation of millimeter waves to be taken into consideration.

Millimetre and submillimetre ranges under the using of active and passive sensing regimes ensure the reliable estimation of content in the atmosphere of certain chlorine compounds, carbon oxide, nitrogen dioxide, ozone, and water vapors, as well allow to determine the wind speed and temperature (Strelkov 1995, 1996). The prospect of these ranges bringing about bi-static radio-translusense of the atmosphere is down to the moderate price of field measurements and existing theoretical results concerning the methodologies used to reconstruct atmospheric spatial distribution parameters along observational routes.

Table 2.20 Calculation of the gases concentrations basing on the measurements of signal relaxation at the frequency ν_a on the atmosphere trace of 10 km (Meriakri 1992)

Gas	Gas concentration (mg m^{-3})	ν_a (MHz)	Atmosphere relaxation (db km^{-1})
CO	1,500	0.3	115.271
	330	6	235.789
N ₂ O	1,600	0.2	100.492
	240	6	351.666
SO ₂	2,300	0.2	104.029
	560	0.4	135.696
H ₂ S	9	1.8	168.763

The application of microwave range for the atmosphere diagnostics can not be effective without the creation of measurement data processing systems. Such systems are based on simulation models that make reconstructing atmospheric characteristics possible by making good use of multichannel sensing data. What is more, the obligatory presence of the optical and IR ranges between the channels of such systems results in an essential gain in monitoring system informativeness.

In framework of the GIMS technology application, a simulation system for the atmosphere pollution physics (SSAPP) was designed as the experimental system for the control and identification of sources polluting the atmosphere basin (Krapivin et al. 1996, 1997a, b; Bondur et al. 2009). The SSAPP is intended to reconstruct multi-component non-stationary pollutant fields and identify local pollutant sources. The SSAPP uses the procedure of adaptive synthesis of simulation model describing the three-components of pollution field as basic algorithm. This procedure consists in dynamic development of the simulation model as a result of estimating the divergence between model output and data registered by means of measuring devices in various ranges of electromagnetic spectrum.

Putting current *a priori* information about the coordinates of measuring devices, pollutant sources, and parameters into a simulation model is brought about through coordination with a topographical map of the territory being controlled. The model optimization and ranges set control are realized with consideration of the presence database and available technical resources. The system is adapted automatically to the spatial scales of territory the pollution of which is simulated. The set of tasks solved by the SSAPP includes:

- calculation of influence area for each source included in the system database;
- determination of sensitivity area for each measuring device;
- reconstruction of spatial distribution of pollutants;
- identification of the causes behind dangerous pollution zones arising;
- search of unknown pollution sources.

The SSAPP foundation is set of models describing the atmosphere dynamics and contaminants spreading over the restricted territory up to whole planet. The meso and micro levels can be imitated by a set of Gaussian models, the choice of which depends on the parameters provided by the monitoring system's database. Global- and macro-levels of the atmospheric contaminants spreading are described with the models of Euler and Lagrange types.

2.8 Microwave Radiometry in Remote Monitoring of the Ocean

The formation of radiothermal field emission of the ocean in the microwave range depends on the water temperature and salinity, surface roughness, concentration of chlorophyll and other components of oceanic environment. Remote registration of this field demands to take into account also such factors as evaporation, precipitation,

foam-formation, cloudiness, intensity variations of direct and scattered solar radiation. That is why the design of microwave remote monitoring systems on the base of registration of ocean emission in microwave range comes to the solution of set of complex mathematical tasks. Parameters reflecting the state of the *atmosphere-ocean* system have an important influence on how the spatial structure of the radiothermal field of this system is formed. So, outside zones of rain, snow and hail clouds when for wavelength $\lambda \geq 0.8$ cm total absorption by the atmosphere is insignificant, phenomenological theory of radiation transmission is applied to determine the radiobrightness temperatures, T_j , for the *atmosphere-ocean* system. In zones of drop clouds presence, relative contribution of scattering processes for the emission on wavelength $\lambda \geq 0.8$ cm to the formation of field $\{T_j\}$ consists from 5 to 50 %. This means that in these zones the scattering effects are to be taken into account under the microwave radiometry data processing received from the ocean surface.

In common case, when the registration of T_j is realized by satellite-based system from the height H under the observation angle θ respect to the local vertical for wavelength λ the following functional correlation of radiobrightness temperature with thermodynamic and physical characteristics of *atmosphere-ocean* system is valid (Savorskij 1992):

$$T_j(\lambda, \theta) = Q_1 + \cos^{-1} \theta \int_0^H Q_2(u) du + Q_3 \int_0^\infty Q_4(u) du, \quad (2.7)$$

where

$$\begin{aligned} Q_1 &= \kappa_\lambda T_{SO} \exp[-\tau_\lambda(0, H)/\cos\theta], \\ Q_2 &= T(u) \gamma_\lambda(u) \exp[-\tau_\lambda(u, H) \cos^{-1} \theta], \\ Q_3 &= (1 - \kappa_\lambda) \exp[-\tau_\lambda(0, H) \cos^{-1} \theta] \cos^{-1} \theta, \\ Q_4 &= T(u) \gamma_\lambda(u) \exp[-\tau_\lambda(0, u) \cos^{-1} \theta], \end{aligned}$$

$\gamma_\lambda(u)$ is the total relaxation coefficient by the atmosphere on the altitude u , $T(u)$ is the thermodynamic temperature on the altitude u , κ_λ is the surface emissive ability, T_{SO} is the ocean surface temperature, $\tau_\lambda(u_1, u_2)$ is the optical thickness of atmosphere layer situated between the levels u_1 and u_2 on the wavelength λ :

$$\tau_\lambda(u_1, u_2) = \int_{u_1}^{u_2} \gamma_\lambda(z) dz.$$

Formula (2.7) is basic for the calculation of the ocean parameters using the measurements $\{T_j\}$. The variety of modifications and simplifications of expression (2.4) is determined by the radiation models set of the *atmosphere-ocean* system, where the dependencies κ_λ and γ_λ from the parameters of this system have theoretical

or empirical character. The coefficients of water surface emission on the horizontal, κ_λ^h , and vertical, κ_λ^v , polarizations are calculated with the Frenel formulae:

$$\kappa_\lambda^h = 1 - \left| \frac{\varepsilon_\lambda \cos \theta - (\varepsilon_\lambda - \sin^2 \theta)^{1/2}}{\varepsilon_\lambda \cos \theta + (\varepsilon_\lambda - \sin^2 \theta)^{1/2}} \right|^2, \quad (2.8)$$

$$\kappa_\lambda^v = 1 - \left| \frac{\cos \theta - (\varepsilon_\lambda - \sin^2 \theta)^{1/2}}{\cos \theta + (\varepsilon_\lambda - \sin^2 \theta)^{1/2}} \right|^2, \quad (2.9)$$

where ε_λ is the water dielectric permittivity at the wavelength λ being the function of salinity, temperature and other parameters of upper ocean layer; $\varepsilon_\lambda = \varepsilon'_\lambda - i\varepsilon''_\lambda$ ($\varepsilon'_\lambda = 5.5 + a_1$; $\varepsilon''_\lambda = \lambda_S \lambda^{-1} a_1$),

$$a_1 = [\varepsilon_S - 5.5] / [1 + (\lambda_S / \lambda)^2], \quad \varepsilon_S = 0.0081t^2 - 0.40885t + 88.2, \quad t = T_{SO} - 273, \\ \lambda_S = 1.466 \exp\{-0.0634t\} + 0.000136t^2 - 0.0272t + 1.8735.$$

A correction to the value ε_λ with consideration of water salinity variations S can take into account by the approximate formula: $\varepsilon_S(S) = \varepsilon_S(0) - 17.2S$. From expressions (2.8) and (2.9) under vertical observation ($\theta^\circ = 0^\circ$) we receive: $\kappa_\lambda^h = \kappa_\lambda^v = \kappa_\lambda^o = P_\kappa$, where

$$P_\kappa = 4|\varepsilon_\lambda|^{1/2} \cos(\delta_\lambda/2) / [|\varepsilon_\lambda| + 2|\varepsilon_\lambda|^{1/2} \cos(\delta_\lambda/2) + 1],$$

angle δ_λ is determined by the expression $\operatorname{tg} \delta_\lambda = \varepsilon''_\lambda / \varepsilon'_\lambda$.

Andreev et al. (1984) analyzed Shepvalov's invariant $(\kappa_\lambda^h)^2 / (2\kappa_\lambda^h - \kappa_\lambda^v) = 1$ and proposed a constructive algorithm to calculate the surface temperature T_S with the measurements of $T_{j,h}$ and $T_{j,v}$ under the observation angle $\theta = 45^\circ$: $\dot{O}_S = (\dot{O}_{j,h})^2 / (2T_{j,h} - T_{j,v})$. This algorithm has the precision less ± 3 K. It is valid for the calculation both T_{SO} and land thermodynamic temperature. The T_j practically depends on T_{SO} linearly with the slope from 0.35 to 0.5. An increase of salinity from 0 to 40 ‰ is provided with the increase of T_j under $\lambda < 3$ cm by values no exceeding 3 K and with essential decrease of T_j under $\lambda \in [8, 10]$ cm by the values up to 40 K. The dependence slope of this decreasing as the function of S is function of T_{SO} .

Knowledge of the radiation dependencies of water surface properties on the total spectrum of water surface parameters is the essential basis of a radiometric control system of the ocean surface.

In the case of water object with great conductivity (sea water) for the decimetre range the following correlation is valid: $\kappa \cong 0.5(f/\sigma)^{1/2}$, where f is the radiowave frequency, σ is the water conductivity. This expression allows to estimate the water conductivity if the water thermal emission is measured. If the substance dissolved in the water and its conductivity are known the dissolved substance concentration is

calculated by the using of thermal radioemission. Hence the microwave radiometry can be used for the monitoring of reservoirs pollution.

The emissive and reflective abilities of a sea surface in microwave region is very connected with ocean environment parameters such as the water temperature, salinity, dielectric constant, and roughness. Sasaki et al. (1988) shown that 6.7–18.6 GHz band has high informativity to diagnose the *atmosphere-ocean* system. It was established that correlation between radiobrightness temperatures of atmosphere and sea surface has linear character and that reflective ability on horizontal polarization at the frequency 18.6 GHz is higher then on vertical polarization. Moreover, it is observed that there exists an obvious dependence of radiobrightness temperature fluctuations of the sea surface on wind speed. It equals for the horizontal polarization to 0.5 and 1.0 K m⁻¹ s at 6.7 and 18.6 GHz, respectively. In the case of vertical polarization these values equal to 0.3–0.8 and 0.6–1.5 K m⁻¹s, respectively.

The sensitivity of the sea surface brightness temperature, $T_{BP}(K)$, for the polarization P -type to the variations in the wind speed, $V(m\ s^{-1})$ is determined by value (Figs. 2.30 and 2.31):

$$\omega = \left. \frac{\partial T_{BP}}{\partial V} \right|_{a_1, \dots, a_k = const},$$

where a_i ($i = 1, \dots, k$) are the oceanic environmental parameters contributing to T_{BP} change except for wind speed. The value of ω is almost linearly correlated with wind speed at constant sea surface temperature and salinity, so $\partial^2 T_{BP} / \partial V^2 \approx 0$. Then $T_{BP} = T_{BOP}(\theta) + V \partial T_{BP}(\theta) / \partial V$, where T_{BOP} is the brightness temperature of the calm sea surface (K), θ is the zenith angle of incident radiation. According to the Kirchoff's law we have the following wind speed sensitivity of reflectivity: $\partial \gamma_P(\theta) / \partial V = -\partial \epsilon_P(\theta) / \partial V$. It gives the following expression for reflectivity at

Fig. 2.30 Empirical dependence of brightness temperature of ocean surface on the wind speed at various wavelengths and the observation angles (Sasaki et al. 1988). The frequencies in GHz are given on the curves

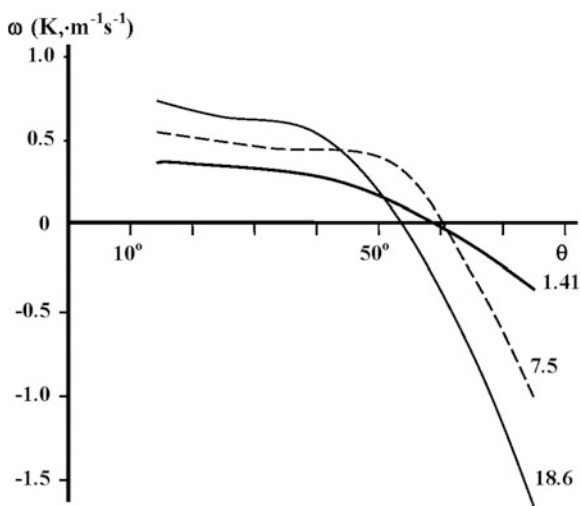
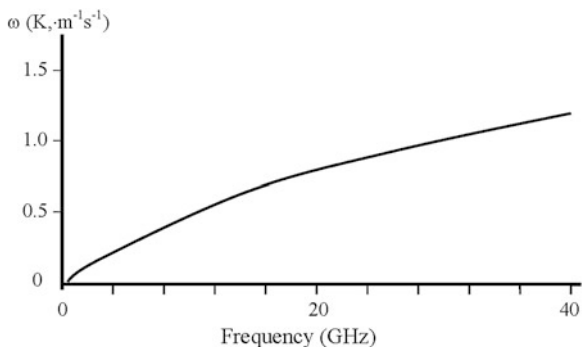


Fig. 2.31 Empirical dependence of brightness temperature sensitivity on the wind speed when the observation is realized by the nadir (Sasaki et al. 1988)



arbitrary wind speed: $\gamma_P(\theta) = \gamma_{OP}(\theta) - (V/T_{SO}) \times \partial T_{BP}(\theta)/\partial V$, where T_{SO} is the sea surface temperature, γ_P and γ_{OP} are the reflectivity of the roughened and the calm sea surface, respectively.

According to Sasaki et al. (1987a, b, 1988) the wind speed sensitivity of the sea surface brightness temperature at satellite level is

$$\frac{\partial T_{BP}^{sat}(\theta)}{\partial V} = \frac{\partial T_{BP}(\theta)}{\partial V} \cdot \frac{T_{SO} - \{T_B^{\downarrow,sky}(\theta) + T_B^{space}\}}{T_{SO}},$$

where $T_B^{\downarrow,sky}$ is the downward sky brightness temperature at sea surface (K), T_B^{space} is the galactic noise (K).

The sea surface brightness temperature at arbitrary wavelength can be represented in the form:

$$T_{BP}^{\lambda}(\theta) = \varepsilon_{1P}(\theta)T_{SO} + \gamma_P(\theta)T_B^{\lambda,sky}(\theta_S, \phi_S),$$

where θ_S and ϕ_S are the zenith and azimuthal angles,

$$\gamma_P(\theta) = \frac{1}{4\pi} \int_0^{2\pi} \int_0^{\pi/2} \gamma_P(\theta, \theta_S, \phi_S) \sin \theta_S d\theta_S d\phi_S.$$

Under conditions of wind-induced sea roughness, when sea wave are so big that radio waves of the centimeter and decimeter ranges cannot be used, scattering and emission characteristics can be estimated by means of Kirchhoff's approximation.

In the range of centimetre waves, where electrophysical properties of water are comparatively known, the expression (2.7) allows to determine water surface temperature when its radiothermal emission is measured.

In common case the task of ocean surface diagnosis comes to the reverse of function $T_j = F(a_1, \dots, a_k)$ in the relation of geophysical parameters set $\{a_i\}$. The function F reflects the type of aquatory radiation model. Linear models allowing to

calculate a standard deviation of T_j are widely used: $\delta_i = k_i \delta a_i$, $k_i = \partial F / \partial a_i$, where δa_i is the standard deviation of parameter a_i . The estimations of κ_i are given by Nelepo et al. (1985).

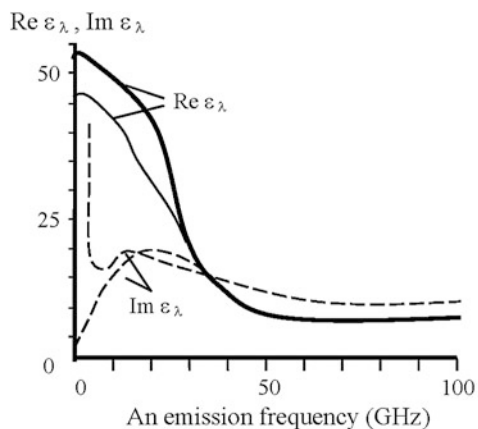
Having synthesized a radiation model, F can then be used to control ocean surface pollution and the *atmosphere-ocean* system is considered as a three-layers environment: *atmosphere-pollutant-water*. For calculation of Frenel's coefficients to estimate the emissive property κ_λ of this system, knowledge of the dielectric permeability of the pollutant layer is needed. Therefore, for oil spills in the microwave range there is weak dependence of the dielectric constant on λ and the values of losses are typically small. For example, the raw oil spill is characterized by value $\text{Re} \varepsilon_\lambda \in [1.6, 3]$. Specifically, for $\lambda = 0.8$ cm we have $\varepsilon_\lambda = \delta_i = k_i \delta a_i$, $k_i = \partial F / \partial a_i$. Certainly ε_λ is changed depending on the oil quality and time interval of its placing in the water.

Any pollutant of water environment forms on the water surface some emulsion layer which exists during certain time interval. Dielectric permeability of this layer can be calculated by means of the mixture formula: $\varepsilon_\lambda = [(1 - W_1)(\varepsilon_{\lambda,1})^{1/3} + W_1(\varepsilon_{\lambda,2})^{1/3}]^3$, where W_1 is the water content in the emulsion volume, $\varepsilon_{\lambda,1}$ and $\varepsilon_{\lambda,2}$ are the dielectric permeabilities of pollutant and water, respectively. Figure 2.32 demonstrates the frequency of ε_λ for the case of oil pollution.

The methodics of radiation model synthesis for three-layers environment is applied to the microwave diagnostics of the ice cover. Here ε_λ is explained as dielectric permeability of the ice layer (Melentyev et al. 1998).

Variety of theoretical and experimental investigations of the ocean/atmosphere system includes the application of remote sensing technologies based on microwave monitoring. For example, Grankov and Milshin (2009) studied experimentally (in the laboratory) a behavior of characteristics of the water surface being initially under the room temperature and sharply cooled with liquid nitrogen: variations of an intensity of natural microwave radiation at the wavelength 2.25 cm and infrared heat radiation in the window 10.5 μm , as well as a value of the heat content

Fig. 2.32 Dielectric properties of oil mixture with the fresh (solid line) and saliny (dashed line) water



(enthalpy) in the upper water surface layer. A comparison of evolutions of the heat contents computed from the difference between temperatures of upper and bottom boundaries of the subsurface layer with evolutions of microwave and infrared radiation intensity is conducted.

Here, it is again necessary to remark that difference between microwave and infrared ranges consists in their response on the atmosphere state:

- intensity of super high frequency is defined by means of the product of emissivity coefficient (κ) and thermodynamic temperature (T) within the limits of efficient radiation layer (l_{ef}) where $dT/dz \leq 0.5$ and l_{ef} equals to the part of centimeter; and
- IR-range methods can be used only in the cases when the atmosphere is free from aerosols, hydrometeors, and clouds as well as l_{ef} equals to the part of millimeter.

Usually, the values of sensible q_h and latent q_e heat at the air-sea boundary are calculated by means of well known in the meteorology formulae:

$$q_h = c_p \rho c_t (t_s - t_a) V; \quad q_e = L \rho (0.622/P) c_e (e - e_o) V, \quad (2.10)$$

where t_a is the air temperature, P is the atmospheric pressure; e is the atmosphere humidity, V is the wind speed in the near-surface atmosphere, t_s is the ocean surface temperature, e_o is the the air humidity, c_t is the numbers of Schmidt (heat exchange), c_e is the number of Dalton (moisture exchange), L is the specific heat of evaporation, c_p is the specific air heat under constant pressure, and ρ is the atmosphere density.

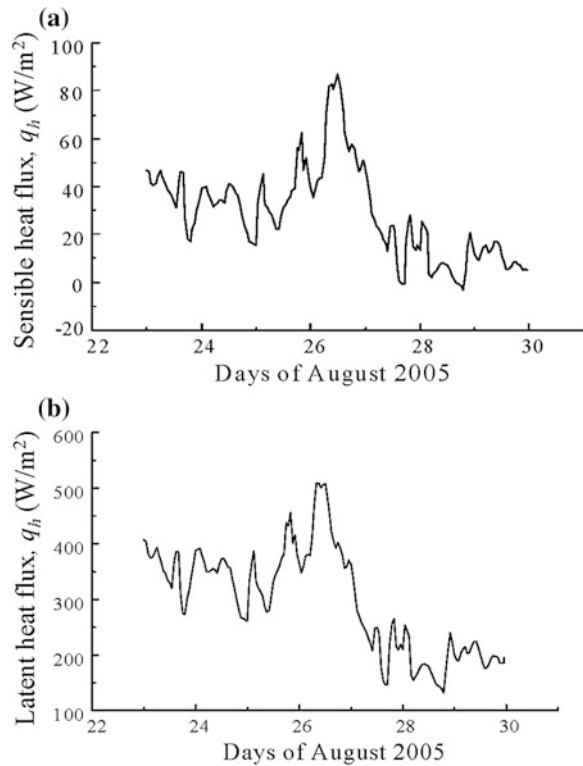
Formulae (2.10) can be used for calculation of sensible and latent heat fluxes only in aquatories that are serviced by meteorological stations. Figure 2.33 represents such calculations for NDBC SMKF1 during hurricane Katrina evolution.

Capability of satellite SHF-radiometric methods to evaluate the characteristics of large-scale heat and dynamic interaction of the atmosphere and ocean is based on the use of resonance absorption of radiowaves 1.35 cm by atmospheric moisture. In this case different models are used (Skou 2008; Pampaloni and Paloscia 2000). One of such simple model is usually used:

$$I = I_1 + I_2 + I_3$$

where $I_1 = I_s \exp[-\tau(H)]$ is the intensity of natural radiation of the oceanic surface I_s attenuated in the atmosphere; the coefficient $\exp[-\tau(H)]$ is the index of the absorption; $I_2 = \int_0^H I_a(z) \exp[\tau(z) - \tau(H)] dz$ is the intensity of upgoing atmospheric radiation; $I_3 = R \int_0^H I_a(z) \exp[-\gamma(z) - \tau(H)] dz$ is the intensity of atmospheric emission reflected from the water surface; $\tau(z) = \int_0^H \gamma(z') dz'$ is the integral

Fig. 2.33 Variations of sensible (a) and latent (b) heat fluxes at the ocean surface in an area of the station SMKF1 responsibility during the period of tropical hurricane Katrina effect in August 2005



attenuation in the atmosphere; H is the height of the troposphere; R is the reflectivity of water surface.

An intensity of natural radiation of the water surface is determined as:

$$I_s = \begin{cases} \kappa T_s & \text{at microwave range,} \\ \delta B(T_s) & \text{at infrared range.} \end{cases}$$

where T_s is the thermodynamic (kinetic) temperature of the ocean surface, κ and δ are the emissivity coefficient of the ocean surface at microwave and infrared ranges, respectively.

The intensity of atmospheric radiation related to the level z is determined as:

$$I_a(z) = \begin{cases} \gamma(z)T_a(z) & \text{at microwave range,} \\ \gamma(z)B(T_a) & \text{at infrared range.} \end{cases}$$

2.9 An Adaptive Technology to Classify and Interpret Remote-Sensing Data of the Water Surface Qualitatively

Collecting and processing information in a geoinformation monitoring system can only be done by effective monitoring of the object under consideration and involves using simulation modeling, information collecting, and information processing (Armand et al. 1987; Burkov and Krapivin 2009).

From the position of system analysis, the system of collection and processing of the information in geoinformation monitoring represents the structure uniting the computers of various classes, databases and the advanced problem-oriented software. Creation of such system demands the development of formalized description of the information flows and unique methodology of its processing.

Development of geoinformation monitoring systems requires the decision of a set of problems related to the formation of data measurement flows to be solved. The problem of classification of aquatories using the remote sensing measurements is one of important among them. Various algorithms of the theory of image recognition, statistical decisions and cluster analysis are used to solve this problem.

At the present time, there are many image recognition methods, mainly because of the variety of statements about concrete tasks. The problem of recognition consists in the division of some group of objects into the classes at the base of certain requirements. The objects having general properties are related to one class. An initial data for the solution of a recognition problem are results of some observations or the direct measurements that are named initial attributes.

Method of taxonomy (clustering) is one of the important methods of recognition and classification of images.

Let's assume set of M it is required to divide by not crossed subsets (clusters), and the elements included in the same clusters should be close to each other enough from the point of view of the chosen criterion of nearness, and elements from different clusters should be far enough from each other. In one of many possible statements of this task two numbers, a and b ($0 < a < b$), are given. It is considered, that two elements x and y are close to each other enough, if $p(x, y) < a$, and are far enough from each other, if $p(x, y) > b$.

King's method is well known in taxonomy and gives good results when the quantity of available information in assumed clusters is moderate. According to this method the distance between groups of points in space of attributes is defined as distance between centers of masses of these groups. Clustering in this case is based on the assumption that sites of the increased density in the space of attributes correspond to similar situations.

The feature of remote measurements is information acquisition, when the data of measurements, acquired during tracing of flying system along routes of survey, are directed to input of the processing system. As result the two dimensional image of investigated object is registered. Statistical model of spottiness for investigated space is one of models for this image.

In real conditions, the study of spots, the acquiring of their statistical characteristics and their using in a problem of detection is enough a complex problem. Criteria have to be developed to distinguish spots from other phenomena. For example, it is necessary to determine such threshold the exceeding of which is the spot indicator. Also it is necessary to develop model presentation of processes of spots detection.

The method of the thresholds determination is the most obvious and simple way for spots definition. In this case that part of space belongs to area of spots, on which the parameter of environment measured within the chosen channel exceeds value (I^+) or, on the contrary, does not exceed value (I^-) a threshold. Let $y = y(x_1, x_2)$ is function of coordinates (x_1, x_2) of points within considered region. If “level surface” $y = \text{const}$ is outlined at the region surface, then the closed curves of level y that bound the spots are projected on it.

Algorithms for simulation of spottiness are based on the numerical solution of the algebraic inequalities determining coordinates of internal points of spots. It is impossible to write the equation of spots contours in a general.

Therefore contours of spots are described by system of the simple algebraic equations connected among themselves by equation $\Sigma \varphi_i(x, y) = 0$, where $\varphi_i(x, y)$ is the equation of an elementary curve. For simplification of software realization of simulation of spottiness image as the equations $\varphi_i(x, y)$ the equation of a circle with varied coordinates of the centre and radius is accepted. Complex forms of spots are formed by overlapping on a plane of the drawing of several circles with different parameters that is defined by system of inequalities of a kind:

$$\sum \left\{ (x - a_i)^2 + (y - b_i)^2 - r_i^2 \right\} \leq 0$$

where x, y are the cartesian coordinates of internal points of spots, a_i, b_i , and r_i are coordinates of the centre and radius i th circle, respectively, n is quantity of the circles composing the modeled image.

To simulate the randomness of background distribution for spottiness the spottiness model parameters a_i, b_i , and r_i are set by means of random-number generators. By changing laws of distribution of random numbers and their statistical parameters, it is possible to receive statistically different spottiness images.

The list of software items of the simulation system for classification of the phenomena on a terrestrial surface is given in Table 2.21. An important point about the system’s algorithms and the software is the possibility of spatial interpolation and data restoration using remote and in situ measurements.

One of main aspects of the practical importance of developed system is qualitative interpretation and visualization of results of remote measurements.

For primary processing of remote measurements it is useful to apply an overage-connecting method of cluster analysis to detect the specific informational zones. That method is effective under small volumes of sampling. Two variants of this approach can be brought about by the way in which algorithms and index spaces are organized.

Table 2.21 Software modules of the simulation system for classification of the phenomena on a terrestrial surface

Software	The functional characteristic of a software
REICM	Reduction of the experimental information in a computer memory
DRHIM	Data reconstruction by means of the harmonics interpolation method
SIDSM	Spatial interpolation of the data by means of a spline method
DRMOT	A method of optimal interpolation
CASRS	Cluster analysis focused on sings space of remote sensors
CALRS	Cluster analysis focused on the account of local reading of sensors
RSC	Research of spottiness characteristics
RRAMDA	Realization of recognition algorithm by a method of the discriminant analysis
CSAIRM	Sorting and accumulation of the in-situ and remote measurements
CMS	Computer mapping of the spots

In the system designed to classify phenomena on a terrestrial surface automatically the two variants of this approach are program modules CASRS and CALRS, distinguished by the way in which attribute spaces and comparison algorithms are organized.

Software item CASRS is focused on the attribute space of remote sensors. The CALRS module allocates areas of equal instability based on local variations in sensor data. Distinction between the algorithms of comparison in these items consists in the taking into account or neglecting of interrelations of the neighbouring counts of sensors. Item CASRS forms clusters without taking into account a geographical generality of radiometers indications. Item CALRS forms continuous spatial clusters.

CASRS and CALRS automatically exclude from consideration the calibrations information. Item CASRS consists from six groups of operators. The first group carries out the organization of data files. Averaging of the information using final set of radiometer readings is made by the second group of operators. The third group of operators finds minimal cluster distances then two points on which this distance is realized are allocated. The fourth group of operators investigates changes of minimal cluster distances on the given step of procedure and in case of occurrence of sharp changes carries out visualization of clusters structure. The fifth group of operators unites the nearest clusters and recalculates their characteristics. The sixth group of operators develops a criterion for the algorithm to stop.

Analysis of statistical characteristics of “spottiness” for three types of areas of Atlantic and Pacific oceans was conducted. These statistical characteristics were determined for the most informative thresholds. At that time statistical characteristics of “spottiness” for the same areas, selected using criteria of minimal value of coefficient of correlation for joint sample of positive and negative spots. Analysis of these characteristics showed, that the statistical characteristics of “spottiness” coincide for areas with temperate sea roughness and storm zones. Minimum for the coefficient of correlation ρ_{\min} is run down for a case of most informative thresholds. But for quiet area the situation is different.

From the aforesaid follows that statistical characteristics for “spottiness” of brightness temperatures in microwaves can be used for detection and classification of the phenomena on a surface of the ocean that was caused by a degree of sea roughness.

Analysis of empirical histograms for spottiness of brightness temperatures in microwaves shows that in most cases (I^+ , I^-) are characteristics that can be coordinated with the exponential distribution while their amplitude can be coordinated with the normal distribution. Therefore, to detect and classify phenomena on ocean surfaces it is necessary to apply the best possible algorithms when programming/teaching the computer to make statistical decisions about distributions.

2.10 A Device to Measure Geophysical and Hydrophysical Parameters

According to algorithms of the multi-channel microwave monitoring discussed by Krapivin and Shutko (2012), it is possible to promptly measure the wind speed, sea surface roughness and water temperature as the base characteristics to calculate other parameters of the environment. From these measurements, a mutual control of the accuracy of correction of the estimates of the atmosphere-ocean gas exchange is realized. Solution of the correction equations in a general case requires the use of the criterion of discrepancy between theoretical and empirical estimates of the parameters or correlations. Usually for this purpose, a criterion of mean square deviation is used. The reliability and efficiency of determination of solutions for the system of equations relating the theoretical and empirical estimates can be increased if their dispersive characteristics are taken as a criterion of discrepancy of these solutions (Nitu et al. 2013a).

Let the proper emission of the sea be measured simultaneously with the help of n radiometers, each operating at a fixed wavelength λ_j ($j = 1, \dots, n$). As a result at the moment t_i at the output of each radiometer the values Z_{ij} ($i = 1, \dots, M$) are fixed, so that $Z_{ij} = T_j + \xi_{ij}$, where T_j is the brightness temperature of a sea site at the wavelength λ_j , and ξ_{ij} is the random value (noise) with the zero mean and dispersion σ_j^2 .

Let the correlation between the brightness temperature and m parameters of the sea be linear:

$$\begin{aligned} A_{11}x_1 + \dots + A_{1m}x_m &= T_1 + \xi_1 \\ &\dots \\ A_{n1}x_1 + \dots + A_{nm}x_m &= T_n + \xi_n \end{aligned} \quad (2.11)$$

where A_{ij} are the coefficients determined in the regime of monitoring the sea site with the known parameters $\{x_i\}$. The x_i^* parameter should be estimated for the x_i^0 parameters so that, first, the average x_i^* coincided with the accurate solution of the system (2.11), that is, $\bar{x}_i^* = x_i^0$ ($i = 1, \dots, m$), and second, a dispersion of the x_i^*

estimate was at a minimum, that is, $D[x_i^*] \leq D[\tilde{x}_i]$, where \tilde{x}_i is the estimate of the x_i^0 parameter obtained by any other method.

And finally, third, let the procedure of estimation of the x_i^* parameters be as simple as possible and permit to judge about the best discrete set of radiometric channels needed to realize the two conditions above.

Let the totality of the x_i^* estimates meeting these conditions be σ -solution of the system of linear equations with the disturbed right-hand part. Multiply step by step the i th solution of the system (2.11) by c_{1i}, \dots, c_{mi} , and let

$$\sum_{i=1}^n c_{ji} A_{il} = \delta_{jl}, \quad (2.12)$$

where

$$\delta_{jl} = \begin{cases} 1 & \text{for } j = l \\ 0 & \text{for } j \neq l \end{cases}$$

As a result, we have

$$x_1^0 = \sum_{i=1}^n c_{1i} T_i, \quad \tilde{x}_1 = \sum_{i=1}^n c_{1i} T_i + \sum_{i=1}^n c_{1i} \xi_i, \quad D[\tilde{x}_1] = \sum_{i=1}^n c_{1i}^2 \sigma_i^2$$

For \tilde{x}_i ($i \geq 2$) we write similar relationships. Derive an auxiliary expression:

$$\varphi(c_{11}, \dots, c_{1n}) = \sum_{i=1}^n c_{1i}^2 \sigma_i^2 + \mu_1 \left(\sum_{i=1}^n c_{1i} A_{i1} - 1 \right) + \sum_{j=2}^m \mu_j \sum_{i=1}^n c_{1i} A_{ij},$$

where μ_j are the non-estimated Lagrange multipliers. Putting first derivative functions φ to zero, we obtain:

$$2c_{1k} \sigma_k^2 + \sum_{j=1}^m \mu_j A_{kj} = 0 \quad (k = 1, \dots, n)$$

These equalities together with conditions (2.12) form the system $(m + n)$ of equations whose solution enables one to find desired optimal values of c_{ij}^* . As a result, $D[x_1] = -\mu_1/2$, and the remaining μ_j ($j \geq 2$) values meet a system $m \times n$ of equations:

$$\sum_{j=1}^m \mu_j \sum_{i=1}^n A_{ij} A_{il} \sigma_i^{-2} = -2, \quad \sum_{j=1}^m \mu_j \sum_{i=1}^n A_{ij} A_{il} \sigma_i^{-2} = 0, \quad (l = 2, \dots, m)$$

For $m = 2$ we have:

$$\begin{aligned}
c_{1,k}^* &= \left(A_{k1} \sum A_{i2}^2 / \sigma_i^2 - A_{k2} \sum_{i=1}^n A_{i1} A_{i2} / \sigma_i^2 \right) \Delta^{-1} \sigma_k^{-2}, \\
c_{2,k}^* &= \left(A_{k2} \sum A_{i1}^2 / \sigma_i^2 - A_{k1} \sum_{i=1}^n A_{i1} A_{i2} / \sigma_i^2 \right) \Delta^{-1} \sigma_k^{-2}, \\
\Delta &= \sum_{i=1}^n A_{i1}^2 \sigma_i^{-2} \sum_{i=1}^n A_{i2}^2 \sigma_i^{-2} - \left(\sum_{i=1}^n A_{i1} A_{i2} \sigma_i^{-2} \right)^2, \\
x_j^* &= \sum_{i=1}^n c_{ji}^* Z_i, \quad (j = 1, 2); \quad D[x_1^*] = \Delta^{-1} \sum_{i=1}^n A_{i2}^2 \sigma_i^{-2}; \\
D[x_2^*] &= \Delta^{-1} \sum_{i=1}^n A_{i1}^2 \sigma_i^{-2}
\end{aligned}$$

For the real use of this algorithm in the radiometric monitoring system the following arrangement can be suggested. Put the n -channel commutation unit and n units of dispersion calculation between the outputs of radiometers and respective inputs of the microprocessor in series. At the radiometers' inputs we plug in switches, which are connected through a control unit with the first group of outputs of the microprocessor, and to the second group of the microprocessor's outputs are linked up the *resolver*, whose second group of outputs is connected, respectively, with the radiometers' outputs. Each unit to calculate dispersion consists of the in-series connected quantizers of the mean value calculator, divisor, summator and second divisor, and the quantizers output is connected with the second input of the summator. The *resolver* consists of identical channels, each containing a summator, n outputs of which are connected with n multipliers. Some inputs of the multipliers form the first group of the *resolver's* inputs, others—the second group of its inputs, the number of channels being equal to the number of the parameters to be measured.

Figure 2.34 shows the structural scheme of an arrangement to measure the parameters of geophysical and hydrophysical objects. The scheme in Fig. 2.35 explains the structure of the unit to calculate dispersion. The *resolver* is characterized in Fig. 2.36. The apparatus operates as follows. When radiometers 1 are calibrated, the signals Z_{ij} from their outputs through the multi-channel switching unit 2 enter the unit 3 of the dispersion calculator. The antennas are switched off from radiometers. In unit 3 the dispersion is calculated using the algorithm.

$$\sigma_j^2 = \frac{1}{M-1} \sum_{i=1}^M (Z_{ij} - M_j), \quad M_j = \frac{1}{M} \sum_{i=1}^M Z_{ij}$$

The M_j parameters are calculated in the units of the mean calculations. The summator calculates:

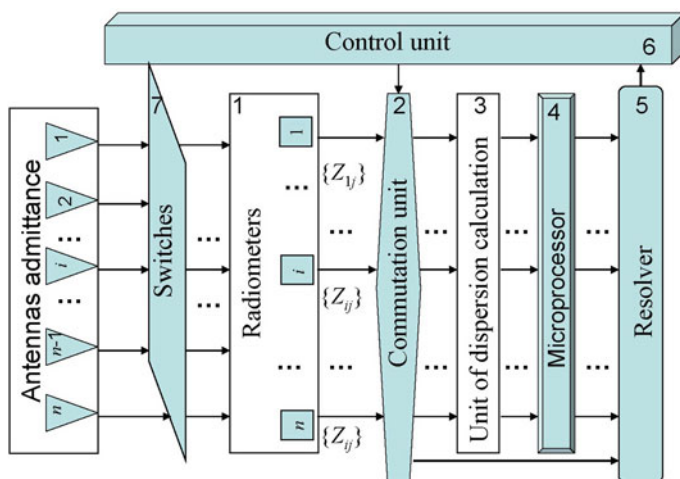
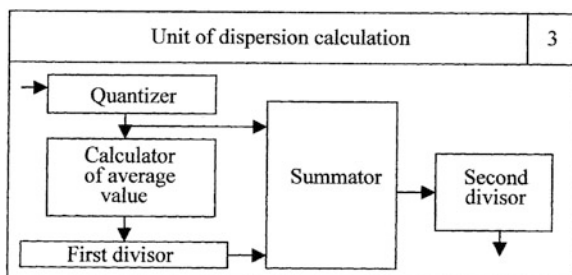


Fig. 2.34 The structural scheme of the arrangement to measure the geophysical and hydrophysical parameters in the regime of the microwave monitoring

Fig. 2.35 Scheme of operations in the unit of dispersion calculation

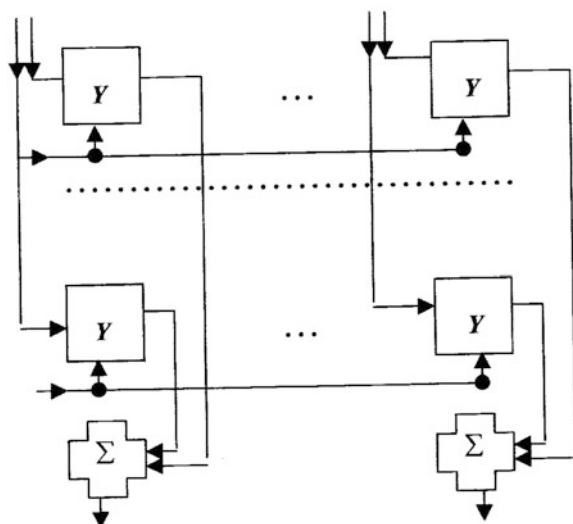


$$\sum_{i=1}^M (Z_{ij} - M_j)$$

The calculated values σ_j^2 enter the microprocessor 4 to calculate partial coefficients c_{jl} . From the first group of its outputs they enter the *resolver* 5 where they are used to solve a system of equations, and from the second group of outputs they enter the control unit 6 which forms the signal that switches off radiometers 1, for which the partial coefficients are equal or close to zero, that is, the information channels automatically get excluded. At the same time, the systems of equations to be solved get compressed. This step makes it possible to contract not only the volume of calculations but also to increase the accuracy of estimating the parameters of the environmental objects being sounded.

Fig. 2.36 Resolver. *Note*

Y = multiplier,

 Σ = accumulator

Once dispersions have been determined, the commutator 2 blocks the input of data from non-information channels. The data from information channels enter the *resolver* 5. The signal at the multiplier's output corresponds to the value of one of the parameters to be estimated.

2.11 Direct and Inverse Problems of Microwave Monitoring

2.11.1 Typical Inverse Task of the Microwave Radiometry

An approach to the inverse problem of microwave monitoring is based on assuming a linear functional correlation between radiobrightness contrasts and the characteristics of the monitored object. The search of analytical relationships relating the radiobrightness temperature of the environment to its thermodynamic and electro-physical characteristics covers more general classes of the functional models. The most general form of such dependence is as follows:

$$T_{bi} = \kappa_i \int_0^{\infty} T(h) \gamma_i(h) \exp \left[- \int_0^h \gamma_i(x) dx \right] dh, \quad (2.13)$$

where $T(h)$ is the thermodynamic profile of the environment, T_{bi} is the radiobrightness temperature at the frequency ν_i , $\gamma_i(h)$ is the profile of the absorption coefficient of the environment, κ_i is the emissivity of the environment.

Relationship (2.13) makes it possible using $T(h)$ and $\gamma_i(h)$ to find T_{bi} (direct problem) and by T_{bi} to calculate $T(h)$ and $\gamma_i(h)$ (inverse problem). The proposed method to solve these problems is based on the use of $T(h)$ and $\gamma_i(h)$ and their derivatives at the point $h = 0$ with some additional limitations resulting from the transformations made below. Write the relationship (2.13) in the form:

$$T_{b\lambda} = -\kappa_\lambda \int_0^\infty T(h) dF_\lambda(h), \quad (2.14)$$

where

$$F_\lambda(h) = \exp \left[- \int_0^h \gamma_\lambda(x) dx \right]$$

λ is the wavelength.

Integrating (2.14) by parts, we obtain:

$$T_{b\lambda} = \kappa_\lambda \left[T_0 + \int_0^\infty T'(h) F_\lambda(h) dh \right] = \kappa_\lambda [T_0 + J_1] \quad (2.15)$$

Let $J_1 = 0$, then $T_{b\lambda} = \kappa_\lambda T_0$. If $dT(h)/dh \equiv 0$, then $J_1 = 0$. Therefore find conditions under which $J_1 = 0$. Let the following relationships be valid:

$$\gamma_\lambda(h) \equiv c_\lambda > 0, \quad T(h) = \sum_{k=0}^n B_k h^k \quad (2.16)$$

It follows from (2.16) that if the coefficients B_k meet the condition:

$$\sum_{k=1}^n k! \frac{B_k}{c_\lambda^k} = 0, \quad (2.17)$$

then $J_1 = 0$.

Integrating (2.15) by parts, we obtain:

$$T_{b\lambda} = \kappa_\lambda \left[T_0 + \frac{T'_0}{\gamma_\lambda(0)} + \int_0^\infty \frac{T''(h)\gamma_\lambda(h) - \gamma'_\lambda(h)T'(h)}{\gamma_\lambda^2(h)} F_\lambda(h) dh \right] \quad (2.18)$$

Equate the integral in (2.18) to zero. It gives

$$T(h) = c \int \gamma_\lambda(h) dh,$$

where c is an arbitrary constant. The integral in (2.18) will be equal to zero if

$$\sum_{k=2}^n B_k k(k-1)k!c_\lambda^{1-k} = 0 \quad (2.19)$$

Further integrating of (2.18) by parts gives

$$T_{\mathcal{H}\lambda} = \kappa_\lambda \left[T_0 + \frac{T'_0}{\gamma_\lambda(0)} + \left(\frac{T'}{\gamma_\lambda(h)} \right)' \frac{1}{\gamma_\lambda(h)} \Big|_{h=0} + J_3 \right],$$

where

$$J_3 = \int_0^\infty \frac{T'''(h)\gamma_\lambda(h) - 3T''(h)\gamma'_\lambda(h) - T'(h)\gamma''_\lambda(h) + 3T'(h)[\gamma'_\lambda]^2}{\gamma_\lambda^4} F_\lambda(h) dh$$

This integral will be equal to zero at

$$T(h) = c \int \gamma_\lambda(h) \int \gamma_\lambda(u) du dh$$

If the condition (2.16) is not met then $J_3 = 0$ at

$$\sum_{k=3}^n B_k k(k-1)(k-2)k!c_\lambda^{2-k} = 0$$

With the process of integration of (2.18) continued N times, we obtain

$$T_{\mathcal{H}\lambda} = \kappa_\lambda \left[\sum_{k=1}^N P_k(0) + \int_0^\infty P'_N(h) F_\lambda(h) dh \right], \quad (2.20)$$

where

$$P_1(h) = T(h), \quad P_2(h) = T'(h)/\gamma_\lambda(h) \dots, \quad P_k(h) = P'_{k-1}(h)/\gamma_\lambda(h)$$

but

$$J_N = \int_0^\infty P'_N(h) F_\lambda(h) dh = 0$$

for

$$\sum_{k=N}^n B_k k(k-1) \cdots (k-N+1) k! c_\lambda^{N-1-k} = 0, \quad (n > N)$$

Consider the case when

$$\gamma_\lambda(h) = \exp\{c_\lambda h\}$$

From (2.20) we obtain:

$$T(h) = \sum_{k=0}^{N-1} B_k \exp[kc_\lambda h]$$

Now we move on to the inverse problem. Let measurements be made at wavelengths $\lambda_1, \dots, \lambda_N$. Solve the equation:

$$P'_{N-1}(h) = c\gamma_\lambda(h)$$

and find

$$P_{k-1}(h) = \int \gamma_\lambda(h) P_k(h) dh, \quad (k = 1, \dots, N)$$

Let $\gamma_\lambda(h) = \varphi(\lambda)\psi(h)$, that is, the dependence of the absorption coefficient on the frequency and depth of the layer be divided by the product of the known function $\varphi(\lambda)$ and an unknown function $\psi(h)$. As a rule, the function $\varphi(\lambda)$ is set from the empirical table and its analytical approximation can be constructed. Then, excluding from (2.20) the second right-hand term (it is equal to zero), we write the relationship:

$$T_{b\lambda} = \kappa_\lambda \sum_{k=1}^N T^{(k-1)}(0) F_k \left[\varphi(\lambda), \psi^{(N-k-1)}(0), \dots, \psi'(0), \psi(0) \right] \quad (2.21)$$

and the solution of the inverse problem is reduced to the solution of a system of algebraic equations with regard to functions:

$$T(0), T'(0), \dots, T^{(N-1)}(0), \psi(0), \dots, \psi^{(N-1)}(0)$$

Consider the case $\psi(h) = \text{const}$, that is, $\gamma_\lambda = \varphi(\lambda) > 0$. Equation (2.21) is re-written:

$$T_{b\lambda} = \kappa_\lambda \sum_{k=1}^N T^{(k-1)}(0) / \varphi^{(k-1)}(\lambda) \quad (2.22)$$

In the simplest version, if $T_{b\lambda}$ was measured at N different wavelengths $\{\lambda_i; i = 1, \dots, N\}$, then the determinant of the system (2.22) will be equal to:

$$\Delta = \prod_{i=1}^N \kappa_i \prod_{i>k}^N [\varphi(\lambda_i) - \varphi(\lambda_k)] / [\varphi(\lambda_i)\varphi(\lambda_k)]$$

If $\varphi(\lambda_i) \neq \varphi(\lambda_k)$ with none of combinations $i \neq k$, then $\Delta \neq 0$ and the system (2.22) has a single solution. Now let

$$\psi(h) = h^m$$

Then, it follows from (2.20) that

$$T(h) = \sum_{k=0}^{N-1} B_k h^{k(m+1)}$$

and we obtain a system of algebraic equations

$$P_k(0) = (m[k-1])_{(m+1)}! \dots! b_{k-1} / \varphi^{k-1}(\lambda)$$

with the following determinant:

$$\Delta = \prod_{i=1}^N \kappa_{\lambda_i} \prod_{p=1}^N [m(k-1)]^{N+1-p} \prod_{t>k}^N [\varphi(\lambda_t) - \varphi(\lambda_k)] / [\varphi(\lambda_t)\varphi(\lambda_k)]$$

The case when the function ψ is approximated by a polynomial is considered in a similar way.

2.11.2 Estimation of Radiobrightness Response Function of the Ocean-Atmosphere System on Variations in Heat Fluxes

The problem of using the satellite passive microwave radiometric methods for the analysis of the roles of the ocean and atmosphere (in respect of their priority) in heat interaction over various space and time scales is one of important for solution in tropical cyclogenesis. This problem is long attracts the specialists engaged in the oceanology, meteorology, atmospheric sciences, etc. Some data of measurements from the Meteor-3M MTVZA device (Module of Temperature and Vlazhnost (humidity) Zonding of the Atmosphere), data of the DMSP (SSM/I) and EOS-Aqua (AMSR-E) radiometers can be used for solving this problem.

The phenomena of a time delay of the ocean/atmosphere system brightness temperature response in the resonant spectral domains 5.9 and 13.5 mm on the variations of surface heat fluxes is described by the Duamel's integral equation:

$$T_b(t, \lambda) = \int_0^t q(\tau) r(t - \tau) d\tau \quad (2.23)$$

where $T_b(t, \lambda)$ is radiobrightness temperature for wavelength λ (K), $q(t)$ is heat flux on the ocean-atmosphere interface ($\text{W/m}^2/\text{h}$), τ is time delay (hours), $r(t)$ is response delay function ($\text{K}/(\text{W/m}^2/\text{h})$).

Solution of Eq. (2.23) can be theoretically realized by traditional methods which are used for solution of inverse tasks in the form of integral equation of the first type. But in real case, functions $T_b(t, \lambda)$ and $q(t)$ have discrete form as restricted in the time numerical sets. Therefore, traditional methods such as Laplace transformation or iterative procedure (Tricomi 1960) lead to large errors. More effective method for solution of Eq. (2.23) was proposed by Grankov and Soldatov (2005). It consists in the use of exponential approximation:

$$r(t) = \sum_{i=1}^N a_i \exp(-b_i t)$$

where coefficients a_i and b_i are defined from condition:

$$M = \min_{\{a_i, b_i\}} (1/n) \sqrt{\sum_{i=1}^n [T_{\mathcal{R}}(t_i) - F(t_i)]^2},$$

where $t_i = i\Delta t$,

$$F(t_i) = \sum_{s=0}^{i-1} q(t_i - t_s) \sum_{k=0}^N (a_k/b_k) \exp(-b_k t_s) [1 - \exp(-b_k \Delta t)]$$

Numerical calculations in Fig. 2.37 show that such approach to solution of Eq. (2.23) gives errors no more 5–7 %. We see that time delay exists between radiobrightness temperature and heat flux. This is important for calibration of satellite measurements. Calculation of the function $r(t)$ of the brightness temperature T_b response (sensitivity) to the total heat fluxes q the variation is clearly demonstrated. In this case, brightness temperatures were calculated from the oceanographic, meteorological, and aerological data, observed in the experiment with ATLANTEX-90 synchronized with use of the DMSP F-08 heat fluxes data q obtained from the vessel *Victor Bugaev* during the cyclone of 9–13 April 1990.

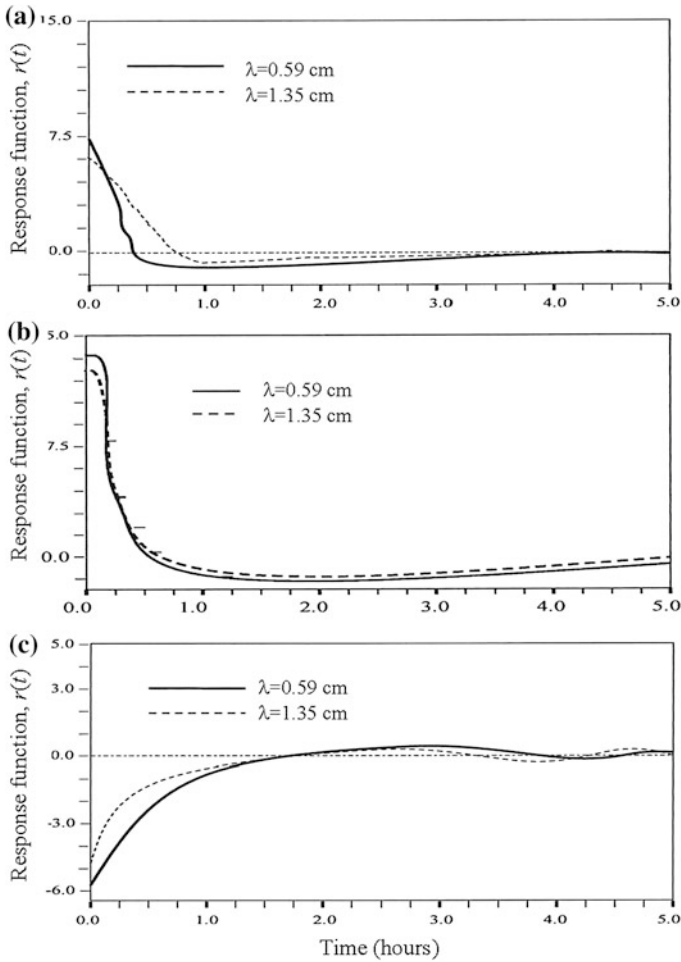


Fig. 2.37 Calculation of response function $r(t)$ ($\text{K}/(\text{W}/\text{m}^2/\text{h})$) as solution of Eq. (2.66) for measurement data received by ships Bugaev (a), Volna (b) and Musson (c) during ATLANTEX-90

2.12 Algorithms for Remote Data Processing

2.12.1 Introduction

Spatial reconstruction of the vegetation radiometric image, based on fragmentary data, demands the development of new algorithms. There exist many approaches to this task. For example, Yoshioka (2004) discussed the problem of extraction of useful information from satellite imagery by means of algebraic manipulation. The concept of vegetation isolines was underpinned for the three-layer system

Table 2.22 Assessments of standard value for parameter R_0 that is used for statistical regulation of experimental measurements (Dally et al. 1984)

n	2	3	4	5	7	10	25	50	100	300	500
R_0	1.15	1.38	1.54	1.65	1.80	1.96	3.33	2.57	2.81	3.14	3.29

soil-canopy-atmosphere. The relationship between the reflectances at two different wavelengths (650 and 940 nm) over this system comprising atmosphere, canopy, and soil layers was derived. Below several algorithms are proposed.

Realization of measurements usually is connected with complex model choice and its planning. Evaluation of initial data and coefficients for model needs the statistical method application. Here, the task of representative sampling definition is arisen. Important problem consists in the choice of criterion that gives a possibility to form this sample. One of possible criterion is based on calculation of value of $R = (\xi_i - \bar{\xi})/S_{\xi}$, where $\bar{\xi}$ is the average value,

$$S_{\xi}^2 = \frac{1}{n} \sum_{i=1}^n (\xi_i - \bar{\xi})^2$$

Formation of representative sampling is realized with the following rule: if $R \leq R_0$ then ξ_i is registered and is taken into account as effective signal; if $R > R_0$ then ξ_i is considered as noise and does not fix into set $\{\xi_i\}$. Parameter R_0 is defined in Table 2.22.

It is evident that statistical data that is used to draw conclusions and inferences should be accurate and consistent. This is important in order to ensure the validity of all the inferences drawn on the basis of the raw data. Statistical analysis as a research methodology for ecological studies comes into collision with the problem of raw data non-stationary what needs new approaches and tools for the decision making and scientific conclusions.

2.12.2 Data Reconstruction Using the Harmonic Functions

The process of spreading of heat in the plane homogeneous media G with constant thermophysical characteristics (density ρ , specific heat C and conductivity coefficient K ; $\rho, C, K = \text{const} > 0$) is described by the equation:

$$\partial T / \partial t = a^2 (\partial^2 T / \partial \varphi^2 + \partial^2 T / \partial \lambda^2), \quad (2.24)$$

where $T = T(\varphi, \lambda, t)$ is the temperature of the media at the point with spatial coordinates $(\varphi, \lambda) \in G$ at time t ; $a^2 = K/C\rho$ is the temperature-conductivity coefficient of G , φ and λ are the latitude and longitude respectively.

If the thermal transport process is stationary then Eq. (2.24) transforms to the Laplace equation:

$$\operatorname{div} \cdot \operatorname{grad} T = \partial^2 T / \partial \varphi^2 + \partial^2 T / \partial \lambda^2 \quad (2.25)$$

The solution of Eq. (2.25) is the harmonic function of the spatial coordinates φ and λ . In accordance with the Rayleigh-Jeans law (DeWitt and Nutter 1988) the brightness temperature as a result of remote microwave measurements is $T_a(\varphi, \lambda) = T_a(\varphi, \lambda, \mu, \theta)$, where μ is the wavelength, θ is the observation angle and $(\mu, \theta = \text{const})$. It is proposed that for the any small area V_M at an arbitrary point $M \in G$ the brightness temperature is a linear function of the temperature of the media:

$$T_a(\varphi, \lambda) = A_M + B_M T(\varphi, \lambda); \quad (\varphi, \lambda) \in V_M, \quad (2.26)$$

where A_M and B_M are constants.

Formula (2.26) follows from the theoretical and experimental estimations of T_a (Krapivin and Potapov 2001; Burkov and Krapivin 2009). For media which are homogeneous in depth, the formula $T_a = \kappa T$ is valid. Here $\kappa = \kappa(\mu, \theta, \varepsilon)$ is the media radiation coefficient where ε is the dielectrical permeability. According to the experimental estimations the radiance of fresh water measured by means of radiometers with wavelengths of 5–8 cm is a linear function of T . The slope of this dependence is 0.35–0.50 K/°C. An increase in the water salinity S from 0 to 16 ‰ is accompanied by a decrease in the sensitivity of the irradiation field to the temperature variations. This effect is observed for wavelengths from 10 to 50 cm. The sensitivity of the irradiation field to variations in T is a minimum when the following conditions are realized: $\mu S \cong 700$; $0 \leq T \leq 30$ °C; $0 \leq S \leq 180$ ‰; $0 \leq \theta \leq 25^\circ$.

From Eq. (2.26) it follows that T_a at every point $M \in G$ satisfies the following condition:

$$T_a(\varphi, \lambda) = \frac{1}{2\pi} \int_0^{2\pi} T_a(\varphi + r \cdot \cos a, \lambda + r \cdot \sin a) da,$$

where the integral is over a circle of radius r centered at (φ, λ) .

This condition is valid for any r ($0 < r < r_M$) where r_M is the radius of the area V_M . Therefore T_a is a harmonic function within G . A typical task here is the search of the harmonic function $T_a(\varphi, \lambda)$ within G when $T_a(\varphi, \lambda) = \tilde{T}_a(u)$ on the boundary Γ of G ($u \in \Gamma$, $u = \varphi + i\lambda$). Such a function is the real part of some analytic function $W(z)$ given by:

$$W(z) = \frac{1}{2\pi} \int_{\Gamma} \mu(\zeta) / (\zeta - z) d\zeta, \quad (2.27)$$

where $\mu(\zeta)$ is the real density, $\zeta \in \Gamma$ and $z = \varphi + i\lambda$ is an arbitrary internal point of G . We have $\operatorname{Re}[W(u)]$ and $\operatorname{Im}[d\zeta/(\zeta - u)] = -\cos(r, n) d\sigma/r$ where r is the distance between ζ and u , $d\sigma$ is an element of Γ and n is the external normal to Γ . As $z \rightarrow u \in \Gamma$, $\mu(u)$ is approximated by the solution of the integral equation:

$$\mu(u) - \frac{1}{\pi} \int_{\Gamma} \mu(\zeta) r^{-1} \cos(r, n) d\sigma$$

When G is the circle $|z-z_o| < R$ the solution of this task is the Poisson integral:

$$T_a(r, \psi) = \frac{1}{2\pi} \int_0^{2\pi} \tilde{T}_a(a) \frac{R^2 - r^2}{R^2 + r^2 - 2Rr \cos(\psi - a)} da,$$

where $\varphi + i\lambda = z_o + re^{i\psi}(r < R, 0 \leq \psi \leq 2\pi)$; and

$$\tilde{T}_a(a) = \tilde{T}_a(z_0 + R \cdot e^{ia}), \quad 0 \leq a \leq 2\pi.$$

The combination of this procedure with other algorithms of spatial-temporal interpolation gives a full representation of the environmental objects on the observation area by means of the parametrical estimations. For example, the GIMS database was formed on the basis of the measurements traced by the flying laboratory using the set of analogous harmonic algorithms. Table 2.23 illustrates the

Table 2.23 An example of the hydrophysical field reconstruction in the lagoon Nuoc Ngot

U (m ³ s ⁻¹)	M (m ³ s ⁻¹)	Error (%)	R (m ³ s ⁻¹)	Error (%)
10.3	11.3	10.1	11.6	12.9
−4	−3.6	9.5	−4.4	9.8
−8.7	−15.3	12.4	−9.9	13.3
−14.2	−12.3	13.1	−16	12.6
−24.1	−22.7	5.7	−22.2	7.7
−22.4	−24.4	8.9	−20.4	9
−16.3	−17.9	9.6	−18.2	11.5
2.3	2.6	11.5	2	11.4
15	13.2	12.3	12.6	15.8
35.1	30.9	12.2	30.1	14.2
39.2	35.1	10.4	43	9.7
38.2	42.6	11.6	33.2	13.1
34.8	39.6	13.8	30	13.7
26.5	25.2	4.8	28.5	7.6
19.2	21.1	9.9	21.2	10.3
Average error (%)	10.4	−	11.5	−
Maximal error (%)	13.8	−	15.8	−
Minimal error (%)	4.8	−	7.6	−

Field measurements was realized during March–April of 2001. Signs correspond to the water inflow (“+”) and outflow (“−”). This lagoon is situated in the Central Vietnam, South-China Sea U is the measured value of water flow (m³ s⁻¹) on the boundary *lagoon-sea*, M and R is the calculated values of this flow with the methods differential approximation and harmonic functions, respectively

precision of this algorithm as compared with the measured values and the differential approximation method.

2.12.3 Method for Parametric Identification of Environmental Objects

Radiometers determine the brightness temperatures Z_{ij} ($i = 1, \dots, M; j = 1, \dots, n$) given by $Z_{ij} = T_j + \xi_{ij}$, where M is the number of measurements, n is number of radiometers, T_j is the real value of the brightness temperature for wavelength μ_j and ξ_{ij} is the noise with zero mean and dispersion σ_j . The problem is to determine the correlation function $T_j = f_j(X)$, where $X = \{x_1, \dots, x_m\}$ are geophysical, ecological, biogeochemical or other parameters. There are many algorithms for the definition of the function f . As a general rule, the mean-square criterion is used for this purpose. But such an approach has one defect: the impossibility of taking the dispersion properties of the noise $E = \{\xi_{ij}\}$ into consideration.

Let the function f be linear. Then we have the following system of equations for parameters A_{ij} :

$$\| A_{ij} \| X = T + E \quad (2.28)$$

It is necessary to solve Eq. (2.28) such that its solution has minimum dispersion. Such a solution is called the σ —solution.

The i th equation of system (2.28) is multiplied by the set of parameters c_{1i}, \dots, c_{mi} . An additional condition is given:

$$\sum_{i=1}^n c_{ji} A_{il} = \delta_{jl} \quad (2.29)$$

where

$$\delta_{jl} = \begin{cases} 1 & \text{for } j = l \\ 0 & \text{for } j \neq l \end{cases} (l, j = 1, \dots, m) \quad (2.30)$$

Under the conditions (2.29) and (2.30) we have

$$x_1^o = \sum_{i=1}^n c_{1i} T_i \quad (2.31)$$

From (2.28) to (2.31) we obtain:

$$\tilde{x}_1 = \sum_{i=1}^n c_{1i} T_i + \sum_{i=1}^n c_{1i} \zeta_i \quad (2.32)$$

The dispersion of solution (2.32) is

$$D[\tilde{x}_1] = \sum_{i=1}^n c_{1i}^2 \sigma_i^2 \quad (2.33)$$

Dispersions of \tilde{x}_i ($i = 2, \dots, m$) are calculated by analogy with (2.33). To calculate the $\min D[\tilde{x}_1]$ the following additional equation is used

$$\psi(c_{11}, \dots, c_{1n}) = \sum_{i=1}^n c_{1i}^2 \sigma_i^2 + \tau_1 \left(\sum_{i=1}^n c_{1i} A_{i1} - 1 \right) + \sum_{j=2}^m \tau_j \sum_{i=1}^n c_{1i} A_{ij}$$

The first derivatives of ψ are equal to zero, giving the following set of equations:

$$2c_{1k} \sigma_k^2 + \sum_{j=1}^m \tau_j A_{kj} = 0, \quad (k = 1, \dots, n) \quad (2.34)$$

The conditions of (2.29), (2.30) and (2.34) consist of a system of $(m + n)$ equations to be solved.

We have $D[x_j] = \tau_j/2$, where the set of τ_j are defined as solution of the following equations:

$$\sum_{j=1}^m \mu_j \sum_{i=1}^n \frac{A_{ij} A_{i1}}{\sigma_i^2} = -2; \quad \sum_{j=1}^m \mu_j \sum_{i=1}^n \frac{A_{ij} A_{il}}{\sigma_i^2} = 0, \quad (l = 2, \dots, m)$$

These algorithms are used as sub-blocks of the Aral-Caspian Expert System (ACES) (Bondur et al. 2009). The forecast of the ACES state is obtained from the GIMS.

2.12.4 Method of Differential Approximation

Databases of the environment monitoring systems not always correspond to the parametrical fullness in framework of the GIMS technology standard. Therefore an algorithm that allows to adapt the database to this standard is considered. Let us suppose that N characteristics, x_i ($i = 1, \dots, N$), of environment are measured at the times t_s ($s = 1, \dots, M$). Formal dependence between x_i is represented by the system of differential equations with unknown coefficients $\{a_{ijk}, b_{ij}\}$:

$$\frac{d\zeta_i}{dt} = \sum_{k,j=1}^N [a_{ijk}\zeta_j(t)\zeta_k(t) + b_{ij}\zeta_j(t)] \quad (2.35)$$

Putting the initial conditions as

$$\zeta_i(0) \quad (i = 1, \dots, N) \quad (2.36)$$

the reconstruction task of $\zeta_i(t)$ for the arbitrary time $t \in [0, T]$ comes down to the simple task of determining unknown coefficients based on the criterion:

$$E = \sum_{s=1}^M \left\{ \sum_{i=1}^N [\zeta_i(t_s) - \zeta_i(t_s)]^2 / N \right\} / M \quad (2.37)$$

where $0 \leq t_1 \leq \dots \leq t_M \leq T$.

Coefficients $\{a_{ijk}, b_{ij}\}$ can be evaluated as solution of the following optimization task:

$$E_0 = \min_{\{a_{ijk}, b_{ij}, \zeta_i(0)\}} E \quad (2.38)$$

There are many methods to solve this task. One of them is based on the Bellman's dynamic programming method (Bellman and Roth 1966; Krapivin and Kondratyev 2002; Krapivin 1969; Ram 2010). In this case search of minimal value of function E comes to the dynamic programming task. Let us supposed that coefficients $\{a_{ijk}, b_{ij}\}$ are functions of time:

$$Y(t) = \begin{pmatrix} \zeta_1(t) \\ \vdots \\ \zeta_N(t) \\ a_{111}(t) \\ \vdots \\ a_{NNN}(t) \\ b_{11}(t) \\ \vdots \\ b_{NN}(t) \end{pmatrix} \quad (2.39)$$

We can consider that $a_{ijk} = a_{ikj}$. Then adding the system (2.35) Cauchy problem (2.35), (2.36) comes to the following task:

$$dY/dt = G(Y) \quad (2.40)$$

where function G has components:

$$\begin{aligned} G_i(Y) &= 0 \quad \text{for } i = N + 1, \dots, N_c, \\ G_i(Y) &= \sum_{k,j=1}^N [a_{ijk} \zeta_j(t) \zeta_k(t) + b_{ij} \zeta_j(t)] \quad \text{for } i = 1, \dots, N; \end{aligned} \quad (2.41)$$

where $a_{ijk}(0) = \bar{a}_{ijk}$, $b_{ij}(0) = \bar{b}_{ij}$, $N_c = N + N^2 + N^2(N + 1)/2$.

The Newton-Raphson method (Ram 2010) gives a possibility to solve system (2.40), (2.41). Let, introduce series of functions $Y^{(1)}(t), \dots, Y^{(n)}(t)$ such that $Y^{(1)}(t)$ is the first approximation of solution for system equations (2.40). Then, n th approximation is solution of the following linear system:

$$dY_i^{(n)}(t)/dt = G_i[Y^{(n-1)}(t)] + \sum_{j=1}^{N_c} \left\{ dG_i[Y^{(n-1)}(t)]/dY \right\} [Y_j^{(n)} - Y_j^{(n-1)}] \quad (2.42)$$

As it was shown by Bellman and Dreyfus (1962), iterative process (2.42) is convergent by the quadratic law. Solution of Eq. (2.42) is described in the following form:

$$Y^{(n)}(t) = P(t) + \sum_{k=1}^{N_c} C_k H^{(k)}(t) \quad (2.43)$$

where $P(t)$ is the particular solution of the Eq. (2.42), $H^{(k)}(t)$ is vector solution of homogeneous system. To define function $P(t)$ it is needed to solve the Eq. (2.42) under initial conditions: $Y_i(0) = 0$ ($i = 1, \dots, N_c$). Functions $H^{(k)}(t)$ are determined as solutions of the Cauchy problem:

$$dY_i^{(n)}(t)/dt = \sum_{j=1}^{N_c} \left\{ dG_i[Y^{(n-1)}(t)]/dY \right\} [Y_j^{(n)} - Y_j^{(n-1)}] \quad (i = 1, \dots, N_c) \quad (2.44)$$

$$H^{(1)}(0) = \begin{Bmatrix} 1 \\ 0 \\ \vdots \\ 0 \end{Bmatrix}, H^{(2)}(0) = \begin{Bmatrix} 0 \\ 1 \\ \vdots \\ 0 \end{Bmatrix}, \dots, H^{(N_c)}(0) = \begin{Bmatrix} 0 \\ 0 \\ \vdots \\ 1 \end{Bmatrix}, \quad (2.45)$$

As it is followed from Eqs. (2.42)–(2.45), constants C_k are unknown initial conditions of system of equations (2.41). Therefore, constants C_k are defined from condition:

$$E = \sum_{s=1}^M \sum_{i=1}^N \left[P_i(t_k) + \sum_{k=1}^{N_c} C_k H_i^{(k)}(t_s) - \hat{\xi}_i(t_s) \right]^2 = \min_{\{C_k\}} \quad (2.46)$$

Let demand:

$$\partial E / \partial C_k = 0 \quad \text{for } k = 1, \dots, N_c \quad (2.47)$$

From Eqs. (2.46) and (2.47) it is followed that

$$\sum_{k=1}^{N_c} A_{km} C_k + B_m = 0, \quad m = 1, \dots, N_c, \quad (2.48)$$

where

$$A_{km} = \sum_{s=1}^M \sum_{i=1}^N H_i^{(k)}(t_s) H_i^{(m)}(t_s), \quad B = \sum_{s=1}^M \sum_{i=1}^N [P_i(t_s) - \hat{x}_i(t_s)] H_i^{(m)}(t_s)$$

Finally, every iteration of (2.42) needs to solve the system of equations (2.48). Unfortunately, the convergence of this procedure depends on the successful selection of initial conditions.

2.12.5 Quasi-Linearization Method

The number of problems that crop up in ecoinformatics leads to the necessity of integrating generally non-linear integro-differential equations; but, in a majority of cases, these equations are not integrable by elementary or special functions. To solve them, as a rule, it is necessary to make use of the latest achievements of calculating methods and technics. In many problems the use of well-known numerical methods to solve initial value problems—even by means of modern high-speed electronic computers—does not come up with desired results. The existing approximate methods of solving integro-differential equations are based as rule on replacing derivatives by finite differences and represent a complicated multi-step process, which in practical problems cannot be solved on computers reasonably quickly. Therefore in solving practical problems we have to search other means of approximate solutions for integro-differential equations, without using the finite-difference methods.

In the method considered here, the integro-differential equation is substituted in each subinterval of the independent variable by an easily integrable ordinary differential equation with constant coefficients; this method is not a new theoretical idea for it was known to Euler. However, here the error estimations are obtained for the first time, and methods applicable to various problems are developed in detail.

2.12.5.1 Method of Solution and Estimation of Error

Let us consider the equation

$$L[y] - \lambda W[y] = f(x, y), \quad (2.49)$$

$L[y]$ being the differential operator

$$L[y] = \sum_{i=0}^n P_i(x, y, y', \dots, y^{(m_i)}) y^{(n-i)}, \quad (m_i < n) \quad (2.50)$$

and $W[y]$ the generalized Volterra operator

$$W[y] = \int_a^x \sum_{j=0}^r K_j(x, \xi) y^{(j)}(\xi) d\xi, \quad (r < n) \quad (2.51)$$

λ —a real number, $P_i(x, y, y', \dots, y^{(m_i)})$ and $f(x, y)$ —continuous functions with respect to their arguments in the finite interval $[a, b]$, $P_0 \neq 0$ and kernels $K_j(x, \xi)$, $j = 0, 1, \dots, r$ are continuous functions in the region $G\{a \leq \xi \leq x \leq b\}$.

The initial conditions are

$$y^{(s)}(a) = y_0^{(s)}, \quad s = 0, 1, \dots, n-1 \quad (2.52)$$

Assuming that Eq. (2.49) with the initial conditions (2.52) has a unique continuous solution $y(x)$, let us construct an approximate solution $\tilde{y}(x)$ in $[a, b]$. Let us divide the interval $[a, b]$ by a sequence of points $x_0 = a, x_1, \dots, x_m = b$, $h_k = x_{k+1} - x_k$. On each subinterval $[x_k, x_{k+1}]$, $k = 0, 1, \dots, m-1$ let us replace Eq. (2.49) by the following linear differential equation of the n th order with constant coefficients

$$\tilde{L}_k[y] = \lambda \tilde{W}_k[y] + f(x_k, \tilde{y}_k) \quad (2.53)$$

with the initial conditions:

$$y^{(s)}(x_k) = \tilde{y}_k^{(s)}, \quad s = 0, 1, \dots, n-1, \quad (2.54)$$

where

$$\tilde{L}_k[y] = \sum_{i=0}^n P_i(x_k, \tilde{y}_k, \tilde{y}_k', \dots, \tilde{y}_k^{(m_i)}) \tilde{y}^{(n-i)}, \quad (2.55)$$

$$\tilde{W}_k[y] = \sum_{j=0}^r (K_{j,k,0} \tilde{y}_0^{(j)} h_0 + K_{j,k,1} \tilde{y}_1^{(j)} h_1 + \dots + K_{j,k,k} \tilde{y}_k^{(j)} h_k) \quad (2.56)$$

The general solution of Eq. (2.53) is known:

$$\tilde{y} = \tilde{y}(x, c_1^{(k)}, c_2^{(k)}, \dots, c_n^{(k)}), \quad (2.57)$$

where the constants are determined from the initial conditions at the beginning of each interval $[x_k, x_{k+1}]$. The calculations are carried out successively beginning with the interval ($k = 0$).

Let us estimate the error in solution of Eq. (2.49). Let $y(x)$ and $\tilde{y}(x)$ be the exact and the approximate solutions respectively. Let us denote

$$\begin{aligned} \tilde{P}_{ik} &= P_i(x_k, \tilde{y}_k, \tilde{y}'_k, \dots, \tilde{y}_k^{(m_i)}), \quad \tilde{f}_k = f(x_k, \tilde{y}_k), \\ \varepsilon_k &= y(x_k) - \tilde{y}(x_k) \end{aligned} \quad (2.58)$$

Let us integrate times Eqs. (2.49) and (2.53) from x_k to x , and consider the final results for $x = x_{k+1}$. For the sake of convenience and brevity let us denote

$$\int_{x_k}^{x_{k+1}} \int_{x_k}^x \cdots \int_{x_k}^x \varphi(x) dx \cdots_n dx = \int_{x_k}^{x_{k+1}} \varphi(x) dx,$$

we have

$$\begin{aligned} y_{k+1} &= y_k + y_k^{\odot} h_k + h_k^2 \sum_{s=2}^{n-1} y_k^{(s)} \frac{h_k^{s-2}}{s!} - \sum_{i=1}^n \int_{x_k}^{x_{k+1}} P_i y^{(n-i)} dx \\ &\quad + \int_{x_k}^{x_{k+1}} f(x, y) dx + \lambda \int_{x_k}^{x_{k+1}} W[y] dx \end{aligned} \quad (2.59)$$

$$\begin{aligned} \tilde{y}_{k+1} &= \tilde{y}_k + \tilde{y}'_k h_k + h_k^2 \sum_{s=2}^{n-1} \tilde{y}_k^{(s)} \frac{h_k^{s-2}}{s!} - \sum_{i=1}^n \int_{x_k}^{x_{k+1}} \tilde{P}_{ik} \tilde{y}^{(n-i)} dx \\ &\quad + \int_{x_k}^{x_{k+1}} \tilde{f}_k dx + \lambda \int_{x_k}^{x_{k+1}} \tilde{W}_k[y] dx \end{aligned} \quad (2.60)$$

From (2.59) and (2.60) we get:

$$\begin{aligned} \varepsilon_{k+1} = & \varepsilon_k + \varepsilon'_k h_k + h_k^2 \sum_{s=2}^{n-1} \varepsilon_k^{(s)} \frac{h_k^{s-2}}{s!} - \sum_{i=1}^n \int_{x_k}^{x_{k+1}} [P_i y^{(n-i)} - \tilde{P}_i \tilde{y}^{(n-i)}] dx \\ & + \int_{x_k}^{x_{k+1}} [f - \tilde{f}_k] dx + \lambda \int_{x_k}^{x_{k+1}} \{W[y] - \tilde{W}_k[y]\} dx \end{aligned}$$

We know that

$$\int_{x_k}^{x_{k+1}} \tilde{f}_k dx = \frac{\tilde{f}_k h_k^n}{n!}, \quad \int_{x_k}^{x_{k+1}} \tilde{W}_k[y] dx = \frac{\tilde{W}_k[y]}{n!}$$

Let us denote

$$\begin{aligned} E_k &= \max_j |\varepsilon_k^{(j)}|, \quad h_{\max} = \max_k h_k, \quad p_i = \max_{[a,b]} |P_i|, \quad M_{n-i} = \max_{[a,b]} |y^{(n-i)}|, \\ L_i &= \max_{[a,b]} |\tilde{P}_{ik}|, \quad N_{n-i} = \max_{[a,b]} |\tilde{y}^{(n-i)}|, \quad F = \max_{[a,b]} |f|, \quad G_0 = \max_{[a,b]} |\tilde{f}_k|, \\ T &= \max_G |\tilde{W}_k[y]|, \quad s = |b-a| \sum_{j=0}^r \max_G |K_j(x, \xi)| M_j \geq \max_G |W[y]|, \\ l &= \frac{1}{n!} \left[\sum_{i=1}^n (p_i M_{n-i} + L_i N_{n-i}) + F + G_0 + |\lambda|(T + s) \right], \\ g &= 1 + \sum_{s=2}^{n-1} \frac{h_{ax}^{s-1}}{s!}, \end{aligned}$$

and $M_{n-i} \approx N_{n-i}$. Then we get the following recurrent error estimation

$$E_{k+1} \leq (1 + gh_{\max})E_k + lh_{\max}^n \quad (2.61)$$

Hence we get

$$E_k \leq (1 + gh_{\max})^k \varepsilon_0 + lh_{ax}^{n-1} g^{-1} [(1 + gh_{\max})^k - 1] \quad (2.62)$$

where ε_0 is the maximum error in the initial data. Obviously, if $\varepsilon_0 = 0$, then from (2.62) it follows that if $h_{\max} \rightarrow 0$ then $E_k \rightarrow 0$, i.e. $\tilde{y}(x_k) \rightarrow y(x_k)$.

In case that the Eq. (2.49) has the form:

$$L[y] = f(x, y) + \int_a^x F(x, y, y', \dots, y^{(m)}) dx, \quad x \in [a, b],$$

then the Eq. (2.62) will read

$$E_k \leq (1 + hp^{(0)})^k \varepsilon_0 + \frac{p^{(1)} h^n}{p^{(0)}} [(1 + hp^{(0)})^k - 1],$$

where

$$\begin{aligned} p^{(0)} &= \sum_{s=1}^{n-1} \frac{h^{s-1}}{s!} + \frac{h^{n-1}}{n!} \left[\tilde{b} + \sum_{i=1}^n (p_i + (m_i + 1) \gamma_i \beta_{n-i}) + (b-a)c(m_i + 1) \right], \\ p^{(1)} &= \frac{1}{(n+1)!} \left(\tilde{a} + \tilde{b} \beta_1 + 2B + \sum_{i=0}^n p_{0i} \right) + \frac{(b-a)q}{n!}, \\ \tilde{a} &= \max_{[a,b]} \left| \frac{\partial f}{\partial x} \right|, \quad \tilde{b} = \max_{[a,b]} \left| \frac{\partial f}{\partial y} \right|, \quad \gamma_i = \max_{s, [a,b]} \left| \frac{\partial P_i}{\partial y^{(s)}} \right|, \quad \beta_i = \max_{[a,b]} \{ |y^{(i)}|, |\tilde{y}^{(i)}| \}, \\ c &= \max_{s, [a,b]} \left| \frac{\partial F}{\partial y^{(s)}} \right|, \quad q = 0.5 \left(A + C \sum_{s=0}^{m_i} \beta_{s+1} \right), \quad p_{0i} = \beta_{n-i} \left(l_i + \gamma_i \sum_{s=0}^{m_i} \beta_{s+1} \right) + 2\alpha_i \beta_{n+1-i}, \\ A &= \max_{[a,b]} \left| \frac{\partial F}{\partial x} \right|, \quad B = \max_{[a,b]} \{ |F|, |\tilde{F}| \} \end{aligned}$$

2.12.5.2 Solution of Equation $y^{(n)} = f(x, y, y', \dots, y^{(n-1)})$

Let us apply the approximate method of the solution presented in Sect. 2.12.5.1 to integro-differential equations to solve the initial value problem:

$$y^{(n)} = f(x, y, y', \dots, y^{(n-1)}), \quad (x, y) \in G, \quad (2.63)$$

$$y(x_0) = y_0, \quad y^{(j)}(x_0) = y_0^{(j)}, \quad j = 1, \dots, n-1, \quad (x_0, y_0) \in G, \quad (2.64)$$

where the function f satisfies the Lipschitz condition

$$|f(x, y + \delta_0, \dots, y^{(n-1)} + \delta_{n-1}) - f(x, y, y', \dots, y^{(n-1)})| \leq K \sum_{i=0}^{n-1} |\delta_i| \quad (2.65)$$

Let us divide the interval $[a, b]$ by a sequence of points $x_0 = a, x_1, \dots, x_s = b$ into elementary intervals. Let $E = \{x_0, \dots, x_s\}$. On each interval $[x_v, x_{v+1}]$, let us solve the initial value problem:

$$y^{(n)} = f(x, \hat{y}_v, \hat{y}'_v, \dots, \hat{y}_v^{(n-1)}), \quad (x, \hat{y}_v) \in G, \quad v = 0, 1, \dots, s-1;$$

$$y(x_v) = \hat{y}_v, \quad y^{(j)}(x_v) = \hat{y}_v^{(j)}, \quad j = 1, \dots, n-1, \quad (x_v, \hat{y}_v) \in G$$

Then, if the function f satisfies condition (2.65) and $\max_i [x_{i+1} - x_i] = h$, the solution of this problem

$$\hat{y} = \{y_0, \hat{y}_1, \dots, \hat{y}_s\}, \quad \hat{y}^{(j)} = \{y_0^{(j)}, \hat{y}_1^{(j)}, \dots, \hat{y}_s^{(j)}\}, \quad j = 1, \dots, n-1$$

when $h \rightarrow 0$ tends to the solution of Eqs. (2.63), (2.64) and the estimation for the rate of convergence is as follows:

$$\max_l |y_r^{(n-l)} - \hat{y}_r^{(n-l)}| \leq \varepsilon_0(1 + h\alpha_0)^r + \frac{h\alpha_1}{2\alpha_0} [(1 + h\alpha_0)^r - 1], \quad r = 1, 2, \dots, s$$

where

$$\alpha_0 = \sum_{i=1}^{n-1} \frac{h^{i-1}}{i!} + K \left(n + \frac{h}{2} \sum_{j=0}^{n-1} \sum_{s=0}^{n-j-2} \frac{h^s}{s!} \right),$$

$$\alpha_1 = K \sum_{j=0}^{n-1} \left[M \frac{h^{n-j-1}}{(n-j-1)!} + \sum_{s=0}^{n-j-2} N_{s+j+1} \frac{h^s}{s!} \right],$$

$$M = \max_{[a,b]} |f(x, y, y', \dots, y^{(n-1)})|, \quad N_{s+j+1} = \max_r |\hat{y}_r^{(s+j+1)}|$$

If the initial conditions are exactly given, the error estimation has the form:

$$\max_{1 \leq l \leq n-1} |y_r^{(n-l)} - \hat{y}_r^{(n-l)}| \leq Dh^2, \quad r = 1, \dots, s,$$

where

$$N = \max_{1 \leq r \leq s} |N_r|, \quad D = K(M + nD) \frac{[1 + he^h(1 + 0.5Knh) + Kn]^r - 1}{4[1 + Kh(0.5h + e^{-h})]}$$

2.12.5.3 Solution of a System of Ordinary Differential Equations

For the sake of simplicity let us confine ourselves to the important case of equations, having the canonical form

$$y_i^{(m_i)}(t) = f_i(t, y_1, y'_1, \dots, y_1^{(m_1-1)}, \dots, y_n^{(m_n-1)}), \quad i = 1, \dots, n \quad (2.66)$$

The system (2.66) can be replaced by an equivalent system of $m = m_1 + \dots + m_n$ equations of the first order, relative to the derivatives for all m unknown functions. Then one of the standard software can be used to solve the last system.

Let the functions f_i , $i = 1, \dots, n$ be continuous and differentiable with respect to all arguments. Let us suppose that the solution of system (2.66) with the initial conditions

$$y_i(t_0) = (y_i)_0, \quad y'_i(t_0) = (y'_i)_0, \dots, y_i^{(m_i-1)}(t_0) = (y_i^{(m_i-1)})_0$$

exists and is unique in $t_0 \leq t \leq T$.

Divide the interval $[t_0, T]$ into elementary intervals $\Delta k = [t_k, t_{k+1}]$ by a sequence of points $t_0 < t_1 < \dots < t_l = T$. On each such interval, let us search the solution of system (2.66) in the form of a series:

$$\begin{aligned} \tilde{y}_i(t) &= \tilde{y}_i(t_k) + \sum_{j=1}^{m_i-1} \frac{(t-t_k)^j}{j!} \tilde{y}_i^{(j)}(t_k) + \frac{(t-t_k)^{m_i}}{(m_i)!} (\tilde{f}_i)_k, \\ \tilde{y}_i^{(j)}(t_k) &= \tilde{y}_i^{(j)}(t_{k-1}) + \sum_{s=1}^{m_i-j-1} \frac{(t_k-t_{k-1})^s}{s!} \tilde{y}_i^{(s+j)}(t_{k-1}) \\ &\quad + \frac{(t_k-t_{k-1})^{m_i-j}}{(m_i-j)!} (\tilde{f}_i)_k, \quad (j = 1, \dots, m_i-1) \end{aligned}$$

The error of such a solution can be easily estimated, considering the exact expansion of the functions $y_i(t)$ and $y_i^{(j)}(t)$ in a Taylor series:

$$\begin{aligned} |\varepsilon_i(t_{k+1})| &\leq |\varepsilon_i(t_k)| + \sum_{j=1}^{m_i-1} \frac{h_k^j}{j!} \left| \varepsilon_i^{(j)}(t_k) \right| + M_i \frac{h_k^{m_i+1}}{(m_i+1)!} \\ &\quad + M_i \frac{h_k^{m_i}}{(m_i)!} \sum_{j=1}^n \sum_{s=0}^{m_j-1} \left| \varepsilon_j^{(s)}(t_k) \right| \end{aligned} \quad (2.67)$$

$$\begin{aligned} \left| \varepsilon_i^{(j)}(t_k) \right| &\leq \left| \varepsilon_i^{(j)}(t_{k-1}) \right| + \sum_{s=1}^{m_i-j-1} \frac{h_{k-1}^s}{s!} \left| \varepsilon_i^{(s+j)}(t_{k-1}) \right| \\ &\quad + M_i \left(\frac{h_k^{m_i-j+1}}{(m_i-j+1)!} + \frac{h_k^{m_i-j}}{(m_i-j)!} \sum_{j=1}^n \sum_{s=0}^{m_j-1} \left| \varepsilon_j^{(s)}(t_{k-1}) \right| \right) \end{aligned} \quad (2.68)$$

where

$$M_i = \max_{[t_0, T]} \left\{ \left| \frac{\partial f_i}{\partial t} \right|, \left| \frac{\partial f_i}{\partial y_1} \right|, \dots, \left| \frac{\partial f_i}{\partial y_n^{(m_n-1)}} \right| \right\}$$

Formulas (2.67) and (2.68) give a recurrent estimation for error. From them it is possible to obtain an error estimation applicable to the entire interval $[t_0, T]$:

$$E_k \leq \varepsilon_0(1 + hp_0)^k + \frac{hP_1}{p_0} \left[(1 + hp_0)^k - 1 \right],$$

where the following notations are introduced

$$h = \max_k h_k, \quad E_k = \max_{i,j} \left| \varepsilon_i^{(j)}(t_k) \right|, \quad M = \max_i M_i, \quad v = \min_s m_s,$$

$$P_1 = M \frac{h^{v-1}}{(v+1)!}, \quad p_0 = mM \frac{h^{v-1}}{v!} + \sum_{s=1}^{\mu-1} \frac{h^{s-1}}{s!}, \quad \mu = \max_s m_s$$

2.12.5.4 Solutions of Equations with Known Moments on the Right Side

Let us consider a particular case of Eq. (2.49):

$$L[y] = y^{(n)} + \sum_{i=1}^n p_i y^{(n-i)} = f(x), \quad x \geq 0 \quad (2.69)$$

where p_i is the constant coefficients, $f(x)$ is a single-valued and differentiable function, $f(x) \rightarrow 0$ as $x \rightarrow \infty$ and its moments are known:

$$M_v f(x) = \int_0^\infty x^v f(x) dx < \infty, \quad v = 0, 1, \dots, m \quad (2.70)$$

It is necessary to solve the Eq. (2.69) with the following initial conditions:

$$y^{(s)}(x_0) = y_0^{(s)} \quad (s = 0, 1, \dots, n-1)$$

We shall approximate $f(x)$ in the following manner:

$$f(x) \approx \exp(-kx) \sum_{i=0}^m a_i x^i = P_m(x) \exp(-kx), \quad (2.71)$$

where $m > 0$ is an integer, $k > 0$ and a_i are constants to be determined. Then, from (2.70) and (2.71) we have

$$\tilde{M}_v f(x) = \int_0^\infty x^v \left[\exp(-kx) \sum_{i=0}^m a_i x^i \right] dx = \sum_{i=0}^m a_i \frac{(v+i)!}{k^{v+i+1}}$$

k is fixed from the conditions of best approximation by (2.71). Then the Eq. (2.69) is replaced by the approximate equation:

$$L[\tilde{y}] = \exp(-kx) \sum_{i=0}^m a_i x^i, \quad (2.72)$$

which can be easily solved. For the error $\varepsilon(x) = y(x) - \tilde{y}(x)$, we obtain an equation from (2.69) to (2.72):

$$L[\varepsilon(x)] = f(x) - \exp(-kx)P_m(x) \equiv R_m(x) \quad (2.73)$$

Solving Eq. (2.73), we have

$$|\varepsilon(x)| \leq \frac{\eta}{n!} \sum_{k=0}^{\infty} \frac{(b-a)^{n+k}}{k!} M^k,$$

where

$$M = \max_{a \leq s \leq x \leq b} |K(x, s)|, \quad \eta = \max_{[a, b]} |R_m(x)|, \quad K(x, s) = \sum_{i=1}^n p_i \frac{(x-s)^{i-1}}{(i-1)!}$$

2.12.5.5 Refinements of Approximate Solutions of Volterra Integral Equations

Let us consider Volterra integral equation of the first and of the second kind arising in the remote monitoring problems:

$$\lambda \int_a^x G(x, y) \varphi(y) dy = g(x), \quad (2.74)$$

$$\varphi(x) - \lambda \int_a^x K(x, y) \varphi(y) dy = f(x), \quad (2.75)$$

where $x \in [a, b]$, the kernel $K(x, y)$ and its derivatives $K'_x(x, y)$ are continuous in the region $R\{a \leq y \leq x \leq b\}$, $f(x)$ is a continuously differentiable function in (a, b) , the kernel $G(x, y)$ and $g(x)$ are twice continuously differentiable functions of x , $G(x, x) \neq 0$. Then, as it is known, Eqs. (2.74) and (2.75) have unique solutions $\varphi_1(x)$ and $\varphi_2(x)$ respectively which are continuous and differentiable in $[a, b]$ for any value of λ . The case when $G(x, x) = 0$ for some point in the interval $[a, b]$ or for the entire interval needs special consideration. In our case, Eq. (2.74) is equivalent to the equation of second kind

$$\varphi(x) + \int_a^x \frac{G'_x(x, y)}{G(x, x)} \varphi(y) dy = \frac{g'(x)}{\lambda G(x, x)}$$

Therefore, the argument used to find an approximate solution of (2.75) is valid for Eq. (2.74) as well.

In traditional way the Eq. (2.75) is solved by replacing the integral of the equation by a finite sum of some quadratic formula. Applying this approach let us divide the interval $[a, b]$ by a sequence of points $x_0 = a < x_1 < x_2 < \dots < x_m = b$ into elementary intervals $\Delta j = [x_j, x_{j+1}]$, and instead of (2.75) let us write the equation:

$$\varphi(x_j) - \lambda \sum_{i=0}^{j-1} \int_{x_i}^{x_{i+1}} K(x_j, y) \varphi(y) dy = f(x_j), \quad (j = 0, 1, \dots, m) \quad (2.76)$$

Further, because of the assumptions made on $\varphi(x)$ and $K(x, y)$ we can write

$$\begin{aligned} \varphi(x) &= \varphi(x_i) + (x - x_i) \varphi'(x_i) + \frac{(x - x_i)^2}{2!} \varphi''(\xi_i), \\ (x_i \leq \xi_i \leq x \leq x_{i+1}) \end{aligned} \quad (2.77)$$

and assuming the existence and differentiability of $K'_y(x, y)$ we have

$$\begin{aligned} K(x_j, y) &= K(x_j, x_i) + (y - x_i) K'_y(x_j, x_i) + \frac{(y - x_i)^2}{2} K''_{yy}(x_j, \eta_i), \\ (x_i \leq \eta_i \leq y \leq x_{i+1}) \end{aligned} \quad (2.78)$$

substituting (2.77) and (2.78) in (2.76) we get:

$$\begin{aligned} \varphi(x_j) - \lambda \sum_{i=0}^{j-1} \{ & K(x_j, x_i) \varphi(x_i) + \frac{h_i}{2} [K(x_j, x_i) \varphi'(x_i) + K'_y(x_j, x_i) \varphi(x_i)] \\ & + \frac{h_i^2}{3} K'_y(x_j, x_i) \varphi'(x_i) \} h_i + R_j = f(x_j) \end{aligned}$$

where

$$\begin{aligned} R_j = -\lambda \sum_{i=0}^{j-1} \{ & \frac{h_i^3}{2} \varphi''(\xi_i) [\frac{1}{3} K'_y(x_j, x_i) + \frac{h_i}{4} K'_y(x_j, x_i)] \\ & + \frac{h_i^3}{2} K''_{yy}(x_j, \eta_i) [\frac{1}{3} \varphi(x_i) + \frac{h_i}{4} \varphi'(x_i)] + \frac{h_i^5}{20} \varphi''(\xi_i) K''_{yy}(x_j, \eta_i) \} \end{aligned}$$

Neglecting the small quantity R_j in this expression, we get a recurrent formula for determining $\varphi(x_j)$ from the values of the function $\varphi(x)$ at $x = x_0, x_1, \dots, x_{j-1}$. By differentiating (2.75) we get a formula to calculate the values of the derivative $\varphi'(x)$:

$$\varphi'(x) = f'(x) + \lambda K(x, x)\varphi(x) + \lambda \int_a^x K'_x(x, y)dy$$

From this equation, we have at $x = x_i$

$$\varphi'(x_i) = f'(x_i) + \lambda K(x_i, x_i)\varphi(x_i) + \lambda \sum_{s=0}^{i-1} \int_{x_s}^{x_{s+1}} K'_x(x_i, y)\varphi(y)dy \quad (2.79)$$

where

$$\varphi(x_0) = f(a), \varphi'(x_0) = f'(a) + \lambda K(a, a)\varphi(a)$$

Neglecting the quantity

$$r_i = \lambda \sum_{s=0}^{i-1} \left\{ K''_{xy}(x_i, Q_s) \frac{h_s^2}{2} \left[\varphi(x_s) + \frac{2}{3} \varphi'(x_s)h_s + \frac{h_s^2}{4} \varphi''(\xi_s) \right] + K'_x(x_i, x_s) \frac{h_s^2}{6} \varphi''(\xi_s) \right\}, \quad (x_s \leq \xi_s, Q_s \leq y \leq x_{s+1})$$

Equation (2.79) can be written as:

$$\tilde{\varphi}'(x_i) = f'(x_i) + \lambda K(x_i, x_i)\tilde{\varphi}(x_i) + \lambda \sum_{s=0}^{i-1} h_s K'_x(x_i, x_s) \left[\tilde{\varphi}(x_s) + \frac{h_s}{2} \tilde{\varphi}'(x_s) \right]$$

We get finally the equation for determining $\tilde{\varphi}(x_j)$:

$$\tilde{\varphi}(x_j) - f(x_j) - \lambda \sum_{i=0}^{j-1} [\tilde{\varphi}(x_i)K(x_j, x_i)l_{ji} + h_i \gamma_{ji} \delta_i] h_i = 0, \quad (2.80)$$

where, for sake of brevity, the following notation is introduced:

$$\begin{aligned}
l_{ji} &= 1 + \frac{h_i}{2} \left[\lambda K(x_i, x_i) + \frac{K'_y(x_j, x_i)}{K(x_j, x_i)} \left[1 + \frac{2}{3} \lambda h_i K(x_i, x_i) \right] \right] \\
\gamma_{ji} &= \frac{1}{2} K(x_j, x_i) \left[1 + \frac{2}{3} h_i \frac{K'_y(x_j, x_i)}{K(x_j, x_i)} \right] \\
\delta_i &= f'(x_i) + \lambda \sum_{s=0}^{i-1} h_s K'_x(x_i, x_s) \left[\tilde{\varphi}(x_s) + \frac{h_s}{2} \tilde{\varphi}'(x_s) \right]
\end{aligned}$$

Thus, starting the calculation by formula (2.80) from $j = 1$. We get the values of solution $\tilde{\varphi}_1, \tilde{\varphi}_2, \dots, \tilde{\varphi}_m$ with the error $\varepsilon(x_i)$. Let us estimate the value of modulus of the error $\varepsilon(x)$ from above. Let us introduce the following notation:

$$\begin{aligned}
M &= \max_{[a,b]} |\varphi(x)|, \quad N = \max_{[a,b]} |\varphi'(x)|, \quad L = \max_{[a,b]} |\varphi''(x)|, \\
Q &= \max_R \left\{ \left| K'_y(x, y) \right|, \quad \left| K'_x(x, y) \right| \right\}, \quad G = \max_R |K(x, y)|, \\
B &= \max_R \left\{ \left| K''_{yy}(x, y) \right|, \quad \left| K''_{xy}(x, y) \right| \right\}, \quad h = \max_s |h_s|, \\
l &= \frac{m}{6} \left[B \left(M + \frac{3h}{4} N \right) + L \left(G + \frac{3}{4} Qh + \frac{3}{10} Bh^2 \right) \right], \\
n &= \frac{|\lambda| Bm}{2} \left(M + \frac{2h}{3} N + \frac{h^2}{4} L \right) + \frac{h}{6} BL
\end{aligned}$$

Then we have

$$\begin{aligned}
|\varepsilon_j| &\leq |\lambda| h \left(G + \frac{2}{3} Qh \right) \sum_{i=0}^{j-1} \left(|\varepsilon_i| + \frac{h}{2} |\varepsilon'_i| \right) + |\lambda| lh^3, \\
|\varepsilon'_i| &\leq |\lambda| G |\varepsilon_i| + |\lambda| Qh \sum_{s=0}^{i-1} \left(|\varepsilon_s| + \frac{h}{2} |\varepsilon'_s| \right) + nh^2,
\end{aligned}$$

where $\varepsilon_j = \varphi(x_j) - \tilde{\varphi}(x_j)$, $\varepsilon'_i = \varphi'(x_i) - \tilde{\varphi}'(x_i)$. From these formulas we get roughly

$$\begin{aligned}
|\varepsilon'_i| &\leq |\lambda| \left(G |\varepsilon_i| + hQ \sum_{s=0}^{i-1} |\varepsilon_s| \right) + (n + |\lambda| QNm) h^2, \\
|\varepsilon_j| &\leq |\lambda| h \left(G + \frac{2}{3} Qh \right) \sum_{i=0}^{j-1} \left[\left(1 + \frac{|\lambda| Gh}{2} \right) |\varepsilon_i| + \frac{|\lambda| Gh}{2} \sum_{s=0}^{i-1} |\varepsilon_s| \right] + |\lambda| th^3,
\end{aligned}$$

where

$$t = l + \frac{h}{2}m \left(G + \frac{2}{3}Qh \right) (n + |\lambda QNm|)$$

Let us denote

$$T = |\lambda|(G + 2Qh/3), b = 1 + |\lambda|Gh/2, r = |\lambda|(t + QMTm^2)$$

Then we get

$$|\varepsilon_j| \leq hTB \sum_{i=0}^{j-1} |\varepsilon_i| + rh^3$$

or, finally, we have

$$|\varphi_j - \tilde{\varphi}_j| \leq E_j = \varepsilon_0 Z_1^j + rh^3(1 - Thb_j)^{-1} \leq \varepsilon_0 + rh^3(1 - Thb_j)^{-1},$$

where $h \leq (Tb)^{-1}$, Z_1 is the real root of the equation

$$Z^{j+1} - TbhZ^{j-1}/(Z - 1) = 0$$

between $Z = 1$ and $Z = hTb$.

<http://www.springer.com/978-3-319-13977-7>

New Ecoinformatics Tools in Environmental Science
Applications and Decision-making

Krapivin, V.F.; Varotsos, C.A.; Soldatov, V.Y.

2015, XXXIII, 903 p. 289 illus., 120 illus. in color.,

Hardcover

ISBN: 978-3-319-13977-7